UNIVERSITÀ DEGLI STUDI DI MILANO

Scuola di Dottorato in
Biotecnologie applicate alle Scienze Mediche
XXVII ciclo

Dipartimento di Biotecnologie Mediche
e Medicina Traslazionale

THE ROLE OF THE IRSp53-LIN7 COMPLEX IN CELL MEMBRANE DYNAMICS

COORDINATORE: Prof. Massimo Locati
TUTOR: Dott.ssa Grazia Pietrini

Tesi di Dottorato di:
ILARIA FERRARI
Matricola: R09564

Anno Accademico 2013-2014

INDEX

CHAPTER 1

Abstract

1. Abstract

The insulin receptor substrate protein of 53 kDa is a critical factor in determining neuronal polarisation, as it initiates membrane protrusions to form filopodia and neurites by coupling membrane deformation with F-actin polymerization. With its C-terminal tail, IRSp53 can bind to PDZ domain containing proteins including LIN7, a small scaffold protein possessing a single L27 domain, necessary for membrane recruitment. Here, we investigated the role of the IRSp53-LIN7 complex in cellular mechanisms that heavily rely on membrane deformation, such as the formation of filopodia and neurites or mitochondrial fission.

Concerning the role of the IRSp53:LIN7 complex in filopodia and neurite induction, our findings indicate that the formation of actin-filled filopodia and neurites depends on motifs mediating IRSp53-LIN7 association and filopodia tip localisation. We further showed that co-expression of LIN7 with IRSp53 enhanced the formation of filopodia protrusions in neuronal NSC34 cells, while also preventing the appearance of actin-deficient protrusions induced by the overexpression of IRSp53 alone. The positive regulatory role of LIN7 in IRSp53-mediated extension of filopodia was further demonstrated by live-cell imaging experiments in neuronal N2A cells. Moreover, LIN7 silencing in N2A cells prevented the extension of filopodia and neurites, induced by either the ectopic expression of IRSp53 or serum starvation. Defective neuritogenesis could be rescued by the expression of RNAi-resistant full

length LIN7 or chimeric L27-IRSp53, whereas the expression of full length IRSp53 or the LIN7ΔPDZ mutant lacking the domain for association with IRSp53 was unable to restore neuritogenesis in LIN7 silenced cells. Finally, LIN7 silencing prevented the recruitment of IRSp53 in Triton X-100 insoluble complexes, otherwise occurring in differentiated cells. Collectively, this first set of data identify in LIN7 a novel regulator of the filopodia- and neurites-promoting activity of IRSp53, whose role is to spatially restrict its activity to the plasma membrane for filopodia and neurite initiation, and to further promote the stabilisation of these actin–rich structures.

More recently, we tested the hypothesis of a role for the IRSp53-LIN7 complex in the modification of intracellular membranes. To this regard, we found that endogenous LIN7 and IRSp53 localized in punctuate structures along mitochondria, a fact that prompted us to further investigate the possible effects of modifications in the expression levels of IRSp53/LIN7 on mitochondrial morphology. Eukaryotic cells, in fact, strictly regulate the overall morphology of their mitochondrial network thanks to the existence of protein complexes able to control fission and fusion events. We found that, upon overexpression of LIN7 and/or IRSp53, mitochondria morphology was altered, with a significant increase in the percentage of cells showing a less interconnected mitochondrial network compared to GFP-transfected control cells, a phenotype that was blocked by co-expression of the K38A dominant negative mutant of the fission protein Drp1. Downregulation of

endogenous LIN7 and/or IRSp53 by shRNA, on the other hand, increased the amount of cells with highly fused mitochondria. Mitochondria hyperfusion in the downregulated cells was associated with an increased resistance to NaN_3-induced mitochondrial fragmentation, and by the appearance of cells with aberrantly shaped and often multi-lobed nuclei, a phenotype that we also found in Drp1 K38A-expressing cells, and that others reported to be caused by defective mitochondrial fragmentation during mitosis. Collectively our data strongly suggest a Drp1-dependent function of LIN7 and IRSp53 on mitochondrial division apparatus.

Taken together, our data unravel a role of the IRSp53-LIN7 complex on membrane dynamics that is not restricted to plasma membranes, as previously thought, but may also apply to other cellular mechanisms that heavily rely on membrane deformation, as our data on mitochondrial morphology have shown.

CHAPTER 2

General Introduction

2.1. Cell Polarity

Cell polarity is a common feature in a vast variety of cell types, which require to develop and subsequently maintain specialized functional domains, enabling them to sustain the tissue-specific activity to which they are entitled (Drubin and Nelson, 1996). The main characteristic of a polarized cell is the asymmetric distribution of its organelles, plasma membrane (PM) domains and cytoskeletal components (Bryant and Mostov, 2008). Such morphological and functional asymmetry is peculiar to the specific functions the cell has to perform. The subsequent coordination in space and time of the polarization mechanism will then ensure that the correct asymmetry will be achieved not only at the single-cell level, but also in the tissue that such cells will have formed (Bryant and Mostov, 2008).

2.2 Neuronal polarity

Neurons are perhaps the most highly polarized cells of our entire body. The acquisition of a polarized phenotype is of pivotal importance for neurons to guarantee their capability of integrating and transmitting information within the nervous system (Barnes and Polleaux, 2009).

Our knowledge about neuronal maturation *in vivo* is still quite limited. What is known is that, upon exit from the cell cycle, mammalian

neuronal cells have to migrate a long distance in order to reach their final destination, and it's in the course of such migration that neurons gradually achieve their proper polarity.

The bulk of our knowledge about neuronal maturation come from *in vitro* studies of primary cortical or hippocampal cultures. The events that transform such cells from symmetric spheres to highly compartmentalized structures able to generate and propagate action potentials from the soma to the synaptic bouton can be divided in five main steps (Craig and Banker, 1994):

- Stage 1: When freshly dissociated from embryonic rat brains, neurons appear as symmetrical spheres encircled by a thin lamellipodium, from which a few filopodia emerge.
- Stage 2: A few hours after plating, neurons start emitting neurites which, at this stage, are all morphologically similar.
- Stage 3: About 12 hours after plating, one of the neurites starts to rapidly elongate, subsequently acquiring an axonal phenotype.
- Stage 4: The other neurites acquire a dendritic phenotype in the course of the first week after plating.
- Stage 5: Neurons start to build a network by creating synaptic contacts.

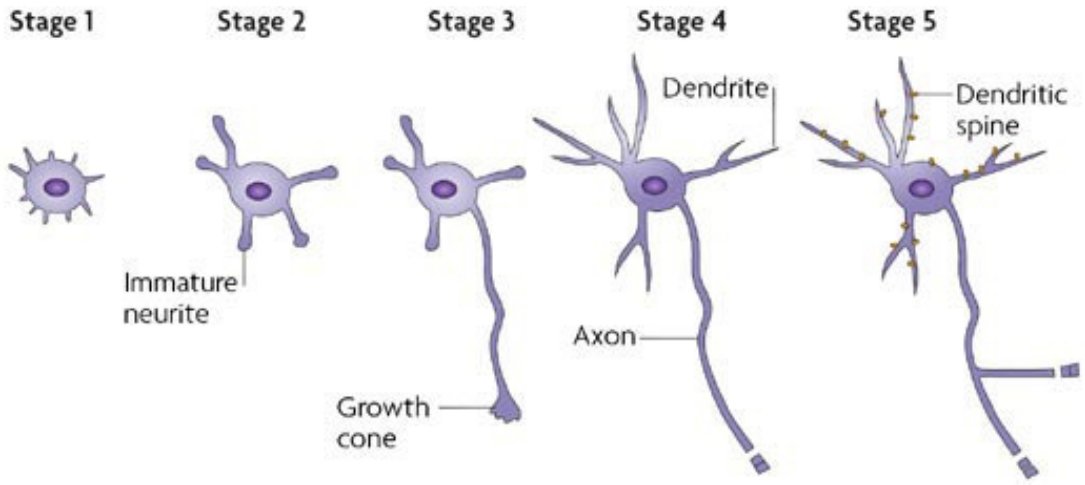

Image 1: neuronal differentiation in vitro (from Arimura and Kaibuchi, 2007)

2.2.1 Stage 1: the extension of membrane protrusions

In order to sense and sample the surrounding environment, the undifferentiated spherical neuron depends on its capacity to extend PM structures called lamellipodia and filopodia. These structures are particularly important for the execution of various tasks, including cell migration. In order to migrate, a call must be able to polarize in response to a variety of extracellular cues. Lamellipodia and filopodia will then arise from the 'leading edge' of the cell, where they act as a link between the cytoskeleton and the extracellular matrix, thanks to the adhesion receptors expressed on their membrane. Such adhesions are necessary to ensure the traction that the cell needs in order to move forward .

In differentiating neuronal cells lamellipodia and filopodia are required for the first steps of differentiation, when the cell has to initiate and subsequently elongate neurites in specific directions. Moreover, filopodia are the precursors of dendritic spines.

2.2.1.1 Role of the actin cytoskeleton in the extension of membrane protrusions

Thanks to its biochemical and mechanical properties, the actin cytoskeleton is the key component in a wide range of cellular processes, such as morphogenesis, polarity establishment and motility. All of these processes are made possible by the fact that actin filaments are able to both resist to and exert force in the cell environment (Blanchoin et al., 2014).

The basic unit for the construction of the double-stranded helical actin filament is the globular actin (G-actin), a 42 kDa protein which possess an intrinsic ATPase activity. G-actin is able to auto-assemble onto a pre-existing filamentos-actin (F-actin) filament through a highly dissipative mechanism, in which the G-actin monomer hydrolizes ATP upon polymerization. The two ends of the actin filament, termed barbed and pointed end, are dynamically different, with the barbed end elongating 10 times faster than the pointed end. At the steady state, this property translates into the fact that only the barbed end actually elongates, whereas at the pointed end depolymerization occurs. The final result is that the actin filament moves forward while maintaining its length unchanged, a process that inside the cell is known as treadmilling (Blanchoin et al., 2014). Once formed, actin filaments can organize into a series of higher order architectures, each of which is suited for a specific physiological function.

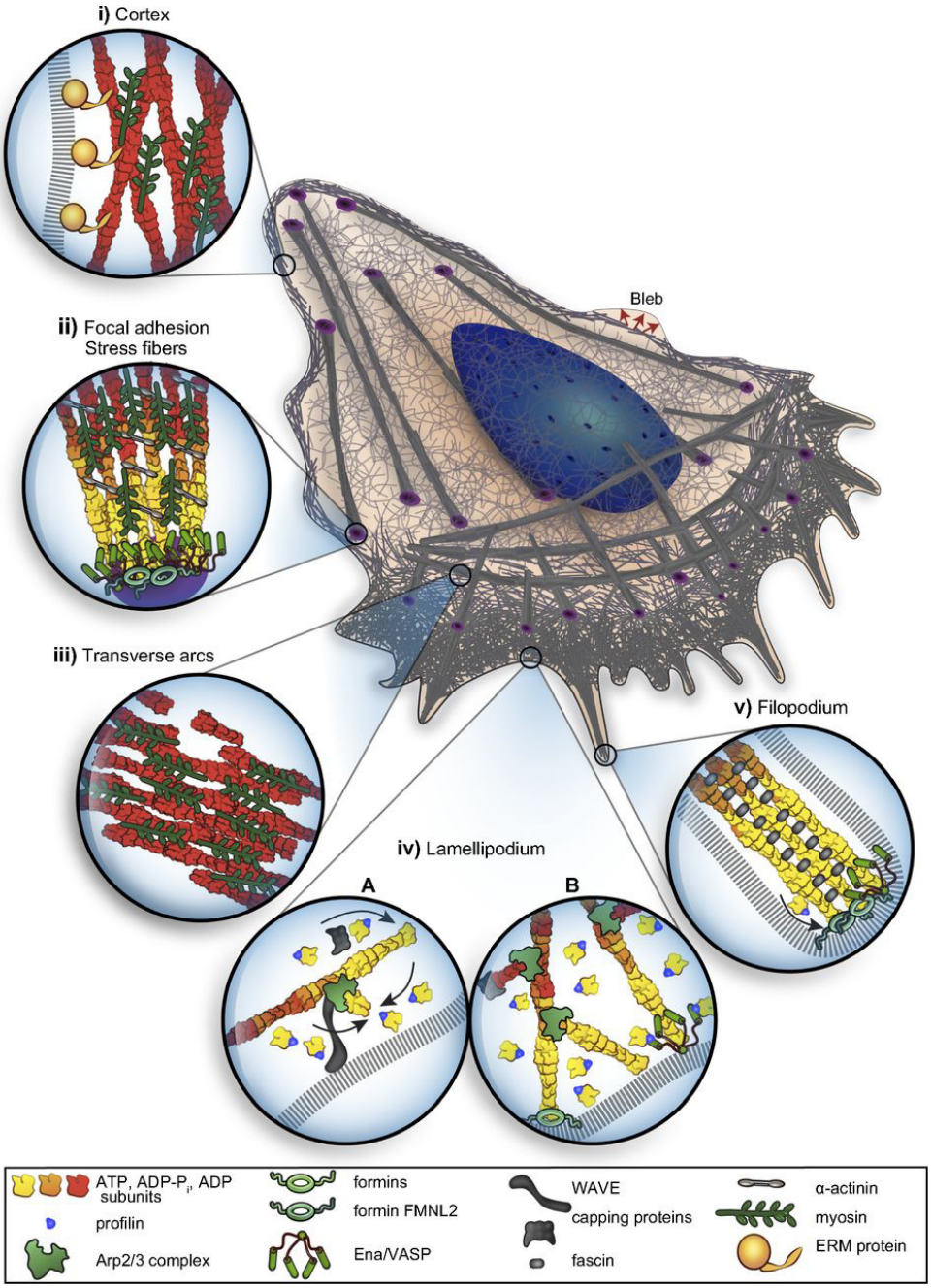

Image 2: actin filaments-based higher order architectures (from Blanchoin et al., 2014)

The control of the actin cytoskeleton morphology is so important for the proper functioning of cells that more than 100 proteins have been found to be involved in various aspects of actin remodelling (Goley and Welch, 2006). Among these proteins, the ones which promote actin nucleation play a central role, as spontaneous actin polymerization is a kinetically

unfavourable phenomenon. Actin nucleating proteins can be divided in two classes: proteins that nucleate new actin filaments starting to the side of a pre-existing one, such as the proteins of the actin-related protein (ARP) 2/3 complex, and proteins that promote the *de novo* formation of linear actin filaments, such as the formins (Goley and Welch, 2006). The ramified actin mesh generated by the activation of the ARP 2/3 complex is the basis for the formation of lamellipodia, whereas linear actin filaments, such as the ones polymerized by formins, are the scaffold for filopodia extension.

The formation of both these membranous structures is regulated by the Ras homolog gene (Rho) family of small GTPases.

2.2.1.2 Role of the Rho GTPases in the extension of membrane protrusions

More than 20 proteins are members of the Rho family of small GTPases. Such proteins are characterized by the capacity to cycle between an active GTP-bound state and an inactive GDP-bound state. Their cycling is regulated by two classes of proteins: the Rho GTPase activating proteins (GAPs) and the Rho guanilate exchange factors (GEFs). The spatiotemporal balance in the activation/inactivation rate of the various Rho GTPases is of crucial importance for many aspects of cell physiology, including morphogenesis, cell migration, neuronal development and cell adhesion (Govek et al., 2011; Heasman and Ridley, 2008).

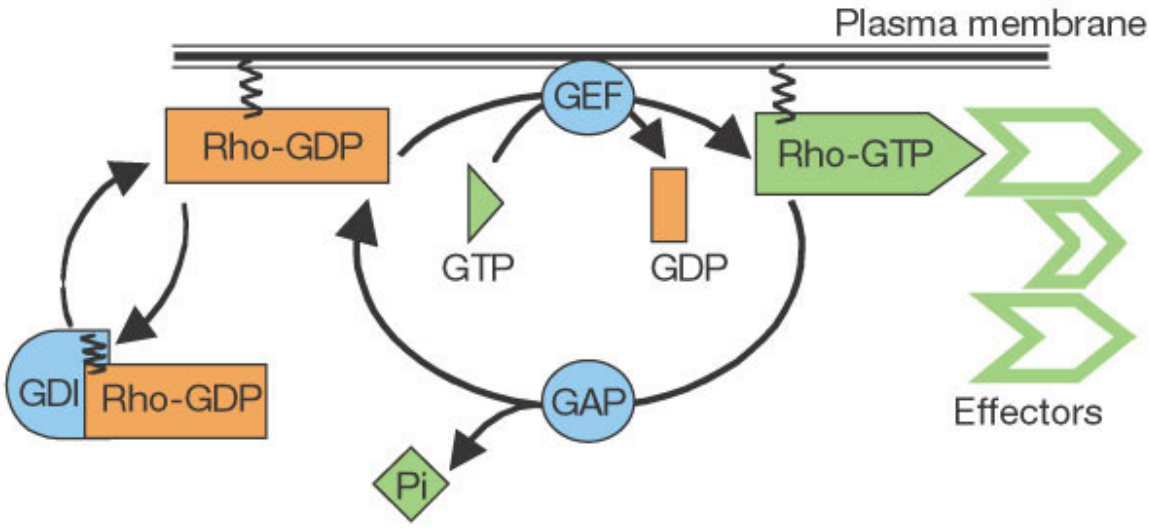

Image 3: Rho GTPases activation (from Etienne-Manneville and Hall, 20002)

Among the Rho family of small GTPases, the Cell division control protein 42 (Cdc42), the Ras-related C3 botulinum toxin substrate 1 (Rac1) and the Ras homolog gene family, member A (RhoA) are by far the most extensively studied. Through its ability to promote actin polymerization by different nucleating factors, Cdc42 plays an important role both in cell polarity and filopodia formation, whereas Rac1 stimulate the extension of lamellipodia. RhoA, on the other hand, is able to induce the formation of stress fibres, which are actin and myosin II-based structures that play an important role in cell adhesion and contractility (Iden and Collard, 2008).

The coordinated interplay between these three GTPases plays a fundamental role in many aspects of neuronal development, such as neurite outgrowth and differentiation, and dendritic spines formation (Govek et al., 2011). In general, the activity of Cdc42 and Rac1 is associated with the promotion of neurite outgrowth and growth cone turning in response to attractive cues, whereas RhoA usually has an

inhibitory effect on neurite formation and is associated with responses to repellent cues (Blanchoin et al., 2014).

2.2.1.3 Lamellipodia

Lamellipodia are actin-based membranous projections that usually appear on the moving edge of a cell. The actin cytoskeleton beneath the membrane of the lamellipodium is organized in a quasi-two-dimensional mesh that is formed by the assembly of new actin filaments starting from the side of pre-existing 'mother filaments' (see Image 2, page 18). Even tough many other nucleating factors have been proposed to participate in actin assembly inside the lamellipodium, it is generally accepted that the main mode of filament assembly is via the ARP 2/3 complex. The ARP 2/3 complex is inactive in the cytoplasm and must be activated by nucleation promoting factors (NPFs). The NPF for the ARP 2/3 complex is represented by the WASP family Verprolin-homologous protein 1 (WAVE1). The function of WAVE1 itself is kept tightly regulated and spatially restricted by assembly into the WAVE regulatory complex (WRC), a five subunit complex that masks the catalytic VCA domain of WAVE1, thus preventing its direct interaction with ARP 2/3. The unmasking of the VCA domain of WAVE1 is mediated by competitive binding of RAC1 to the WRC (Ismail et al., 2009). Thus, Rac1 activation favours actin polymerization into the lamellipodium by promoting WAVE1-ARP 2/3 interaction (Bisi et al., 2013).

Once activated by RAC1, WAVE1 is also able to interact with the inverted Bin–amphipysin–Rvs167 (I-BAR) domain containing protein insulin

receptor substrate protein of 53 kDa (IRSp53). With the convex face of its I-BAR domain, IRSp53 is able to both bind phospholipids at the PM and impose a negative curvature to the PM itself (Mattila et al., 2007).

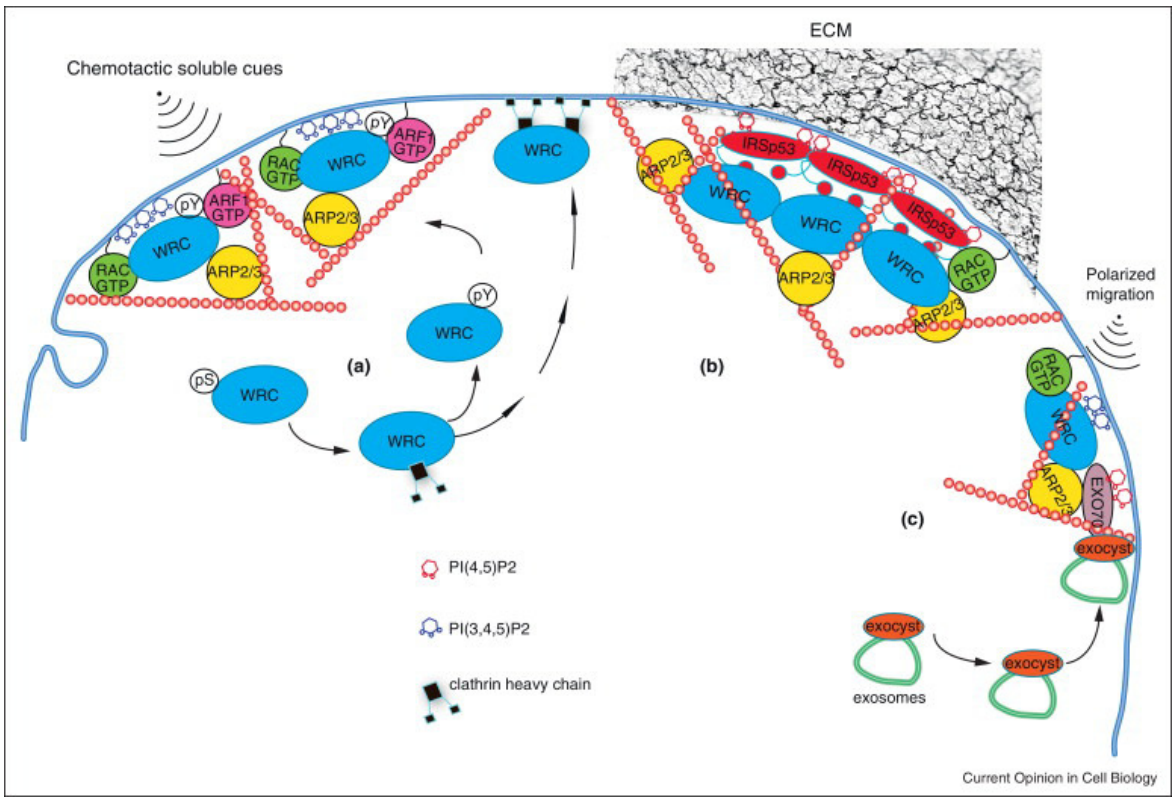

Image 4: proteins involved in lamellipodia formation during chemotaxis or haptotaxis (from Bisi at al., 2013)

Even though biochemical experiments showed that IRSp53 is able to enhance WRC activity and its recruitment to the lamellipodium leading edge (Suetsugu et al., 2006), knocking down IRSp53 in fibroblast cells had no effect on their capability to form lamellipodia and migrate in response to growth factors stimulation (Bisi et al., 2013). Cohen and colleagues, however, provided data demonstrating how IRSp53 activity

seems to be critical for proper cell-extracellular matrix (ECM) adhesion and spreading of epithelial cells (Cohen et al., 2011).

Thus, it would seem that IRSp53, while dispensable for growth factors-mediated migration (chemotaxis), is essential for haptotaxis, which is the ability of a migrating cell to sense ECM gradients on the substrate (Wu et al., 2012). Therefore, IRSp53 interaction with WAVE1 and the WRC may be relevant for cell responses to insoluble environmenttal cues.

Finally, it is important to mention that Block and colleagues demonstrated a role for Cdc42 in lamellipodia formation through activation of the Formin-like protein 2 (FMNL2), of the formin family of proteins (Block et al., 2012), thus suggesting that the ARP 2/3 complex isn't the only NPF contributing to actin polymerization inside the lamellipodium.

2.2.1.4 Filopodia

Filopodia are thin membrane protrusions of a diameter of 0,1 – 0,2 µm and a length between 5 and 15 µm, and containing 15-20 parallel actin filaments. Membrane receptors sensing locally expressed adhesive ligands and extrinsic guidance cues are expressed on their membrane, enabling filopodia to participate in a wide series of physiological events, such as cell migration, wound healing, cell adhesion and, at the neuronal level, neuritogenesis, growth cone path finding and dendritic spines development (Dent et al., 2007; Jang et al., 2010).

The exact mechanism of how filopodia are generated is still partially obscure, but so far two possible models have been proposed:

- Convergent elongation model: according to this model, the parallel actin filaments that act as the skeleton of the filopodium are generated from the actin mesh of the lamellipodium. The hypothesis is that actin filaments braches that are not protected from further elongation by capping proteins become the substrate of formin proteins that elongate them into long and parallel actin filaments that are then bundled together by fascin.
- *De novo* filament nucleation model: according to this model the actin filaments composing the filopodium are simply polymerized *de novo* by formins, then bundled by fascin.

The majority of the experimental data published in literature suggest that the convergent elongation model is the correct one (Blanchoin et al., 2014).

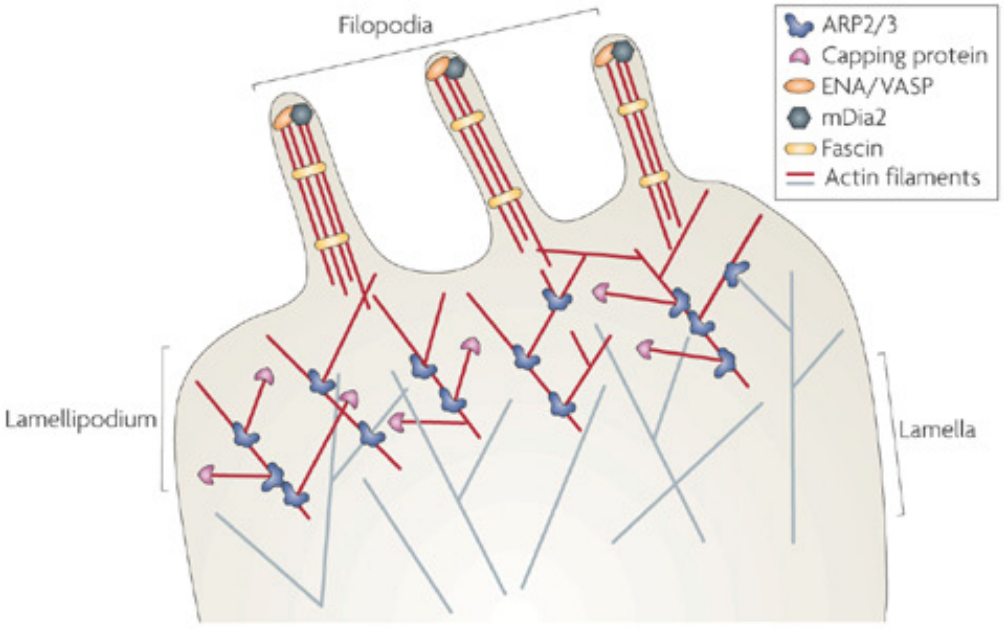

Image 5: Filopodia formation (Heasman and Ridley 2008)

Many proteins have been implicated in filopodial generation and maintenance, such as:

- Proteins of the Enabled (ENA) / Vasodilator-stimulated phosphoprotein (VASP): proteins belonging to this family are localized at focal adhesions, cell-cell contacts, lamellipodia leading edge and filopodia tips. The proteins of the ENA/VASP family are able to prevent capping proteins from binding actin filaments.
- Formins: the proteins belonging to this family have the ability to nucleate actin filaments *de novo*. Once a new actin filament has been nucleated, formins remain attached to its barbed end through their formin homology 2 (FH2) domain and promote filament elongation.
- Myosin X: myosin X belongs to a superfamily of motor proteins which are able to progress along actin filament in an ATP-dependent manner (Berg and Cheney, 2002; Berg et al., 2000). Myosin X has been proposed to exert a role also in filopodia extension as its overexpression induces an increase in the number of filopodia (Mattila and Lappalainen, 2008).
- Fascin: an actin crosslinking protein that generates rigid bundles of several actin filaments, as required inside the filopodium.
- Proteins containing an I-BAR domain: although actin polymerization toward the PM provides a force that pushes the membrane outward, the process of negative membrane bending

is made easier by the action of proteins that contain an I-BAR domain. As already mentioned in paragraph 2.2.1.3, I-BAR domain-containing proteins, such as IRSp53, are able to both bind and deform the PM so to generate a membranous protrusion (Mattila et al., 2007; Suetsugu et al., 2006).

2.2.2 Stage 2: neuritogenesis

A neurite can be defined as a microtubule-based neuronal extension that cannot be classified neither as axon, nor dendrite. Neurites can sample the environment and grow accordingly thanks to the presence, on their distal end, of a growth cone. The growth cone is an actin-based structure formed by a lamellipodium and numerous filopodia, which bare membrane receptors for both adhesive ligands and extrinsic guidance cues. The extension of neurites from the spherical 'stage 1' neuron represents the first symmetry-breaking step of neuronal differentiation. Filopodia are the necessary precursors of neurites, as cultured neurons defective in filopodia formation are blocked at the stage 1 of cell differentiation (Dent et al., 2007). Neurites are generated when a few filopodia located in a given region of the neuronal sphere are invaded by microtubules, which are essential to promote further elongation of the newly extruded neurite (Lowery and Van Vactor, 2009). Neurite extension by the actin and microtubule cytoskeletons must be coupled with an increase in intracellular vesicles fusion with the PM, so to guarantee that enough PM surface is available for neurite elongation.

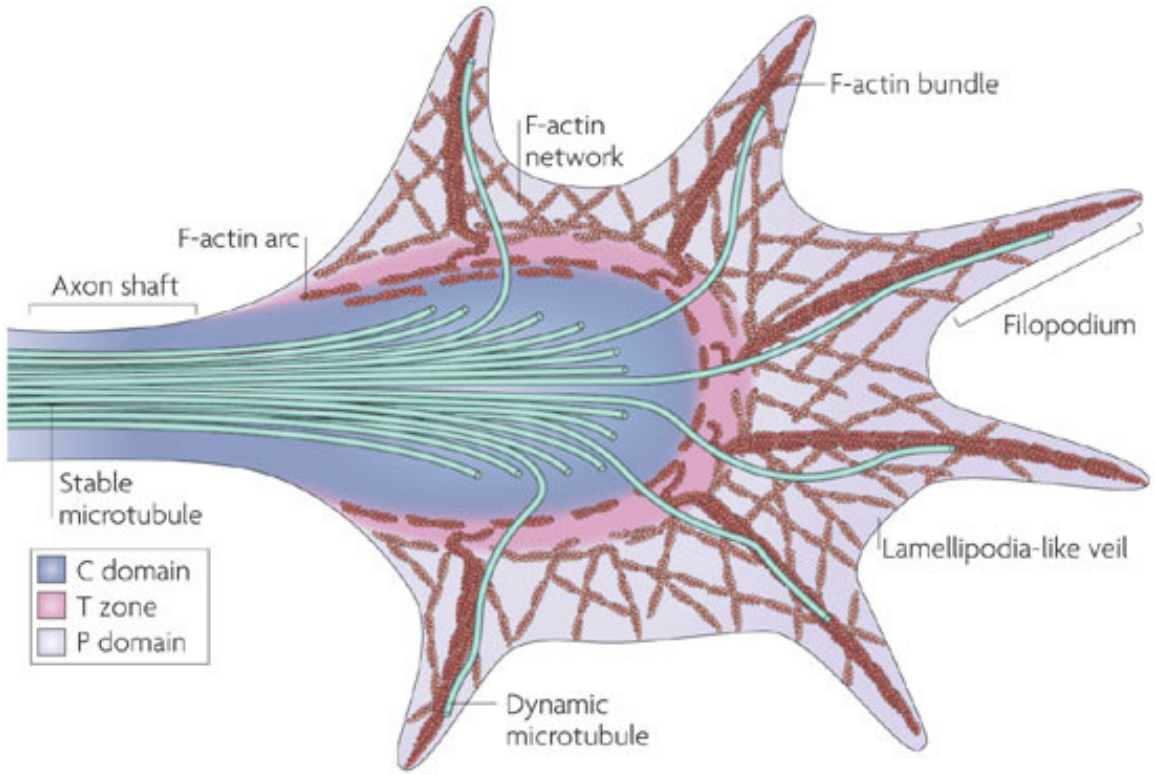

Image 6: the neuronal growth cone (from Lowery and Van Vactor, 2009)

During the stage 2 of differentiation, neurites are in a self-maintained equilibrium that is guaranteed by feedback loops generated by neurites themselves: each single neurite, in fact, releases negative feedback signals to hamper the growth of all the others. The equilibrium is broken when a positive feedback signal (the nature of which is sill partially unknown) is activated in one of the neurites. This single neurite will then be able to both exert a much stronger negative effects on the others' growth and start an auto-activation pathway that will transform it into the axon (Arimura and Kaibuchi, 2007).

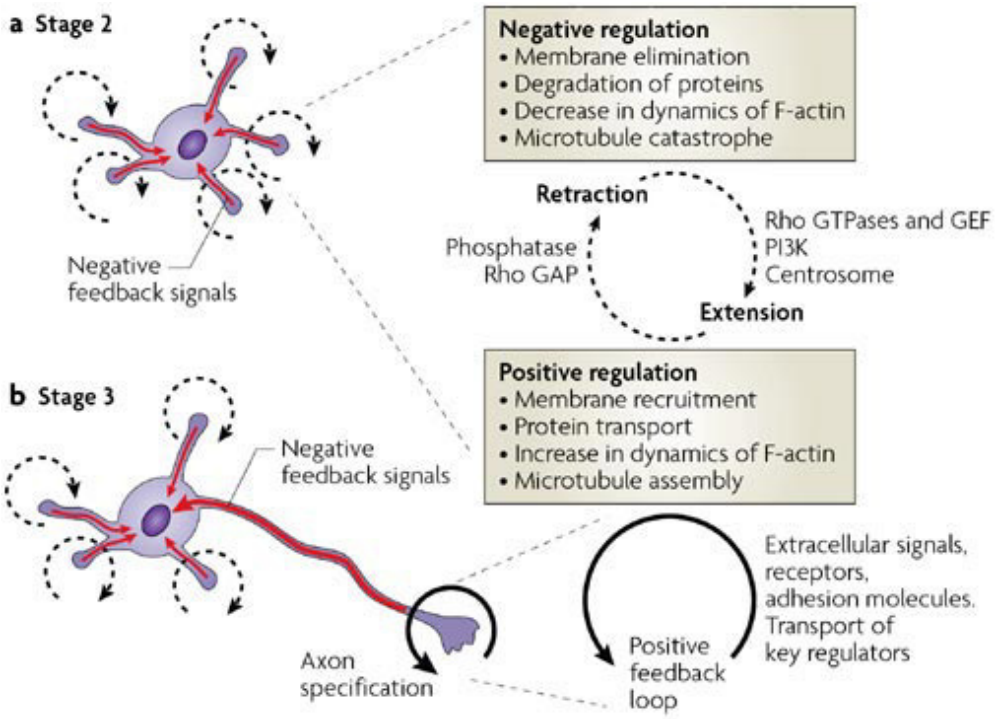

Image 7: Positive and negative feedback loop control neurites maturation (from Arimura and Kaibuchi, 2007)

2.2.3 Stages 3-4: axon and dendrites specification

The hallmark of a neuron that has reached stage 4 of differentiation is the presence of two easily distinguishable compartments which differ both molecularly and morphologically: the axon and the dendrites. Typically, the axon is much longer and thinner compared to the other extensions, and its calibre remains constant all through its length. On the other hand, dendrites are relatively shorter and their calibre decreases toward their end.

What are the molecular pathways whose asymmetric activation/ inactivation either in the axon or the dendrites are responsible for the disruption of the equilibrium between neurites typical of the stage 2 of differentiation? Researcher have found that, at the end of stage 2, the

neurite destined to be the axon start displaying some peculiar features, such as an increased actin network instability, or activation of the Phosphoinositide 3-kinase (PI3K) and apicobasal polarity pathways (Goodrich, 2008).

In cultured hippocampal neurons the polarity proteins Partitioning defective-3 and -6 (Par-3 an Par-6), for instance, are localized at the tip of the differentiating axon. Par-3 and -6 localization at this level is particularly important to couple the activation of the Rho GTPase Cdc42 to that of RAC1. Active Cdc42 is the responsible for the localization of the Par-3/6 complex to the axonal growth cone. Once localized there, Par-6 is able to directly interact with the T-cell lymphoma invasion and metastasis-inducing protein 1 (TIAM1) and the SIF and Tiam 1-like exchange factor (STEF), both of which are GEFs for RAC1. Thus, Par-3 functions as a scaffold to promote localized RAC1 activation at the axonal tip (Arimura and Kaibuchi, 2005).

Concerning the role of the PI3K pathway in axon specification, it is important to note that in stage 3 neurons the activity of this kinase is restricted to the axon, suggesting a role in axon specification and maintenance. At this level, PI3K is able to mediate the activation of the Akt kinase and its recruitment to the PM. Once activated, Akt inactivates the otherwise constitutively active glycogen synthase kinase 3 beta (GSK3β) by phosphorylating it. It's the decrease in GSK3β activity that ultimately promotes axon formation and elongation. Active GSK3β, in fact, interferes with microtubule polymerization, which is essential to support axonal growth. Therefore, by activating a Phosphorylation

cascade, PI3K activation results in axon elongation and maintenance (Yoshimura et al., 2006). In accordance with a specific role of this pathway in axonal formation only, Akt activation by the PI3K pathway in dendrites is prevented in by its degradation.

Unfortunately, not much else is known about the mechanisms involved in dendrite specification. What is known is that dendrites *in vivo*, not unlike axons, elongate by the extension of thin filopodia that, in some cases, are stabilized and then transformed in a dendrite.

It is not clear which signals could be involved in the stabilisation of certain filopodia rather than others. One possibility is that neurotransmitters occasionally released by the developing pre-synapse may bind to receptors on the surface of filopodia, and that only filopodia whose membrane receptors are bound to the neurotransmitter will be further stabilized. Another possibility is that filopodia may physically engage the pre-synapse through their adhesion receptors, which would then inhibit filopodia resorbtion (Heiman and Shaham, 2010). Moreover, some postsynaptic density (PSD) proteins, such as the postsynaptic density protein 95 (PSD-95) and the SH3 and multiple ankyrin repeat domains protein (Shank), have been proposed to exert a role in dendrite development (Vessey and Karra, 2007).

2.2.4 Stage 5: dendritic spines formation

Dendritic spines are specialized protrusions of the mature dendrite which act as the post-synaptic terminal for the majority of the glutamatergic inputs inside the central nervous system (CNS). Dendritic

spines seem to be a recent product of evolution, as they can be found only in those organisms capable of complex functions. *In vivo*, dendritic spines start to appear in the developing foetus only perinatally, and will subsequently maturate in response to the inputs provided by the animal experience. The generation and remodelling of spines is a finely tuned process that continues through life and is responsible for synaptic network organization (Yoshihara et al., 2009).

Morphologically, dendritic spines are protrusions arising from the dendrite and characterized by a narrow neck which supports a 'head' whose volume can range from 0.01 to 0.08 μm^3 (Sala et al., 2008).

It is widely known that filopodia localized to the dendritic shaft are the precursors of the dendritic spines. Dendritic filopodia are very abundant in the developing neurons, whereas in the adult CNS they can be found only in particular conditions, such as during tissue regeneration events. The half-life of a dendritic filopodium can range from a few minutes to a maximum of a few hours. During this time filopodia can transiently interact with excitatory axons. Only a few of such contacts, however, will be stabilized, as approximately 20-30% of dendritic filopodia will actually maturate into a dendritic spine (Yoshihara et al., 2009). The maturation of a filopodium into a dendritic spine is accompanied by the expression on its PM of adhesion molecules that stabilize the new contact, such as neuronal cadherin (N-cadherin) and α-catenin (Sala et al., 2008). Similarly to all the events that rely on actin remodelling, Rho GTPases are involved in spines maturation, with Cdc42 and RAC1 promoting it and RhoA inhibiting it.

On the basis of their morphology, dendritic spines can be divided into 3 categories:

- 'Thin': spines with a thin neck and a small head
- 'Mushroom': spines with a short neck and a large head
- 'Stubby': spines which do not appear to have a neck.

The thin, newly formed spines are generally more responsive to variations in synaptic activities, compared to the mature mushroom ones. The increase in the volume of the spine during maturation directly correlates with an increase in the accumulation of α-amino-3-hydroxy-5-methyl-4-isoxazolepropionic acid (AMPA) receptors on their membrane.

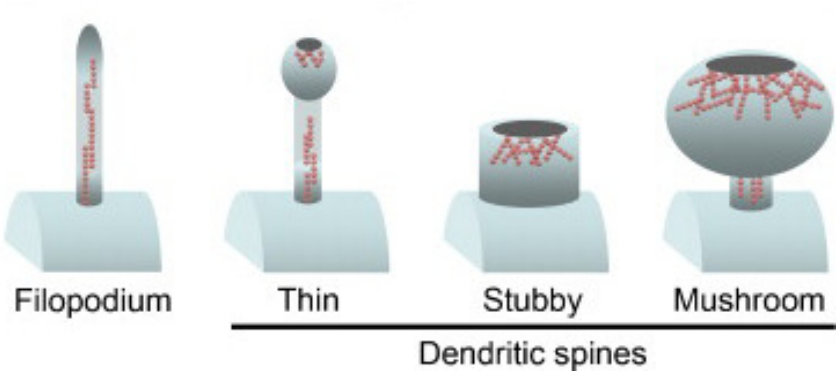

Image 8: Possible morphologies of a dendritic spine (Sekino et al., 2007)

The dendritic spine is particularly rich in F-actin. The actin cytoskeleton inside the spine is constantly remodelled according to the changes in spine morphology (Sekino et al., 2007). This is made possible by the regulated activity of many actin-binding proteins, such as Profillin II,

drebrin, N-cadherin, myosin II and VI and synaptopodin (Newey at al., 2005).

In dendritic spines the space right beneath the PM is occupied by the PSD, a proteinaceous scaffold that accommodates hundreds of proteins, including the AMPA, N-methyl-D-aspartate (NMDA) and metabotropic glutamate receptors, signalling proteins such as the Ca2+/calmodulin-dependent protein kinase II (CAMKII), or the proteins that compose the scaffold itself, such as PSD-95 and Shank. Such proteins localize to the PSD thanks their domains for protein-protein interaction, the most important of which is the post synaptic density protein/Drosophila disc large tumor (PDZ) domain (Sheng and Sala, 2001). The dendritic spine cytoplasm also contains mitochondria and portions of smooth endoplasmic reticulum.

The stabilization of the dendritic spine must be coupled with the maturation of the pre-synaptic compartment, which has to become competent to release the neurotransmitter. During the maturation of the axonal growth cone into the pre-synaptic compartment, vesicles containing key pre-synaptic proteins, such as Piccolo and Bassoon, are transported from the soma to the growth cone, where they fuse with the PM (Sala et al., 2008). Once the pre- and post- synaptic compartments come in contact with each other, their physical interaction is guaranteed by adhesion proteins (Serafini, 1997).

To conclude, it is important to note that once formed, synapses can still be remodelled bi-directionally throughout their existence. In cultured hyppocampal neurons, for instance, it is possible to induce changes in

the structure and morphology of the synapses by applying protocols of long term potentiation (LTP) or long term depression (LTD). Such protocols mimic the effects of animal experience on synapses in vivo (*Wang and Zhou*, 2010).

2.3 Mitochondrial architecture and cell polarity

Within the cell environment mitochondria are organized in an integrated ever-changing network that spans the cell at the micron scale. The overall shape of this network in terms of connectivity and distribution within the cytoplasm can vary from cell to cell and in response to environmental conditions (Rafelski et al., 2013).

As mitochondria are notoriously known as the 'powerhouse of the cell' for their capacity to sustain the bulk of ATP production via oxidative phosporylation (OXPHOS), it is evident how their distribution can directly affect the subcellular regions that have access to higher concentrations of mitochondrial-derived metabolic molecules. Therefore, mitochondria must integrate changes in their network morphology with various aspects of cell behaviour in order to ensure the proper functioning of specialized cells (Jayashankar and Rafelski, 2013).

The overall shape of the mitochondrial network, as well as its distribution within the cell, depends on two highly regulated activities: mitochondrial network remodelling and motility (Palmer et al., 2011; van der Bliek et al., 2013). The proper functioning of these two mechanisms is obviously particularly important in cells that are highly polarized, and

therefore the more polarized and energy demanding a cell is, the more sensitive it will be to defects in mitochondrial division and transport.

With their extremely complex and extended morphology, neurons are perhaps the most polarized of all cell types, and indeed there is extensive literature reporting various defects in neurons that are deficient in the regulation of mitochondrial dynamics (Detmer and Chan, 2007; Chen and Chan, 2009). Ishihara and colleagues, for example, reported how a neuronal cell-specific knockout of dynamin-related protein 1 (Drp1), the main protein involved in mitochondrial fission (see 2.3.1.2.), in the mouse results in a decrease in neurites and defective synapse formation (Ishihara et al., 2009). Moreover, neurons that lack either Drp1 (Verstreken et al., 2005) or the proteins involved in mitochondrial transport Milton (Stower et al., 2002) and Mitochondrial Rho GTPase 1 (Miro) (Guo et al., 2005) show defects in mitochondrial transport that result in a deficiency of mitochondria at axon terminals and a reduced capacity for synaptic transmission.

Another classical example of the importance of mitochondrial architecture in cell polarity is the proper positioning of mitochondria in contracting muscle cells, where most of the mitochondria are tightly aligned with the myofibrils to provide high ATP concentrations very close to the site that needs them most during contraction (Romanello and Sandri, 2013).

Similarly to this, mitochondria must be localized to the immune synapse in T-cells in order to ensure efficient signalling there (Quintana et al., 2007).

The papers mentioned report just a few of the recent discoveries underscoring the importance of mitochondrial dynamics in the generation of cellular architecture and its maintenance. Therefore the importance of proper functioning of the proteins involved in mitochondrial dynamics cannot be forgotten in the context of cell polarity.

2.3.1 Mitochondrial remodelling through fusion and fission

The overall mitochondrial network morphology can be considered a continuous flux between two extreme states: a reticular network of fused mitochondria and a fragmented state. The balance between these two situations is controlled by proteins involved in fission and fusion events.

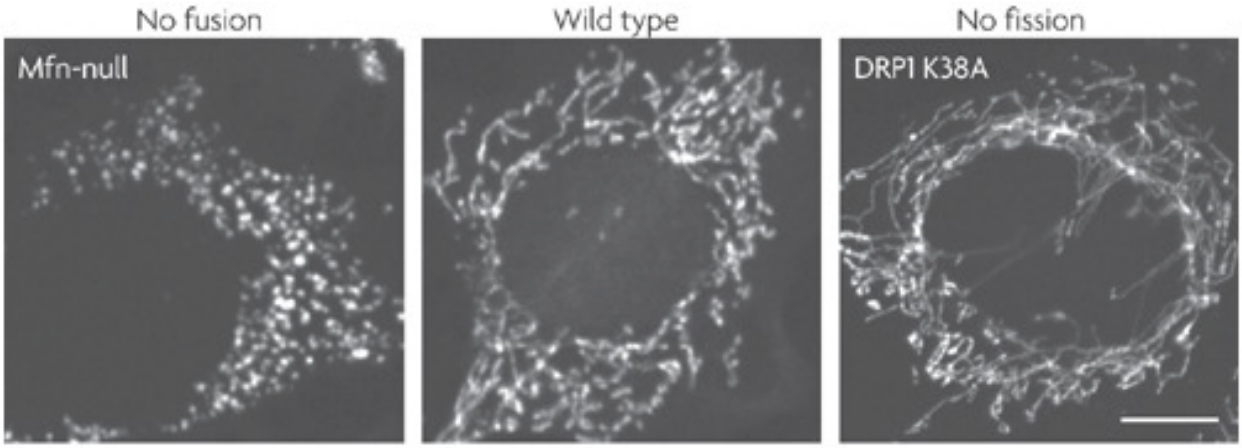

Image 9: fusion and fission events regulate mitochondrial morphology (Detmer and Chan, 2007)

Beside ensuring integration of the mitochondrial network with the overall cell architecture, mitochondrial fusion and fission proteins are also pivotal for guaranteeing the optimal functionality of the organelle

itself. When two mitochondria fuse together, the mixing of their contents enables protein complementation, mitochondrial DNA (mtDNA) repair and equal distribution of metabolites. The importance of such event is underlined by the fact that cells in which fusion is blocked in favour of unopposed mitochondrial fission display a heterogeneous population of organelles with non-uniform mtDNA distribution, decreased capacity to generate ATP, increased generation of reactive oxygen species (ROS) and higher susceptibility of cells to undergo apoptosis (Parone et al., 2008).

On the other hand, fission is particularly important to guarantee equal segregation of mitochondria during cell division, and to favour their motility and distribution along cytoskeletal tracks. In addition, fission is indispensable to get rid of unfunctional segments of mitochondria through mitophagy (Twig et al., 2008). When a segment of mitochondrion defective in the capacity to maintain the inner membrane potential is severed from the network by membrane fission, the segments itself becomes a target of the E3 ubiquitin ligase parkin, which ubiquitylates several mitochondrial outer membrane proteins including Mitofusin 1 (MFN1) and Mitofusin 2 (MFN2), the GTPases involved in mitochondrial fusion. As such, the isolated mitochondrion cannot enter the network anymore, and is eventually removed by mitophagy (Galluzzi et al., 2012).

2.3.1.1 Proteins involved in mitochondrial fusion

The coordinated fusion of inner and outer mitochondrial membranes is ensured by three proteins with a GTPase activity: the outer mitochondrial membrane (OMM) GTPases MFN1 and MFN2 and the inner mitochondrial membrane (IMM) GTPase Optic atrophy 1 (OPA1). The overall importance of mitochondrial fusion proteins has been highlighted by the generation of knock out (KO) mice lacking either MFN1, MFN2 or OPA1, all of which fail to survive past mid-gestation (Chen et al., 2003; Davies et al., 2007).

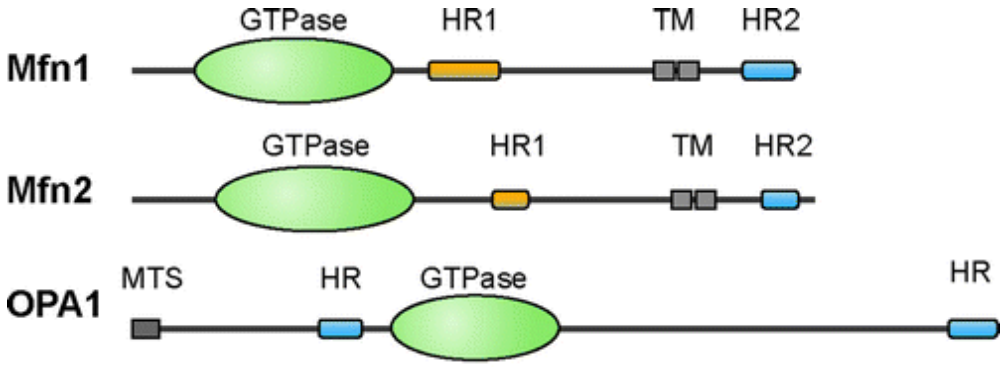

Image 10: struture of the protiens involved in mitochondrial fusion (from Chan at al., 2006)

The two OMM GTPases MFN1 and MFN2 display a very high degree of homology between each other, and present a similar domain structure, composed of a N-terminal GTPase domain, two hydrophobic heptads repeats (HRs) and two transmembrane domains. The two transmembrane domains anchor the proteins to the OMM, with both the N-terminal and C-terminal regions of the proteins protruding into the cytosol (Rojo et al., 2002). MFNs form complexes in *trans* between

adjacent mitochondria through the formation of an anti-parallel coiled coil between the heptad repeats of juxtaposing proteins (Koshiba et al., 2004). These results suggest a model in which GTPases from opposing membranes dimerize and then pull the membranes together with a SNARE-like mechanism not dissimilar to that described for synaptic vesicles fusion.

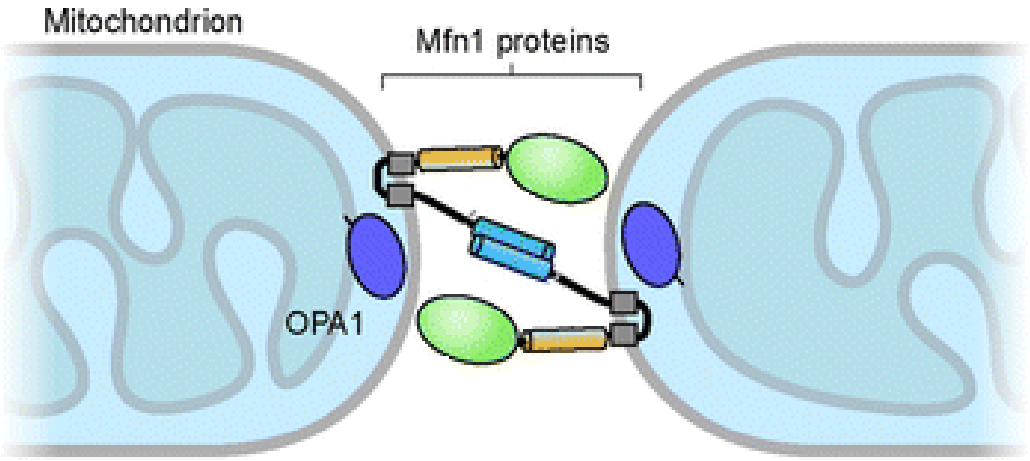

Image 11: fusion of the OMM (adapted from Chan, 2006)

Much less is known about the mechanism by which IMM fusion is achieved. In accordance with its role in IMM, localization studies have confirmed that OPA1 is anchored to the IMM, with the bulk of the protein facing the IMM space (Wong et al., 2000). It is widely known that ionophores that dissipate the mitochondrial membrane potential inhibit mitochondrial fusion, leading to extensive mitochondrial fission (Legros et al., 2002). Even though the link between mitochondrial membrane potential maintenance and mitochondrial fusion is not yet completely understood, Ishiara and colleagues reported that dissipation of the

mitochondrial membrane potential leads to the proteolitic cleavage of OPA1 to a fusion-incompetent short isoform (Ishihara et al., 2006).
Another protein more recently involved in mitochondrial fusion is the Mitochondrial phospholipase D (mitoPLD), a dimeric enzyme bound to the OMM through a C-terminal transmembrane anchor, with its N-terminal catalytic domain facing the cytosol. The enzymatic domain of mitoPLD has a lipid-modifying activity that has been proposed to modify OMM lipids following MFN-mediated mitochondrial tethering. (Choi et al. 2006).

2.3.1.2 Proteins involved in mitochondrial fission

Mitochondrial fission in mammals is mediated by Drp1, a cytosolic protein with an N-terminal GTPase domain thought to provide mechanical force, a dynamin-like middle domain, and a GTPase effector domain (GED) located in the C-terminal region. Drp1 exists as dimers and/or tetramers in the cytoplasm; upon mitochondrial fission, Drp1 assembles into larger oligomers at mitochondrial fission sites, wraps around the mitochondrion and finally severs mitochondrial membranes with a mechanism that depends on GTP hydrolysis (Otera et al., 2013). Approximately 3% of total Drp1 is localized to mitochondria as foci, but only 5% of these foci are involved in fission events each hour (Smirnova et al., 2001).

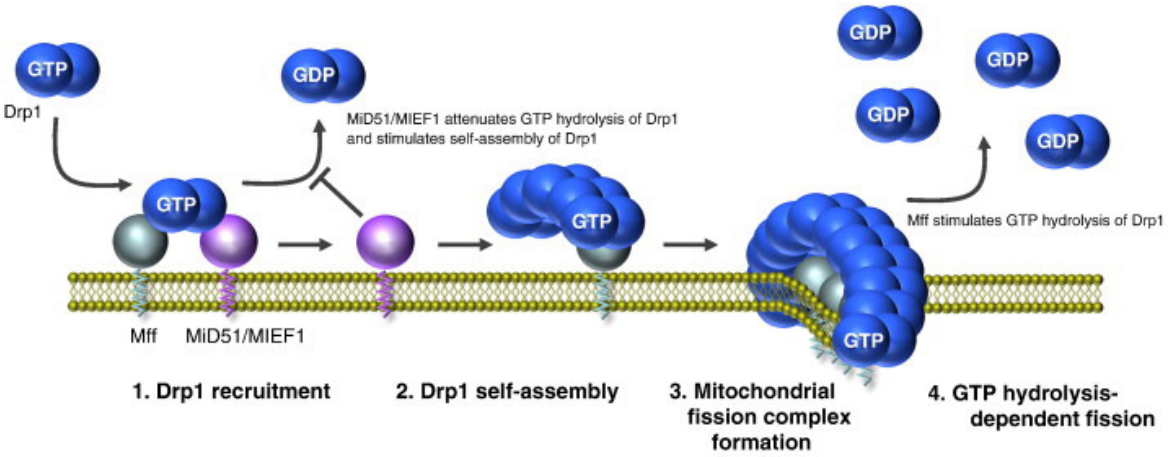

Image 12: Drp1-mediated mitochondrial fission (from Otera et al, 2013)

Similarly to KOs for the fusion GTPases (se paragraph 2.3.1.1), mice lacking Drp1 display developmental abnormalities, which are particularly severe at the level of the forebrain, and die around embryonic day 12.5 (Ishihara et al., 2009).

Depletion of Drp1, as well as inhibition of its activity, results in an extensive elongation and perinuclear clustering of the mitochondrial network in all cell types (Palmer et al., 2011; Loson et al., 2013; van der Bliek et al., 2013). On the other hand, overexpression of Drp1 doesn't have any effect on mitochondrial fission rates. Such results suggest that the regulation of Drp1 properties, such as mitochondrial translocation, post-translational modification, or GTPase activity may be a critical step for the control of fission activity. Indeed, Drp1 phosphorylation has huge effects on its activity, with phosphorylation of Serine (Ser) 616 exerting a pro-fission effect, whereas phosphorylation of Ser373 is inhibitory (Otera et al., 2013).

Despite its high homology with dynamin (DYN), Drp1 lacks the pleckstrin-homology (PH) domain that promotes membrane binding in DYN. Therefore, Drp1 requires membrane receptors for its recruitment to the OMM. The 3- to 4 nm gap between Drp1 and liposome tubes calculated by 3D reconstruction could easily accommodate Drp1 membrane receptor or other cofactors necessary for membrane fission.

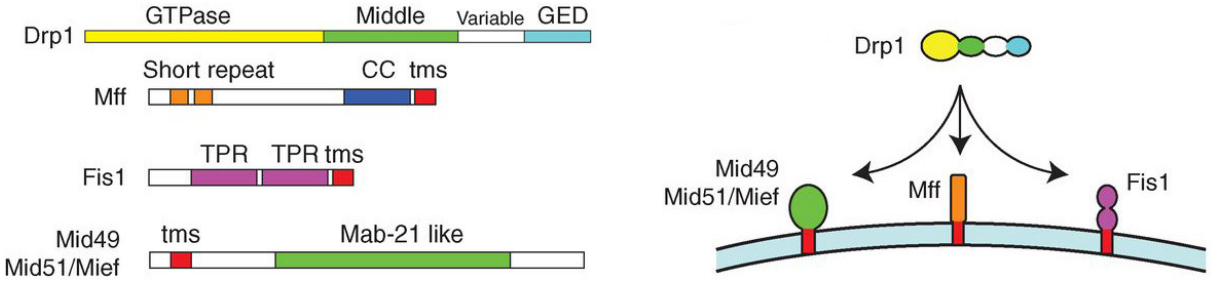

Image 13: Schematice representation of Drp1 and its putative receptors (adapted from van der Bliek et al., 2013)

In yeast cells, Drp1 recruitment to the OMM has been demonstrated to depend on mitochondrial fission protein 1 (Fis1), an integral protein of the OMM (Okamoto et al., 2005). In mammalian cells, however, downregulation of Fis1 decreases mitochondrial fission but has little effect on Drp1 recruitment to the OMM, suggesting that other proteins may be involved in the localization of Drp1 to mitochondria (Lee et al., 2004). Several other OMM proteins have in fact been proposed to support mitochondrial fission by promoting Drp1 localization to the OMM. These proteins are the mitochondrial fission factor (Mff) and the mitochondrial dynamics proteins of 49 and 51 kDa (MiD49 and MiD51, respectively). Knockdown of Mff causes both mitochondrial elongation

and a decrease in the number and intensity of Drp1 foci on mitochondria, thus demonstrating its importance for Drp1 translocation to the OMM (Gandre-Babbe et al., 2008; Loson et al., 2013). Contradictory data are present in literature about a possible role of MiD51 and MiD49 in either mitochondrial fusion or fission (Zhao et al., 2011a). However, Loson and colleagues recently provided evidence that MiD49 or MiD51 can mediate Drp1 recruitment and mitochondrial fission in the absence of Fis1 and Mff (Loson et al., 2013).

A few other proteins have been proposed to participate in Drp1-mediated fission. Tondera and colleagues demonstrated that downregulation of the Mitochondrial protein of 18 kDa (MTP18) resulted in the appearance of highly fused mitochondria, while its overexpression caused excessive mitochondrial fission (Tondera et al., 2005). The topology of this protein is still unknown, but the protein contains three putative transmembrane domains and is not exposed to the cytosol.
Another protein proposed to be involved in mammalian mitochondrial fission is Endophilin B1 (also called Bif-1 and SH3GLB1), a Bin–Amphiphysin–Rvs (BAR) domain-containing protein that, similarly to the mitoPLD enzyme involved in mitochondrial fusion, possesses a lipid-modifying enzymatic domain. Endophilin B1 is a cytosolic protein that is able to deform lipid bilayers into tubules in vitro (Farsad et al. 2001). Additionally, Endophilin B1 interacts with the pro-apoptotic Bcl-2-associated X protein (Bax) during apoptosis, and has been proposed to

participate in apoptosis-induced fission (Karbowski et al., 2004; Takahashi et al. 2005).

Early data supporting the importance of Drp1 function in membrane fission suggested that this protein may be sufficient to both initiate membrane bending and subsequently sever the OMM and IMM. Such model was challenged by the observation that in yeast cells defective for Dnm1 (the yeast ortholog of Drp1) transient constrictions were found along mitochondrial tubules, suggesting the existence of an initial Drp1-indepenent membrane-bending step (Legesse-Miller et al. 2003). Moreover, the diameter of the Drp1 ring was calculated by structural analyses to be 30–50 nm, and therefore smaller than the diameter of the mitochondrion, thus strengthening the hypothesis that some other pre-constriction factors may be needed before Drp1 can assemble around mitochondria (Smirnova et al., 2001; Ingerman et al., 2005).

Recent findings from Korobova and colleagues suggested the possibility that actin polymerization mediated by Inverted formin-2 (INF2), a formin associated to the endoplasmic reticulum (ER), might provide the pushing force that constricts mitochondria to a diameter consistent with that of the Drp1 ring (Korobova et al., 2013). INF2 localization to the ER rather than the mitochondrial membrane also provides a possible explanation for the fact that mitochondrial fission has been shown to occur at sites in which mitochondria contact the ER.

The same group that reported the role of INF2 in membrane fission has provided further evidence of a role of actin polymerization in membrane

fission with a recent paper in which they demonstrated how myosin II-mediated constriction of actin filaments provide further mechanical force for membrane constriction. Moreover, myosin II inhibition decreased Drp1 association with mitochondria, in agreement with the model that Drp1 association with mitochondria can happen only in regions where the organelle has been already squeezed (Korobova et al., 2014; Pon et al., 2014).

This model is somewhat similar to the ones proposed for leading-edge extension or the initial steps of endocytosis, where actin polymerization provides the mechanical force necessary to bend the PM.

2.3.2 The interplay between mitochondrial dynamics and organelle motility

Mitochondrial movement along cytoskeletal tracks is of fundamental importance for many aspects of cell physiology. The relative abundance of mitochondria localized to a specific area of the cytoplasm can directly affect the amount of energy that a given subcellular region will have access to. In neurons mitochondrial movement into the axon is of primary importance, as pre-synaptic terminals cannot depend for their ATP supply on the soma, which can be up to hundreds of millimetres away.

Mitochondrial movement must be coordinated in space and time with changes in the shape of the mitochondrial network, in order to generate organelles small enough to be transported. Defects in both fusion and fission have been reported to impair mitochondrial transport: while it is

easy to understand why tangled and fused mitochondria are impossible to be moved across the cytosol, cells whose mitochondrial network has undergone excessive fission have also been reported to display defects in mitochondrial movement, possibly because the number of mitochondria exceeds that of the adaptor proteins linking them to the cytoskeleton. Moreover, dot-like mitochondria are more prone to swelling, a condition that would make their transport difficult (Otera et al., 2013).

As well as defects in fusion and fission impair mitochondrial motility, it is also true that mitochondrial transport rates and directionality affect mitochondrial morphology. It has been proposed that during fission motor proteins directed to the opposing sides of a microtubule might bind to the two ends of the same mitochondrion, thus providing further force to split the long mitochondrion in two smaller ones (Bowes et al., 2008).

A similar concept can be applied to mitochondrial fusion: Liu and colleagues demonstrated that fusion events occur between mitochondria that move toward each other along cytoskeletal tracks. If the two merging organelles move toward each other along the same microtubule, a complete fusion event will occur, whereas mitochondria interacting laterally with each other while associated to separate microtubules will engage in a transient fusion, similar to the 'kiss-and-run' fusion described for synaptic vesicles (Liu et al., 2009).

In neuronal cells, mitochondrial transport to axon and dendrites is mediated by the two adaptor proteins Trafficking kinesin-binding protein

1 (TRAK1) and TRAK2. Mitochondria in which TRAK1 works as a scaffold between the mitochondria-anchored protein Miro and kinesin-1/ Kinesin heavy chain isoform 5 (KIF5) will be targeted to the axon, whereas mitochondria bound by TRAK2 will be transported inside dendrites by dynein motors. TRAKs are fundamental for neuronal differentiation, as knockdown of TRAK1 decreases axon length, the number of axonal tips, and the number of axonal branches by 50%, whereas knockdown of TRAK2 decreases total dendritic length and number of primary dendrites by 50% (van Spronsen et al., 2013).

2.3.3 Mitochondrial dynamics and diseases

Health disorders in which mitochondrial dysfunction is unequivocally central to the pathogenesis of the disease are classified as mitochondrial diseases. Mitochondrial diseases can affect any organ, manifest at any age, and can be inherited from an autosome, the X chromosome, or maternally.

Mutations in 228 nuclear and 13 mitochondrial genes have already been associated with the onset of mitochondrial diseases, but only the most recent papers are highlighting how defects of mitochondrial structure can be by themselves causatives of mitochondrial diseases (Archer., 2013).

For instance, the mitochondrial disorders Charcot-Marie-Tooth type 2A disease (CMT2A) and the autosomal dominant optic atrophy (DOA) have both been associated to mutations in genes encoding for pro-fusion proteins.

The Charcot-Marie-Tooth disease (CMT) is one of the most common hereditary neuropathies, and mutations in more than 30 genes have been found to cause it. The CMT2A subtype of the disease is caused by genetic defects that primarily impair metabolic functions of neurons rather than Schwann cells. More than 40 mutations in either the coiled-coil or the GTPase domain of MFN2 have been associated with CMT2A (Zuchner et al., 2004), further corroborating the role of mitochondrial dynamics and organelle motility for neuronal preservation.

DOA is a form of inherited neuropathy affecting the optic nerve, characterized by the progressive loss of visual acuity that often leads to blindness by the second decade of life. Even though inheritance of the disease is associated with several genetic loci, the gene encoding for OPA1 has been found to be the most commonly affected in patients (Alexander et al. 2000, Delettre et al. 2000). The unopposed fission resulting from the loss of OPA1 function has been liked to an increased predisposition of retinal ganglion cells to apoptosis and subsequent degeneration of the optic nerve.

Although no hereditary mitochondrial disorders have been linked to mutations in pro-fission genes, the utmost importance of Drp1-mediated fission for human development was highlighted by the identification of a dominant negative mutation in Drp1 gene in a baby girl who died at 37 days of age, and presented hypotonia, microcephaly, and optic atrophy upon admission to the hospital. Fibroblasts derived from the patient displayed elongated and tangled mitochondria, thus confirming that the

identified mutation had a dominant negative effect on Drp1 function (Waterham et al., 2007).

In addition to pathologies directly linked with genetic alterations in mitochondrial fusion and fission proteins, more and more data are supporting the notions that secondary disorders in mitochondrial dynamics may contribute to the progression of complex diseases, such as cancer, cardiovascular and neurodegenerative diseases. In most of those pathologies an increase of mitochondrial fission, coupled with an increased risk of diseased cells to undergo apoptosis, has been reported. In neurons of patients affected by Huntington's disease, for instance, mutant Huntingtin (Htt) is able to increase Drp1 GTPase activity, leading to the inhibition of mitochondrial transport within the axon and cell death (Song et al., 2011).
In Alzheimer's disease, the increase in Nitric Oxide (NO) production triggered by the beta-amiloid favours activation of Drp1 by S-nitrosylation, leading to synaptic loss and neuronal damage (Cho et al., 2009).
The discovery of the role of disordered mitochondrial dynamics in the pathogenesis of a variety of human diseases, such as the ones briefly described above, will hopefully lead to the identification of drugs able to restore mitochondrial network morphology and thus ameliorate the prognoses of multiple, complex pathologies.

2.4 IRSp53 and LIN7

2.4.1 IRSp53

As its name promptly suggests, IRSp53 (also called brain-specific angiogenesis inhibitor 1-associated protein 2, BAIAP2) was initially identified as a substrate of the insulin receptor kinase that was phosphorylated in response to stimulation with either insulin or insulin-like growth factor 1 (IGF-1) (Yeh et al., 1996).

The mRNA encoding for IRSp53 can undergo different splicing events, which give rise to up to 4 different isoforms. These 4 splicing variants, named IRSp53 –L, -M, -S and –T, have a common N-terminal portion (amino acids 1-511) and a different C-terminal sequence which, depending on the specific isoform, can be from 9 to 41 amino acids long (Miyahara et al., 2003; Scita et al., 2008).

IRSp53 is the founder of a protein family characterized by the presence of a IRSp53 and missing in metastasis domain (IMD), also called the I-BAR domain (Lee et al., 2002), which can bind to both membranes and actin.

Indeed, IRSp53 binds to negatively charged lipids in vitro, such as Phosphatidylinositol 4,5-bisphosphate (PtdIns(4,5)P_2) or Phosphatidylserine (PS) (Futò et al., 2013) , and is able to induce a specific membrane curvature (Yamagishi et al., 2004; Mattila et al., 2007; Millard et al., 2005; Suetsugu et al., 2006; Krugmann et al., 2001). While proteins containing a BAR domain are involved in the formation of positive membrane curvature, such as during endocytosis, proteins

containing an I-BAR domain induce a negative curvature of the PM (Zhao et al., 2011b), thus promoting the formation of membrane protrusions.

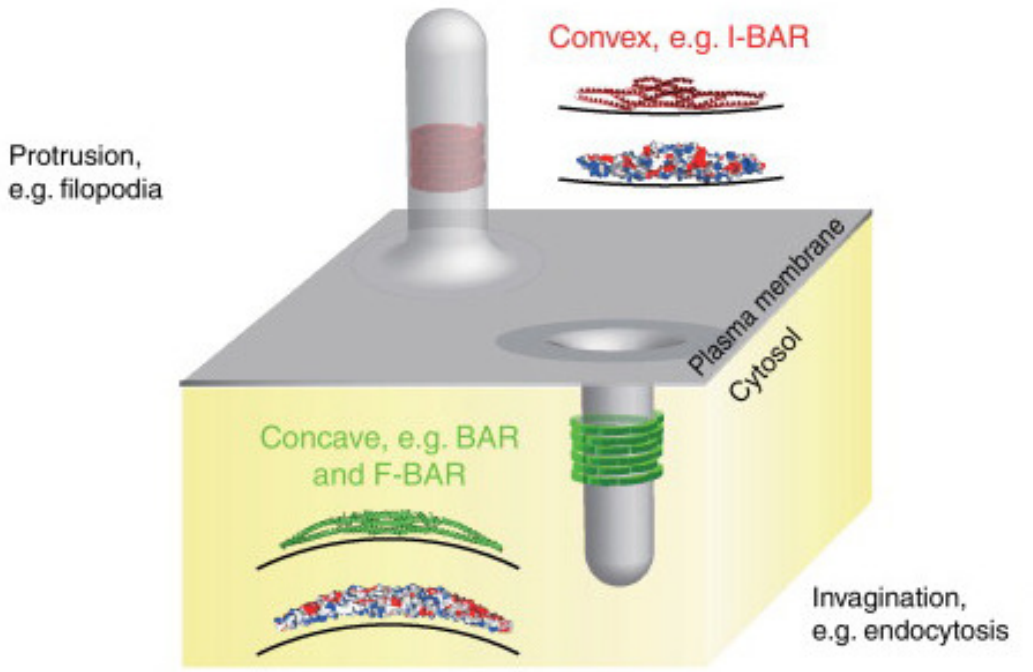

Image 14: membrane curvatures generated by the BAR and I-BAR domains (Suetsugu and Gautreau 2012)

The overexpression of the I-BAR domain of IRSp53 alone is able to promote the formation of membrane protrusions that, unlike proper filopodia, display an erratic behaviour and are poor in F–actin (Yang et al., 2010).

In addition to the IMD domain, IRSp53 also contains a SRC homology 3 (SH3) domain for the interaction with various actin regulators and a Cdc42/Rac interactive binding (CRIB) domain for Cdc42 binding (Scita et al., 2008).

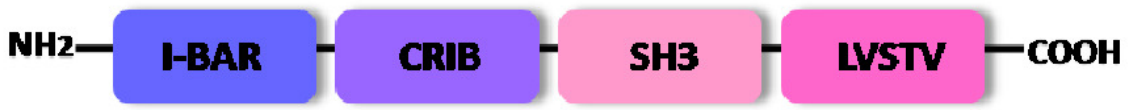

Image 15: schematic structure of IRSp53

The actin regulators whose proline-rich motifs have been demonstrated to bind to the SH3 domain of IRSp53 include: Wave 1 and 2 (Miki et al., 2000), mammalian enabled (Mena) (Krugmann et al., 2001), neuronal Wiskott- Aldrich syndrome protein (N-WASP) (Lim et al., 2008), epidermal growth factor receptor pathway substrate 8 (Eps8) (Funato et al., 2004; Disanza et al., 2006), the mammalian Diaphanous (mDia) isoforms mDia1 and mDia2 (Fujiwara et al., 2000; Goh et al., 2012), and Dynamin (Chou et al., 2014).

All the interactors of IRSp53's SH3 domain have a known role in sustaining the formation of filopodia and/or lamellipodia: the interaction between IRSp53 and Eps8, for instance, promotes filopodia formation by mediating the generation of F-actin bundles (Disanza et al., 2006). Similarly, the formation of a heterotrimeric complex between Rac1, IRSp5 and WAVE 2 is a fundamental step during lamellipodia formation (Miki et al., 2000).

Thus, the coexistence of both the IMD and SH3 domains within a single protein renders IRSp53 able to couple the capacity to deform the PM to the control of actin polymerization.

Given its pivotal role in the formation of membrane protrusions, IRSp53 activity must be tightly controlled. Such control is, not surprisingly,

guaranteed by the Rho GTPases Rac1 and Cdc42, both of which play fundamental roles in the regulation of lamellipodia and filopodia, respectively. The interaction with Cdc42 occurs through IRSp53 CRIB domain, whereas Rac1 binds the IMD (Scita et al., 2008).

When not bound to a Rho GTPase, IRSp53 is present in the cytosol in a closed, self-inhibited conformation (Krugmann et al., 2001), in which the CRIB domain binds to the SH3 domain, thus preventing the latter from binding its effectors (Kast et al., 2014).

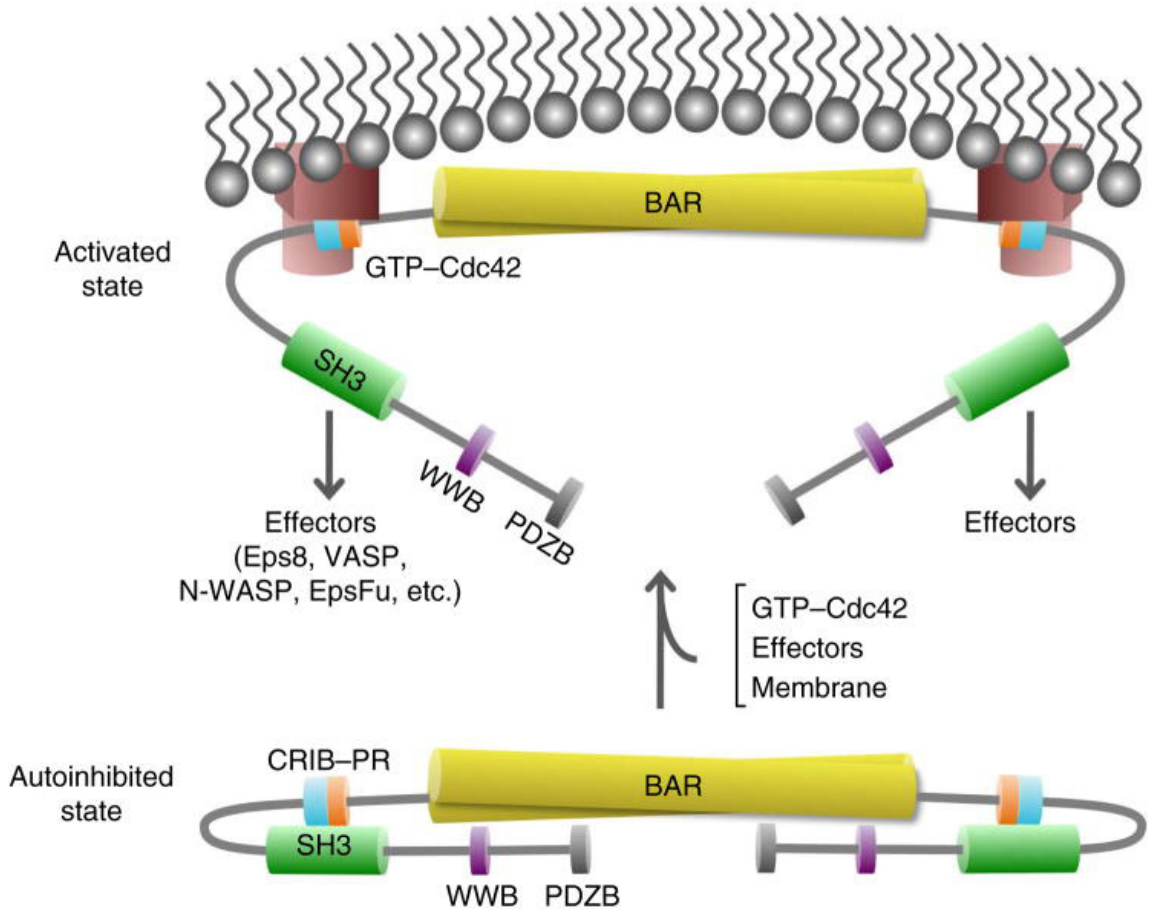

Image 16: IRSp53 auto-inhibited and activated states (from Kast et al., 2014)

It is important to note that IRSp53 activity can be inhibited also by phosphorylation at the level of two threonine residues located in between the CRIB and SH3 domains: such phoshorylated residues favours the interaction of IRSp53 with the 14-3-3 protein, whose binging masks the SH3 domain (Robens et al., 2009).

The extreme C-termini of IRSp53-S terminates with the amino acidic sequence LVSTV, termed the PDZ-binding motif, which allows this isoform to bind to PDZ domain-containing proteins.

The presence of the PDZ-binding motif allows IRSp53 to interact with the PSD core protein PSD-95, thus promoting its localization into dendritic spines (Choi et al., 2005; Soltau et al., 2004). At the level of the PSD, IRSp53 also interacts with Shank1, a protein of fundamental importance for spine maturation (Soltau et al., 2004). In accordance with its localization to the PSD, IRSp53 is highly expressed in various brain areas starting from right after birth (Sawallisch et al., 2009), and its activity has been associated with dendritic spine formation (Kim et al., 2009; Sawallisch et al., 2009).

Another PDZ containing protein which has been demonstrated to interact with IRSp53 is lineage defective 7 (LIN7; also called Mammalian lin-seven protein, Mals or Vertebrate lin-7 homolog, VELI) (Hori et al., 2003).

2.4.2 LIN7

The small scaffolding protein LIN7 was originally identified in C. elegans as a component of a heterotrimeric complex that included the other two

proteins lineage defective 2 (LIN2) and lineage defective 10 (LIN10). Such complex is of fundamental importance to mediate the recruitment of the tyrosin-kinase receptor lethal protein 23 (Let-23) to basolateral junctions in C. elegans vulval precursor cells (Smiske et al., 1996; Kaech et al., 1998). The LIN complex is also found in the more complex organisms, where it plays a role in the formation of PM junctional domains.

LIN7 is the smallest component of the complex, as it contains only one LIN2 and LIN7 domain (L27) domain and one PDZ domain. Such domains are present in all three constituents of the complex, and they enable them to work as scaffolds to organize large protein assemblies. The L27 domain, in fact, is a protein-protein interaction module that is able to hetero-dimerize, or even hetero-tertamerize, with other L27 domains located on protein partners (Li et al., 2004).

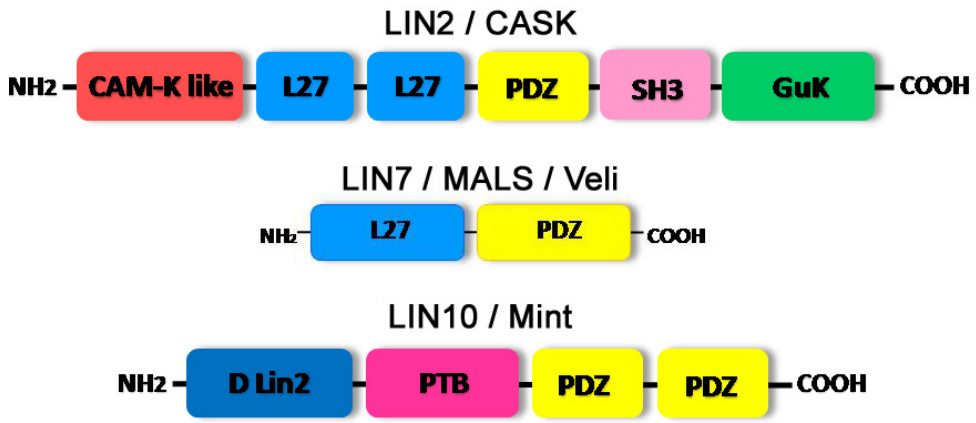

Image 17: Schematic structure of the LIN proteins

The PDZ domain, although different in structure from the L27 domain, plays a similar scaffolding role. PDZ domains recognize specific binding

motifs usually localized in the C-terminal tail of their target proteins. Depending on the target motif recognized, PDZ domains can be divided into 3 different classes (Songyang et al., 1997; Schultz et al., 1998):

PDZ domain	PDZ containing proteins (eg.)	Target proteins (eg.)	PDZ-bindig motif
Class I: -S/T-X-Φ	PSD95 Homer LIN7	NMDAr mGLUR β-catenin BGT-1	-E-**S**-D-**V** -S-**S**-S-**L** -D-**T**-D-**L** -K-**T**-H-**L**
Class II Φ-X-Φ	GRIP LIN2/CASK	AMPAr Syndecan Neurexin	-S-V-K-I -Y/F-X-Φ -E-Y-Y-V
Class III -E-D-X-W-C/S	LIN10/Mint	N-type Ca++ channel	-D-H-W-C

X = any amino acid; Φ = hydrophobic amino acid

PDZ-binding motifs are often found on protein channels and on transmembrane receptors (Kornau et al., 1995; Niethammer et al., 1996). Therefore, even though PDZ domain-containing proteins usually do not have a transmembrane domain themselves, they are often localized to specific regions beneath the PM by virtue of their interaction with transmembrane domain-containing proteins.

LIN7 exists in both non-vertebrate and vertebrate organisms in 3 isoforms, named –A, -B and –C (or -1, -2 and -3), which weight 26, 23 and 22 kDa, respectively. LIN7A and B are primarily expressed in the brain, where they are ubiquitously expressed, and can be detected in rat

tissues such as kidney, liver, thymus and heart already at E13 (Jo et al., 1999).

With its PDZ domain, LIN7 interacts with various proteins, such as the epithelial gamma-Aminobutyric acid (GABA) receptor beataine-GABA transporter 1 (BGT1) (Perego et al., 2000) or β-catenin (Perego et al., 1999; Perego et al., 2002). LIN7 interaction with β-catenin ensures its recruitment from the cytosol to those cell junctions that are rich in β-catenin. At the level of the cell junctions, LIN7 functions to maintain and stabilize proteins that are important for epithelial cell physiology (Straight et al., 2006), such as the aforementioned BGT1 (Perego et al., 2000).

It is important to note that, with its L27 domain, LIN7 also binds to LIN2 (called calcium/calmodulin-dependent serine protein kinase, CASK, in mammals) and together they localize to adherens junctions (AJs). CASK also binds to LIN10, thus working as the scaffold that holds together the LIN complex. The LIN complex is of fundamental importance at the level of the pre-synaptic terminal, where CASK mediates the binding of the LIN complex to neurexin, an adhesion molecule that ensures to juxtaposition between the pre- and post-synaptic terminals by interacting with post-synaptic neuroligin (Hata et al., 1996; Hsueh et al., 1998; Olsen et al., 2005; Olsen et al., 2006). The importance of LIN7 localization to the pre-synaptic terminal is underlined by the fact that KO mice for all three LIN7 isoforms die shortly after birth due to laboured breathing, a phenotype consistent with an impairment in synaptic transmission (Olsen et al., 2005).

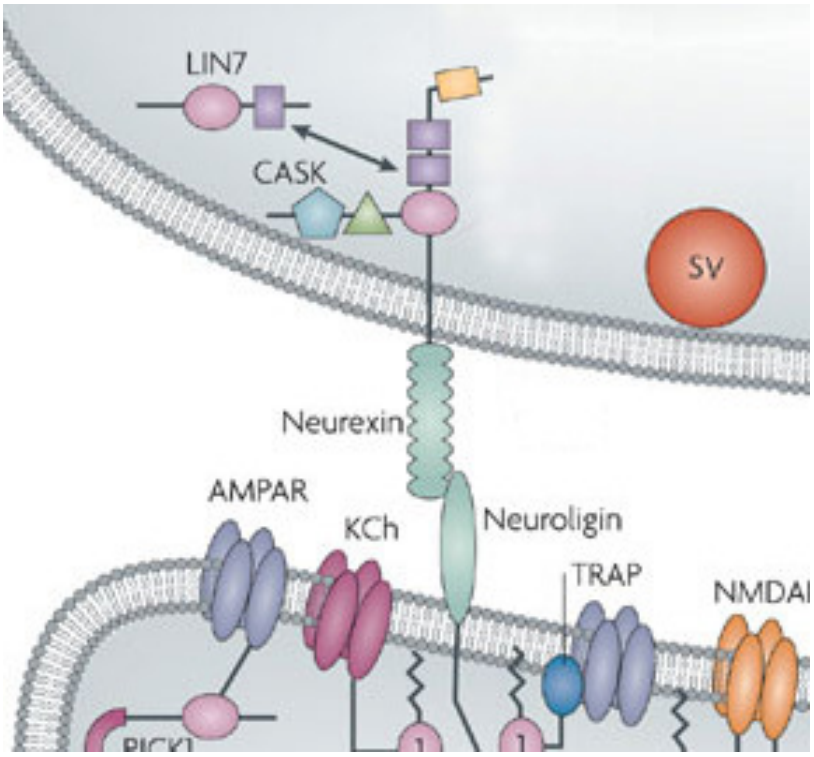

Image 18: LIN7-CASK interaction at the pre-synapse (Neff et al., 2009)

At the post-synaptic level, the LIN complex has been proposed to be involved in the trafficking of the 2B subunit of the NMDA receptor by virtue of the affinity of LIN10 to the transport motor Kinesin-like protein (Kif17) (Rogelj et al., 2006; Setou et al., 2000).

With its PDZ domain, LIN7 binds to IRSp53 (Hori et al., 2003) and participates in filopodia formation (Crespi et al., 2012, and chapter) and in IRSp53 recruitment to tight junctions (TJs) (Massari et al., 2009).

2.4.3 The interaction between IRSp53 and LIN7

The interaction between the PDZ-binding motif of IRSp53-S and the PDZ domain of LIN7 was first demonstrated by Hori and colleagues, by means of two-hybrid screenings and immunoprecipitation (IP) experiments in

Madin-Darby canine kidney (MDCK) cells (Hori et al., 2003). In the same cells, our group further confirmed the physiological relevance of the IRSp53 : LIN7 interaction by demonstrating that LIN7 mediates IRSp53 recruitment to TJs (*Massari et al., 2009*).

Interfering with their interaction by a) expression of a IRSp53 construct lacking the PDZ-binding motif (IRSp53Δ5), b) downregulation of LIN7 or c) expression of a dominant-negative variant of LIN7 (LINΔL27) interfere with MDCK cells polarization. LIN7 and IRSp53 interact not only in epithelial cells, but also in neuronal cell lines. The role of their interaction during filopodia formation and neuronal differentiation will be the topic of chapter 3.

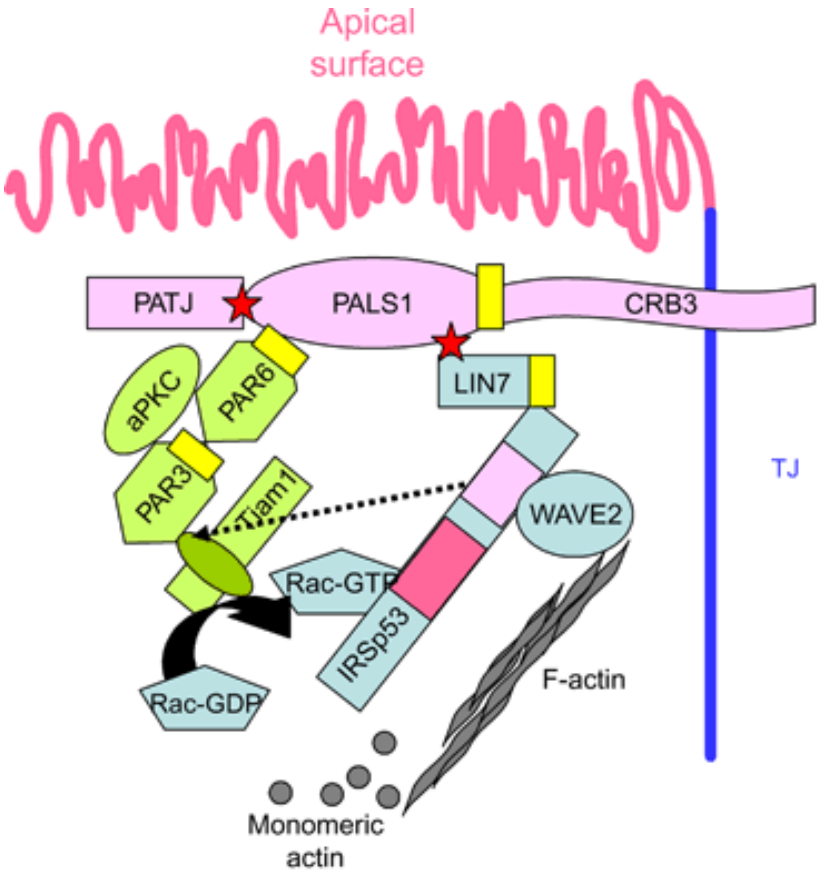

Image 19: LIN7-IRSp53 recruitment to TJs in MDCK cells (from Massari et al., 2009)

2.4.4 IRSP53 and LIN7 involvement in neurological disorders

The formation of functional and efficient synapses is the basis of the correct wiring of the CNS. Anomalies in dendrites morphology or dendritic spines structure compromise efficient signal transmission within the neuronal circuitries, and are related to severe neurological defects, ranging from mental retardation to autism spectrum disorder (ASD) (Chiurazzi et al., 2003; Fiala et al., 2002).

As the same structural and functional anomalies in dendrites and spines are recurrent in different pathologies, it is feasible that alterations in a common range of pathways give rise to different neurological disorders that, depending on the severity of the symptoms are then classified as different pathologies. The attention deficit hyperactivity disorder (ADHD), for instance, is a neurological disorder of infancy characterized by structural and functional anomalies that affect cerebral areas involved in motor and cognitive functions. As the names suggests, children affected by ADHD are impulsive and hyperactive, and have difficulty sustaining attention for long periods of time. It was estimated that this pathology affects 8-12% of children and approximately 3-5% of the adult population (Spencer et al., 2007). Patients affected by ADHD have a higher risk to develop other neurological disorders during their life, such as alchool and drug abuse, anxiety, depression and bipolar disorder (Biederman et al., 2006). Moreover, between 20 and 50% of ADHD affected children display symptoms consistent with a diagnosis of ASD, as well as 30-80% of ASD patients' symptoms are compatible with a diagnosis of ADHD, thus strengthening the hypothesis that these two

pathologies may share common genetic and environmental risk factors (Rommelse et al., 2010; Toma et al. 2010).

Even though various neuronal pathways related to neurotransmitter release and other neuronal-specific functions have been found to be consistently altered in various neurological disorders, more recent genome-wide studies suggested that proteins implicated in more general cellular pathways, such as cell polarity or cytoskeletal remodelling, may also play a pivotal role in the onset of these diseases (Roman et al., 2009). In line with this possibility, certain polymorphisms within IRSp53 and LIN7 have been associated with neurological disorders such as ADHD (Lanktree et al., 2008; Ribasés et al., 2009), ASD (Toma et al. 2010; Shinawi et al., 2011), and, for IRSp53 only, in Gilles de la Tourette syndrome (Paschou et al., 2004).

The association of LIN7 with both ASD and ADHD is also supported by clinical evidences, as Shinawi and colleagues reported that four young patients with ASD and/or ADHD had microdeletions on chromosome 11, in the region (11p14.1) encoding for LIN7 and the Brain-derived neurotrophic factor (BDNF) (Shinawi et al., 2011).

Alterations in the levels of IRSp53 or LIN7 have also been reported in neurodegenerative diseases. A significant decrease in the levels of LIN7B was found in post-mortem pyramidal neurons from patients affected by Huntington's Corea (Zucker et al., 2010), whereas a two-fold decrease in the levels of IRSp53 was observed in PSDs obtained form post-mortem tissues of patients affected by Alzheimer's disease (Zhou et al., 2013). It is interesting to note that in this study IRSp53 was the only one of the 9

core PSD proteins analyzed to be highly downregulated, as the majority of the proteins that were found to be highly decreased by this group had a mitochondrial rather than a PSD origin.

Finally, it is important to mention that a 2011 meta-analysis study highlighted how 53% of the genes found to be associated with ADHD in case-control studies are involved in neurite formation and extension (Poelmans et al., 2011).

This finding is in accordance with those models that classify ADHD as a neurodevelopmental disorder, in which it is conceivable that an unbalance in the levels of proteins involved in neuritogenesis or synapse formation and function, such as IRSp53 and LIN7, could cause structural alterations in neurons, thus giving rise to those dysfunctions typical of ADHD.

CHAPTER 3

Aims of the study

2. Aims of the study

IRSp53 is the founder of a protein family characterized by the presence of a IRSp53 and missing in metastasis domain (IMD), which is a domain able to both bind membranes and induce a conformational change in their curvature. In addition to the IMD domain, IRSp53 also contains a SRC homology 3 (SH3) domain for the interaction with various actin regulators and a Cdc42/Rac interactive binding (CRIB) domain for Cdc42 binding (Scita et al., 2008). The coexistence of both the IMD and SH3 domains within a single protein makes IRSp53 able to couple the capacity to deform the plasma membrane to the control of actin polymerization.

With its C-teminal tail IRSp53 binds LIN7, a small protein with a scaffolding role. We have previously shown that LIN7 regulates epithelial polarity through its binding and recruitment of IRSp53 to tight junctional plasma membrane domains (Massari et al., 2009). IRSp53, however, is mostly known for its capacity to induce filopodia, which are membrane protrusions that participate in a wide series of physiological events, such as cell adhesion, cell migration and, at the neuronal level, neuritogenesis.

Hence, the first of the two aims of this project was to test whether LIN7 regulates the formation of IRSp53-dependent filopodia and neurites. To this end, we investigated by morphological and biochemical means the functional role of LIN7-IRSp53 interaction on filopodia and neurites formation. To assess the effects of either forcing or disrupting of the

IRSp53-LIN7 interaction, different mutants of LIN7 and IRSp5, as well as shRNAs against LIN7, were transfected in neuronal cell lines.

The extension of filopodia and neurites isn't the only cell process that heavily relies on membrane deformation. So, if the IRSp53-LIN7 complex has a role in coupling membrane deformation to actin polymerization at the level of the plasma membrane, it may exert a similar role also on other membranes. The control of the mitochondrial network morphology through fission and fusion event is another process heavily relying on membrane deformation, and therefore it is conceivable that membrane-deforming proteins might be involved. Given these considerations, the second aim of this project was to investigate whether IRSp53 and LIN7 could localize to and have a role on other membranous compartments, such as mitochondria. Localization experiments by means of immunofluorecence staining and biochemical fractionation experiments were performed in HeLa cells because of their large cytoplasm. The morphological and functional effects of modifications in the expression levels of IRSp53/LIN7 on mitochondrial morphology were also evaluated in this cell type.

CHAPTER 4

LIN7 regulates the filopodium- and neurite-promoting activity of IRSp53.

4.1 Summary

The insulin receptor substrate protein of 53 kDa (IRSp53) is crucially involved in the formation of filopodia and neurites through mechanisms that have only partially been clarified. We have investigated the role of the small scaffold protein LIN7, which interacts with IRSp53. We found that formation of actin-filled protrusions in neuronal NSC34 cells and neurites in neuroblastoma N2A cells depends on motifs mediating the LIN7:IRSp53 association, as both the co-expression of LIN7 with IRSp53 or the expression of the L27-IRSp53 chimera (a fusion protein between IRSp53 and the LIN7 L27 domain for plasma membrane protein complexes association) prevented actin-deficient protrusions induced by overexpressed IRSp53, and enhanced the formation of actin-filled protrusions. The regulatory role of LIN7 in IRSp53-mediated extension of filopodia in neuronal N2A cells was demonstrated by live-cell imaging experiments. Moreover, LIN7 silencing prevented the extension of filopodia and neurites, induced by ectopic expression of IRSp53 or serum starvation, respectively, in undifferentiated and differentiated N2A cells. The expression of full-length IRSp53 or the LIN7ΔPDZ mutant lacking the domain for association with IRSp53 was unable to restore neuritogenesis in LIN7-silenced cells. Conversely, defective neuritogenesis could be rescued by the expression of RNAi-resistant full-length LIN7 or chimeric L27-IRSp53. Finally, LIN7 silencing prevented the recruitment of IRSp53 in Triton X-100-insoluble complexes, otherwise occurring in differentiated cells. Collectively these

data indicate that LIN7 is a novel regulator of IRSp53, and that the association of these proteins is required to promote the formation of actin-dependent filopodia and neurites.

The results shown below have been published in 2012 on The Journal of Cell Science in a paper by Crespi et al., and further commented in an addendum (Ferrari et al., 2012) published on Communicative and Integrative Biology.

4.2 Brief introduction

Filopodia are dynamic actin-rich cell surface protrusions involved in cell migration, axon outgrowth and guidance, and wound healing (Mattila et al., 2008). Plasma membrane protrusion and actin dynamics are essential events for filopodium formation and, by coupling these two events, IRSp53 is a key player in this process (Ahmed et at., 2010; Disanza et al., 2006; Yamagishi et al., 2004). Its N-terminal I-BAR domain binds to and deforms the plasma membrane, whereas its C-terminal SH3 domain interacts with various actin regulators, including Mena (Ena/VASP) family proteins, N-WASP, the mammalian Diaphanous (mDia) isoforms mDia1 and mDia2, and Eps8 (Scita et al., 2008). In the inactive state, the SH3 domain of IRSp53 has been suggested to be locked by intramolecular interactions. Binding of the Rho GTPase Cdc42 to a CRIB domain located between the I-BAR and SH3 domains may activate IRSp53 by unmasking the SH3 domain (Lim et al., 2008). With its C-terminal tail, IRSp53 can

bind to PDZ domain containing proteins, including LIN7. LIN7 is a small scaffold protein possessing only a single L27 domain, necessary for membrane recruitment, and a single PDZ1 domain mediating protein-protein interactions, including the one with IRSp53. The absence of either the L27 or PDZ domains causes mislocalization of LIN7 as well as IRSp53 in a polarised epithelial cell lines (Massari et al., 2009).

Here we hypothesised that LIN7 could be a possible partner of IRSp53 in the early steps of filopodia and neurites formation. Using a combination of structure-function studies with different mutants of either LIN7 or IRSp53 together with RNAi-based depletion in neuronal cell lines, we investigated the functional and molecular role of this protein partnership in filopodium formation and in neuritogenesis. Our morphological and biochemical data indicate a positive regulatory role for LIN7 in the formation of IRSp53-mediated actin-filled filopodia and neurites, and provide further evidence that neuritogenesis depends on actin-stabilised filopodia.

4.3 Results

4.3.1 The localisation of LIN7 and IRSp53 in filopodia tips depends on the L27 domain of LIN7 and the PDZ target motif of IRSp53

To gain initial clues as to a role of the IRSp53-LIN7 complex in filopodia, we ectopically expressed various combinations of epitope-tagged, wild type and mutant proteins (Fig. 1A) in NSC34 cells. This motoneuron-like

cell line was chosen as model because it exhibits endogenous filopodia-like protrusions (width of ~1 µm and length of ~5-10 µm) containing actin filaments along their entire length. Both myc-IRSp53 and GFP-LIN7, expressed alone or in combination, localised along the entire shafts and often appeared enriched on their tips. Protrusions with club-shaped tips similar to those shown in Fig. 1B have been previously described in cells expressing constitutively active human formin mDia2 (Yang et al., 2007; Block et al., 2008), suggesting that overexpression of the constructs may activate formins (see also 4.4, Discussion, in relation to this point). The IRSp53Δ5 construct lacking the association motif for the PDZ domain of LIN7 maintained the localisation along the shafts, but completely lost the tip enrichment (Fig. 1B, see plot profiles of the representative filopodia), suggesting that an interaction with PDZ-containing proteins endogenously expressed by these cells, such as LIN7, may be crucial for proper targeting of IRSp53. To strengthen this notion, we used a chimeric construct in which the LIN7-binding-deficient IRSp53Δ5 mutant was targeted to the plasma membrane by adding the L27 domain of LIN7 to its N-terminus (L27-IRSp53Δ5 chimera) (Massari et al., 2009). The L27 domain was sufficient to fully rescue tip localisation of IRSp53Δ5 (compare the plot profile of L27-IRSp53Δ5 chimera in Fig. 1C with that of IRSp53Δ5 in Fig. 1B). The importance of the L27 domain of LIN7 was further supported by the finding that a LIN7 mutant deleted of the L27 domain (LIN7ΔL27) was excluded from protrusions, and caused the sequestration of the co-expressed IRSp53 in the cytoplasm (Fig. 1C).

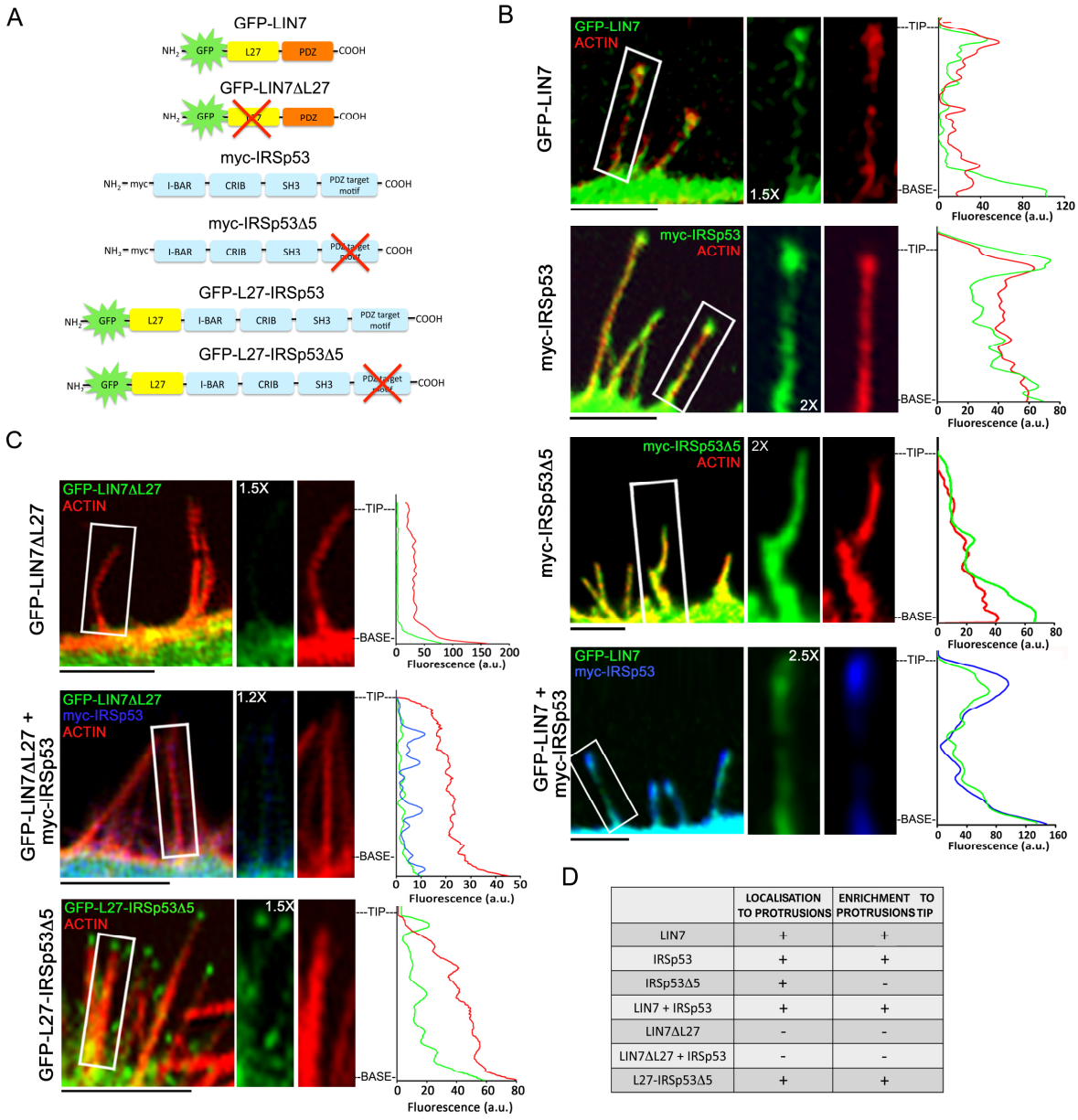

	LOCALISATION TO PROTRUSIONS	ENRICHMENT TO PROTRUSIONS TIP
LIN7	+	+
IRSp53	+	+
IRSp53Δ5	+	-
LIN7 + IRSp53	+	+
LIN7ΔL27	-	-
LIN7ΔL27 + IRSp53	-	-
L27-IRSp53Δ5	+	+

Figure 1

Figure 1: Colocalisation of IRSp53 and LIN7 to protrusion tips depends on the L27 domain of LIN7 and the PDZ target motif of IRSp53. (A) Schematic representation of the domain organisation of LIN7 and IRSp53 constructs used in the study. The myc or GFP tags fused at the N-termini and the domain structures are indicated; deleted domains are indicated with a X. **(B,C)** NSC34 cells were transiently transfected with the indicated cDNAs (left). Three days after transfection, cells were fixed in paraformaldehyde and stained with the myc antibody to visualise IRSp53, and Rhodamine-conjugated phalloidin to visualise F-actin; localisation of LIN7 constructs is revealed by the GFP fluorescence. Merged images and individual staining of the selected magnified protrusions are shown. The signal intensities were quantified using

ImageJ 'plot profile'. Pixel intensity along the corresponding protrusions is expressed in fluorescence arbitrary units (a.u.); the tips and bases of the filopodia are indicated. Scale bars: 5 µm. **(D)** A summary of the localisation analyses, such as those in B and C, shows the examined constructs and their presence or absence in protrusions and protrusion tips.

The localisation data above described for overexpressed constructs were not verified with endogenous LIN7 and IRSp53, because both proteins were under the level of detection at the PM using their specific antibody. However, overexpressed LIN7 and IRSp53 colocalize in protrusions and most prominently at their tips, and these tip enrichments were abolished when interaction between the two proteins was prevented (see a summary of localisation data in Fig. 1D), hence suggesting a role for the LIN7:IRSp53 complex in the extension of membrane protrusions.

4.3.2 LIN7 regulates the protrusion-promoting activity of IRSp53

It is well established that the expression of full-length IRSp53 as well as of its isolated I-BAR domain is sufficient to induce filopodia-like protrusions in a variety of cell lines. Notably, however, these protrusions, particularly when induced by the I-BAR domain of IRSp53, differ from canonical filopodia since they generally display a lower content of organised F-actin. In addition, the transfected proteins are uniformly distributed along the entire shaft, instead of being enriched at the tips of the protrusions (Faix and Rottner, 2006; Mattila et al., 2007; Yang et al., 2009). We obtained similar results in NSC34 cells. In these cells, the expression of IRSp53 or IRSp53Δ5 induced a large number of protrusions

that appeared floppy and branched, and frequently devoid of F-actin, which could, instead, be detected mainly at the bases of these structures (Fig. 2A,B). Notably, however, a 'normal' morphology and structural organisation was restored by the concomitant expression of LIN7 and IRSp53, but not with IRSp53Δ5 (see Fig. 1B for protrusion magnification). Aberrant, actin-deficient protrusions were also virtually absent in cells expressing the chimeric protein L27-IRSp53Δ5 (Fig. 2C and see Fig. 1C for protrusion magnification). Since comparable levels of expression of the IRSp53 constructs were measured by Western blot analysis (data not shown), these data suggest that LIN7 co-expression is necessary and sufficient to prevent the aberrant protrusions induced by overexpressed IRSp53. It is of note that the mean total number of protrusions (actin filled + actin deficient) significantly increased under all conditions of transfection tested (Fig. 2D), albeit it was less pronounced in cells co-expressing LIN7 with IRSp53 or the L27-IRSp53Δ5 chimera alone, which remarkably displayed only actin-filled protrusions. These results therefore reinforce a critical role of LIN7 in promoting IRSp53-mediated, F-actin-positive protrusions. The effect of LIN7:IRSp53 association on F-actin was also analysed by measuring the ratio of F-actin/monomeric G-actin (Fig. 2E). This assay is based on the differential extractability of F- and G-actin from cells by non-ionic detergent (Blikstad and Carlsson, 1982). We found that the F- to G-actin ratio was unaltered in cells expressing IRSp53Δ5, whereas it was significantly increased in cells expressing the L27-IRSp53Δ5 chimera, further supporting that LIN7-

mediated PM recruitment of IRSp53 is necessary for the stabilisation of actin in protrusions induced by the ectopic expression of IRSp53.

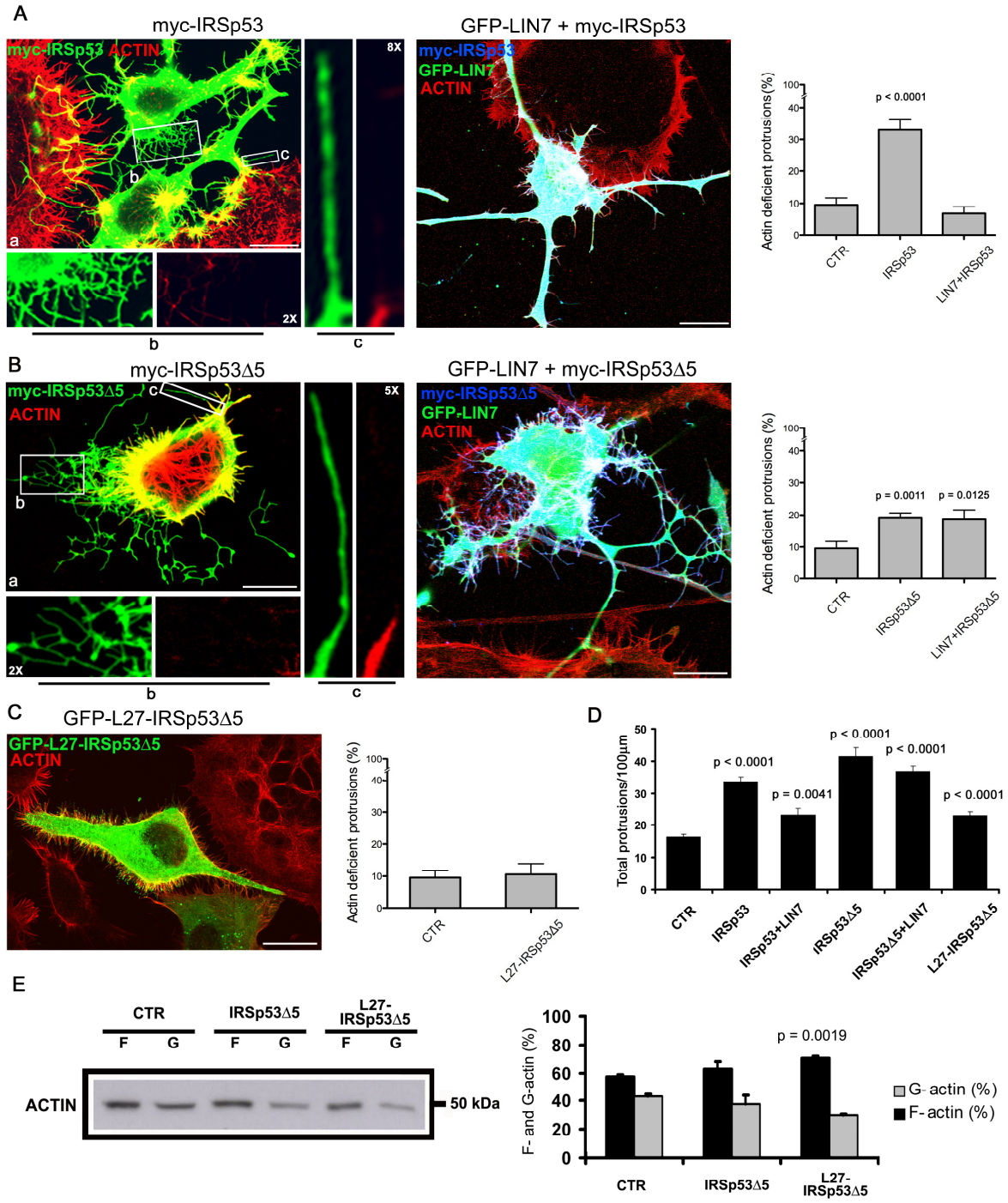

Figure 2

Figure 2: LIN7 regulates the protrusion-promoting activity of IRSp53. NSC34 cells transfected with the indicated cDNAs were analysed by immunocytochemistry **(A-D)** or

western blot **(E). (A-C)** Cells were fixed in paraformaldehyde 3 days after transfection with the indicated cDNAs (top of each image), stained with Rhodamine-conjugated phalloidin to visualise F-actin and anti-myc antibody to visualise IRSp53 constructs; LIN7 constructs were revealed by the GFP fluorescence. GFP-tagged empty vector was transfected as control (CTR). Merged images of the indicated double staining are shown together with magnified views of individual stainings (inset). The histograms represent the percentage of actin-deficient protrusions (linear + branched) measured in 20 different cells (6 mm of total plasma membrane) for each transfectant. Scale bars: 10 µm. (D) Quantification of the average number of protrusions (actin-deficient + actin-filled) in 100 µm of PM, obtained by measuring the protrusions in >20 cells. Data are the means of at least three independent experiments. Error bars indicates ± s.e.m.; P-values (t-test) are indicated. **(E)** Detergent extraction experiment. Equal volumes of insoluble F- and soluble G-actin fractions were separated using 11% SDS-PAGE and blotted onto nitrocellulose; the molecular weight (kDa) is indicated on the right of the blot. The percentage of F- and G-actin (means ± s.e.m.) from three independent experiments (the blot from one of them is shown) is presented; P-value (t-test) is indicated.

4.3.3 Effect of IRSp53 and L27-IRSp53 on filopodia dynamic in live-cell imaging

Based on morphological criteria, the protrusions of 5-10 µm length and width of ~1 µm containing actin for their entire length described in NSC34 cells could be considered filopodia (Yang and Svitkina, 2011). However, filopodia are defined as highly dynamic protrusions undergoing rapid cycles of extension and resorption. We therefore analysed the role of LIN7 in filopodial extension by live-cell imaging experiments. These experiments were performed in neuroblastoma N2A cells because of their high efficiency of transfection and tolerance to the environmental and illumination conditions (laser light) during time-lapse recording. Moreover, N2A cells behave like proliferating, undifferentiated neuroblasts when grown in the presence of serum, while they extend filopodia and neurites upon serum deprivation (Wu et al., 1998).

We compared filopodia induced by 16 h serum starvation in cells expressing GFP-tagged IRSp53 or L27-IRSp53 in reconstitution experiments for length and lifetime. In these experiments, the cells were co-transfected with RFP-pLifeAct to identify F-actin-filled filopodia, and cells transfected with GFP fused to a plasma membrane localisation signal (mGFP) were used as control.

The extent of protrusions induced by IRSp53 or L27-IRSp53 expression in differentiated N2A cells were equivalent to those promoted in NSC34 cells, as total protrusions were, respectively, 1.72-fold (±0.03) and 1.4-fold (±0.16) higher than control. Filopodia were positive for LifeAct and the IRSp53 and L27-IRSp53 along their lengths (Fig. 3A-C), and their average length (3.44±0.36 µm) did not differ significantly from control.

Figure 3: L27-IRSp53 induces dynamic protrusions in differentiated N2A cells. (A–C) Cells were co-transfected with RFP-LifeAct, and membrane mGFP construct as control (A), GFP-IRSp53 (B) or GFP-L27-IRSp53 (C). 24 h after transfection the cells were serum starved for an additional 16 h. Whole cells are shown in the merged images (left), magnifications of the selected areas at the indicated time points are presented separately (green and red channels) and as merged images. Scale bars: 5 µm**. (D-F)** The lifetime of filopodia (D), the percentage of static linear protrusions (absence of assembly/disassembly) (E), and average number of filopodia in 100 µm membrane (F). **(G)** A graph representing the changes in length of filopodia during the 5 min analysis and the unchanged length of four branched actin-deficient protrusions in cells expressing IRSp53; means ± s.e.m. of two independent experiments; P-values (t-test) are indicated.

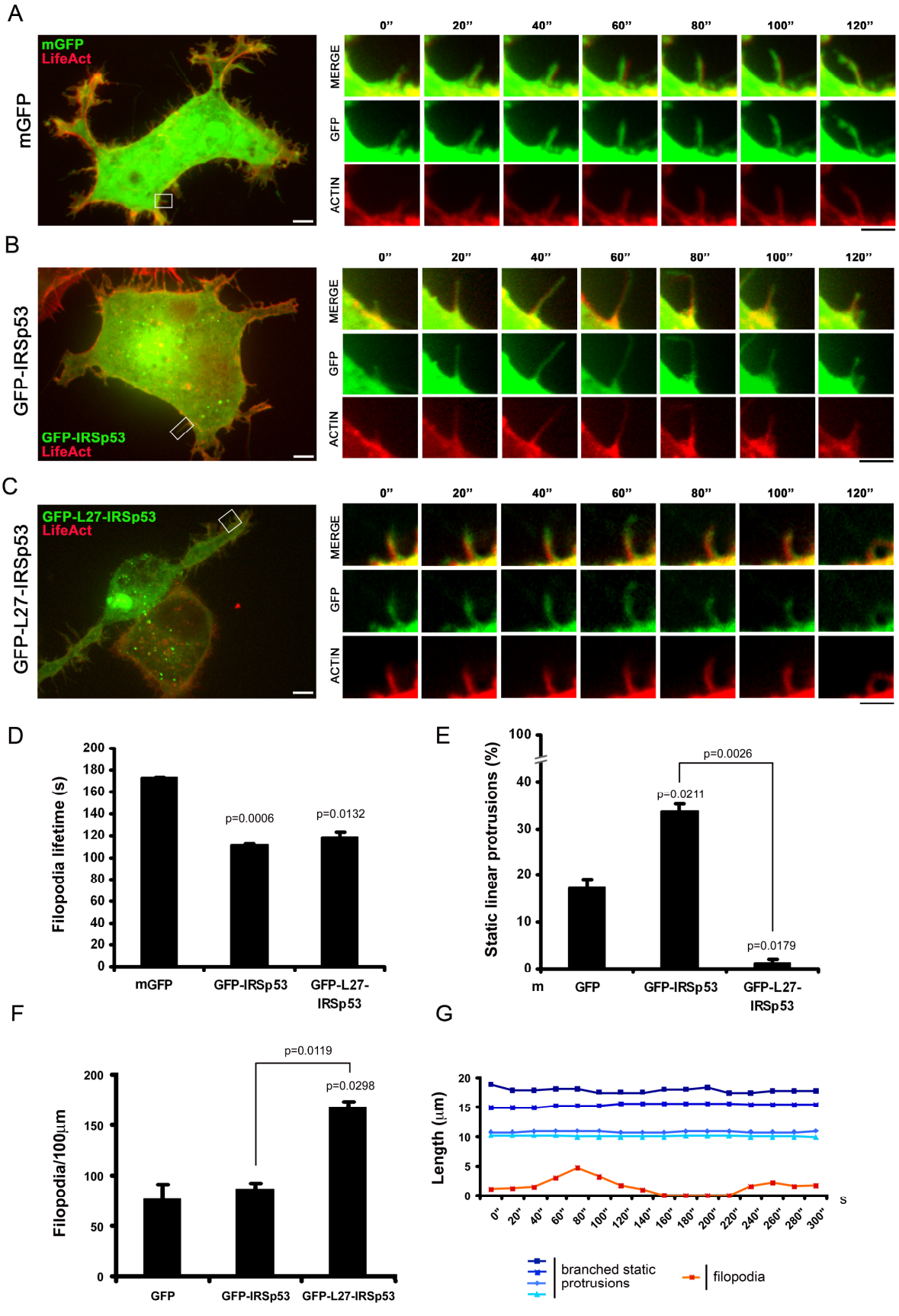
A
mGFP
mGFP
LifeAct
0"
20"
40"
60"
80"
100"
120"
MERGE
GFP
ACTIN
B
GFP-IRSp53
GFP-IRSp53
LifeAct
C
GFP-L27-IRSp53
GFP-L27-IRSp53
LifeAct
D
Filopodia lifetime (s)
p=0.0006
p=0.0132
mGFP
GFP-IRSp53
GFP-L27-IRSp53
E
Static linear protrusions (%)
p=0.0026
p=0.0211
p=0.0179
m
GFP
GFP-IRSp53
GFP-L27-IRSp53
F
Filopodia/100µm
p=0.0119
p=0.0298
GFP
GFP-IRSp53
GFP-L27-IRSp53
G
Length (µm)
s
branched static protrusions
filopodia

Figure 3

The lifetime of filopodia protruding or retracting was significantly decreased from 170 s in the control to 110 s in both IRSp53 and L27-IRSp53 filopodia (examples in Fig. 3A-C, quantification in D). However, the time-lapse analysis indicated a twofold increase in static linear protrusions in IRSp53-transfected cells compared with control (Fig. 3E). Even the abnormal, branched and F-actin-poor protrusions induced by overexpressed IRSp53 were static during the 5 min examined (Fig. 3G). In sharp contrast, static protrusions were drastically reduced in cells expressing the L27-IRSp53 chimera (Fig. 3E), and almost all the protrusions induced by the chimera were dynamic and thus identified as filopodia. In line with these findings, the total number of filopodia protruding or retracting from 100 µm plasma membrane within 5 min doubled the control in L27-IRSp53-expressing cells, whereas it did not differ significantly in IRSp53-expressing cells (Fig. 3F). Since the level of expression of the constructs was comparable (data not shown), these data confirm the results obtained in NSC34 cells concerning the LIN7 control of altered protrusions induced by IRSp53 overexpression and robustly indicate IRSp53 requirement of LIN7 to promote filopodia.

4.3.4 LIN7 is required for IRSp53-induced differentiation of neuronal N2A cells

To further demonstrate the role of LIN7 in filopodia, LIN7 was silenced in N2A cells. Since actin bundling and filopodium formation are critical early steps in neurite formation (Dent et al., 2007), neuritogenesis was analysed in LIN7-silenced N2A cells.

Three different LIN7A, B, C isoforms are frequently ubiquitously expressed: LIN7A is larger with a predicted molecular weight of 29 kDa, LIN7B and C are, instead, smaller and predicted to have a similar 22 kDa molecular weight. We used a pan-LIN7 antibody (which does not distinguish among the three LIN7 isoforms) to asses which isoforms were expressed in N2A cells by immunoblotting. As shown in Fig. 4A, we could only detect a single 22 kDa band, possibly corresponding to LIN7B and C. The pan-IRSp53 antibody predominantly recognised a doublet (~75% of the total bands) migrating at the expected 50–53 kDa molecular weight for IRSp53-S, with the band of lower mobility probably corresponding to phosphorylated IRSp53-S (Cohen et al., 2011), and a 70 kDa band corresponding to mobility of the IRSp53-L isoform (Okamura-Oho et al., 2001; Miyahara et al., 2003). The doublet was immunoprecipitated by the LIN7 antibody but not by the preimmune serum (bands 1 and 2 in the IP). However, bands with molecular weight corresponding to IRSp53-S dimers and tetramers (bands 4 and 5 in the IP) and, surprisingly, also the band of ~70 kDa (band 3 in the IP) was selectively detected in LIN7 immunocomplexes (Fig. 4A). All the unexpected bands might be artefacts due to oligomerisation with IRSp53-S occurring in the immunoprecipitation condition.

The 22 kDa band was greatly reduced in N2A cells silenced for LIN7C (Fig. 4B), and the reduction level correlated with the transfection efficiency in this cell system, thus suggesting that LIN7C is the main, if not exclusive, isoform in N2A cells. The LIN7C silencing did not affect the expression of

all the IRSp53 endogenous isoforms, but completely prevented the extension of protrusions, recognised as filopodia and neurites on the basis of their length and size, induced by 48 h serum starvation (Fig. 5A,B) or promoted by IRSp53 overexpression in undifferentiated N2A cells (Fig. 4C, and quantification in Fig. 4E).

Similar results were obtained with shRNA 2 (data not shown). The requirement of LIN7 for IRSp53-mediated protrusions appears to be specific, as silencing of LIN7C did not prevent neuritogenesis and filopodium formation induced by mDia1 or mDia2 (Fig. 4D, and quantification in Fig. 4E), members of the formin family of proteins that induce filopodia and neurite extension by promoting the nucleation and linear elongation of actin (Faix and Grosse, 2006).

Figure 4: IRSp53 requires LIN7 to induce neurite outgrowth in undifferentiated N2A cells. (A) Western blot characterisation of the expression of LIN7 and IRSp53 isoforms in N2A cells by immunoprecipitation with anti-LIN7 antibodies (IP: LIN7) or preimmune IgG (IP: preimmune serum). Bands 1, 2 correspond to the apparent molecular mass of de-phosphorylated and phosphorylated IRSp53-S; band 3 to IRSp53-L; bands 4 and 5 to IRSp53-S dimers and tetramers, respectively. The arrow indicates the IgG light chain dimers. **(B)** A representative western blot showing downregulation of LIN7C in N2A cells transiently transfected with shRNA 1. The histogram representing the percentage of LIN7 in silenced cells compared with control was obtained by densitometric quantification of the 22 kDa band (corresponding to LIN7B and/or C) normalised to Calnexin. Data are the means ± s.e.m. of four independent experiments; P-value (t-test) is indicated. **(C)** Laser confocal microscopy of undifferentiated N2A cells transfected with the empty vector (pSUPER), GFP-IRSp53 (IRSp53) or co-transfected with GFP-IRSp53 and shRNA LIN7C. The insets show magnifications (2.2×) of the process outlined in the merged image. Scale bar: 20 μm. **(D)** Undifferentiated N2A cells transfected with the cDNA encoding formin mDia2 or co-transfected with mDia2 and shRNA LIN7C cDNAs. Scale bar: 20 μm. **(E)** Quantification of the percentage of cells with neurites (n>150 cells). Data are the means of three independent experiments. Error bars indicate ± s.e.m.; P-values (t-test) are indicated.

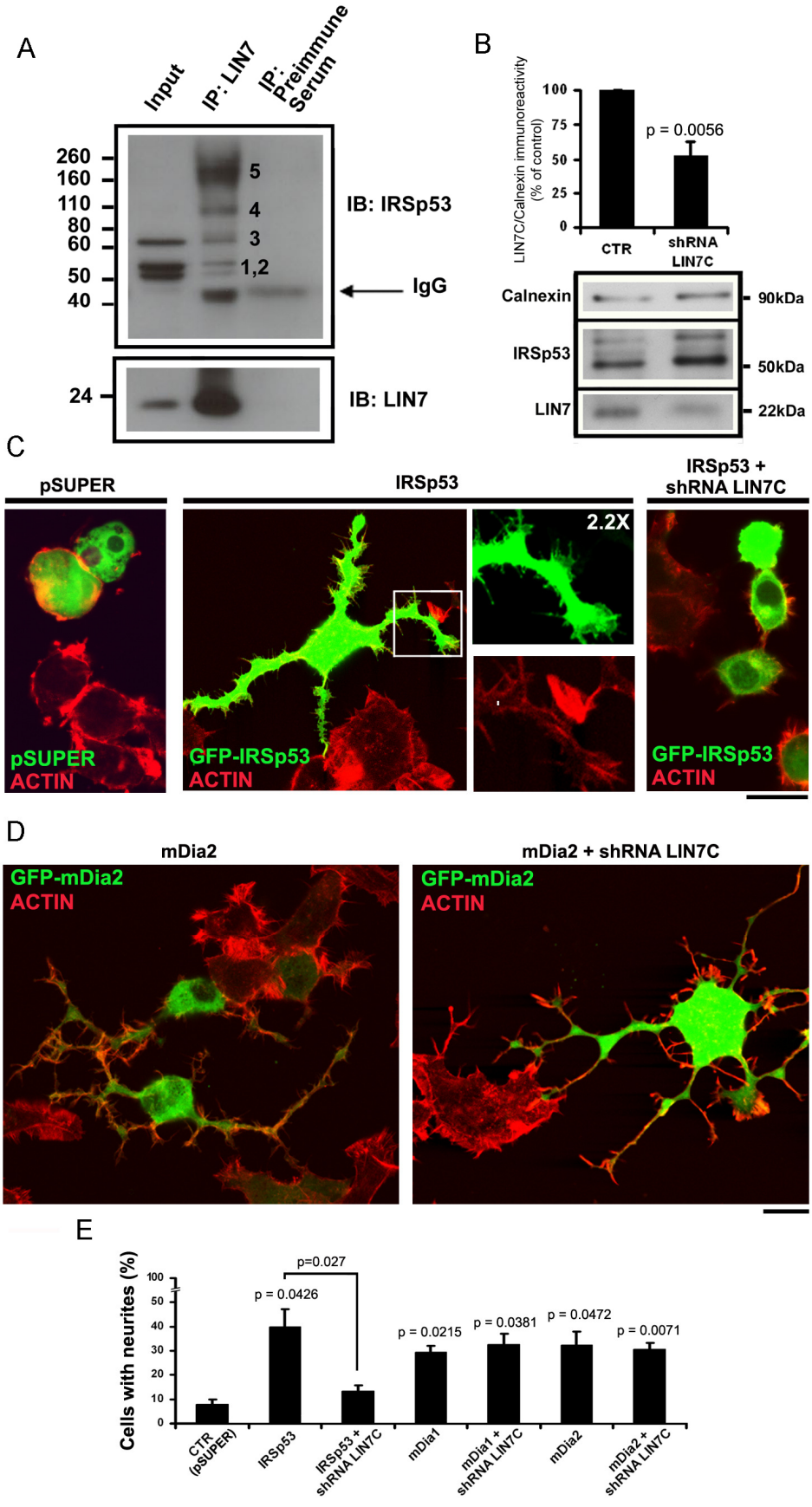
A
Input
IP: LIN7
IP: Preimmune Serum
260
160
110
80
60
50
40
5
4
3
1,2
IB: IRSp53
IgG
24
IB: LIN7
B
LIN7C/Calnexin immunoreactivity (% of control)
100
75
50
25
0
p = 0.0056
CTR
shRNA LIN7C
Calnexin
IRSp53
LIN7
90kDa
50kDa
22kDa
C
pSUPER
IRSp53
IRSp53 + shRNA LIN7C
2.2X
pSUPER
ACTIN
GFP-IRSp53
ACTIN
GFP-IRSp53
ACTIN
D
mDia2
mDia2 + shRNA LIN7C
GFP-mDia2
ACTIN
GFP-mDia2
ACTIN
E
Cells with neurites (%)
100
50
40
30
20
10
0
p=0.027
p = 0.0426
p = 0.0215
p = 0.0381
p = 0.0472
p = 0.0071
CTR (pSUPER)
IRSp53
IRSp53 + shRNA LIN7C
mDia1
mDia1 + shRNA LIN7C
mDia2
mDia2 + shRNA LIN7C

Figure 4

4.3.5 Differentiation of N2A cells requires the L27 and PDZ domains of LIN7

We further analysed the role of LIN7 in IRSp53-mediated neurite outgrowth and the requirement of the LIN7 domains. To this end, N2A cells were transfected (green signal) with the empty vector (pSUPER) or with cDNA encoding shRNA LIN7C, and 24 h after transfection the cells were cultured in serum-free medium for 48 h to induce differentiation (Fig. 5).

Analysis of phase contrast images (Fig. 5A), and their corresponding quantifications (Fig. 5B), indicate highly significant reduction of neurites induced by serum-starvation in LIN7C-silenced cells, confirming the essential function of the LIN7C isoform in neurite extension. The expression of IRSp53 in LIN7C-silenced cells did not restore neuritogenesis, which was, instead, fully rescued by the expression of the RNA silencing resistant LIN7A isoform. Notably, neuritogenesis was not re-established by the expression of the LIN7 variant lacking the PDZ domain, but it was fully restored by the L27-IRSp53 chimera.

Figure 5: IRSp53 requires LIN7 association for neurite outgrowth. (A) Phase contrast images of differentiated N2A cells transfected with the pSUPER empty vector (CTR) or the vector encoding shRNA LIN7C, or co-transfected with shRNA LIN7C and the indicated constructs. Transfected cells are identified by the green signal. Twenty-four hours after transfection, cells were serum-starved for an additional 48 h to induce neurite outgrowth, before fixation in 4% paraformaldehyde. Scale bar: 40 μm. **(B)** The histogram represents the effects of the transfectants on differentiated N2A cells; neurite outgrowth was scored by evaluating the percentage of cells with neurites. Data are the means ± s.e.m. of three independent experiments; processes in >100 cells for each experiment were evaluated. P-values (t-test) compared with the control are indicated.

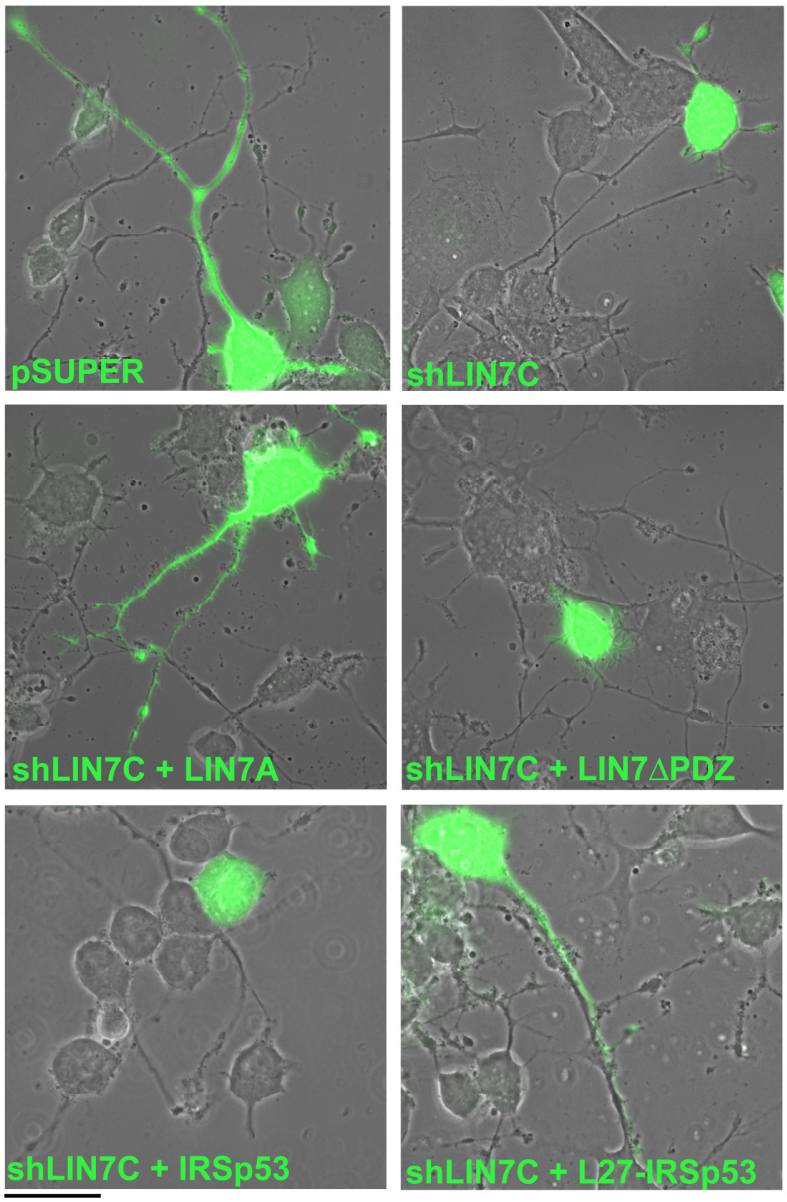
pSUPER
shLIN7C
shLIN7C + LIN7A
shLIN7C + LIN7ΔPDZ
shLIN7C + IRSp53
shLIN7C + L27-IRSp53

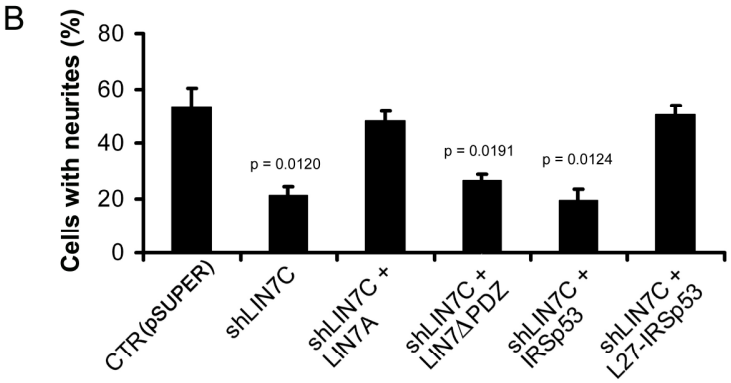
B
Cells with neurites (%)
80
60
40
20
0
p = 0.0120
p = 0.0191
p = 0.0124
CTR(pSUPER)
shLIN7C
shLIN7C + LIN7A
shLIN7C + LIN7ΔPDZ
shLIN7C + IRSp53
shLIN7C + L27-IRSp53

Figure 5

Since the levels of expression of the constructs were comparable (data not shown), these data further demonstrate the requirement of both domains of LIN7 for IRSp53-mediated neuritogenesis.

4.3.6 LIN7 is required to relocate IRSp53 in Triton X-100-insoluble complexes in differentiated N2A cells

If formation of actin-filled protrusions (neurites) during N2A differentiation depends on LIN7 recruitment of IRSp53 to PM sites, we might expect an increased amount of the latter protein to remain associated with fractions rich in PMs and cytoskeletal elements. Insolubility of a protein to non-ionic detergent is largely dependent on the strength of its association with actin cytoskeleton (Gilbert and Fulton, 1985). We therefore investigated the Triton X-100 solubility of LIN7 and IRSp53 in control and silenced N2A cells (Fig. 6). Undifferentiated (+FBS) or serum-free medium differentiated (–FBS) N2A cells were lysed in 0.5% Triton X-100 for 10 min at 0°C, and equal volumes of soluble (S) or insoluble (I) fractions were analysed by immunoblotting. The amount of LIN7 and IRSp53 recovered in the Triton X-100-insoluble cytoskeletal-associated fraction increased in differentiated cells, reaching ~60% after 48 h in serum-free medium (Fig. 6A). This finding suggests that under conditions of neurite outgrowth there is an increased association of LIN7 and IRSp53 with the F-actin cytoskeleton.

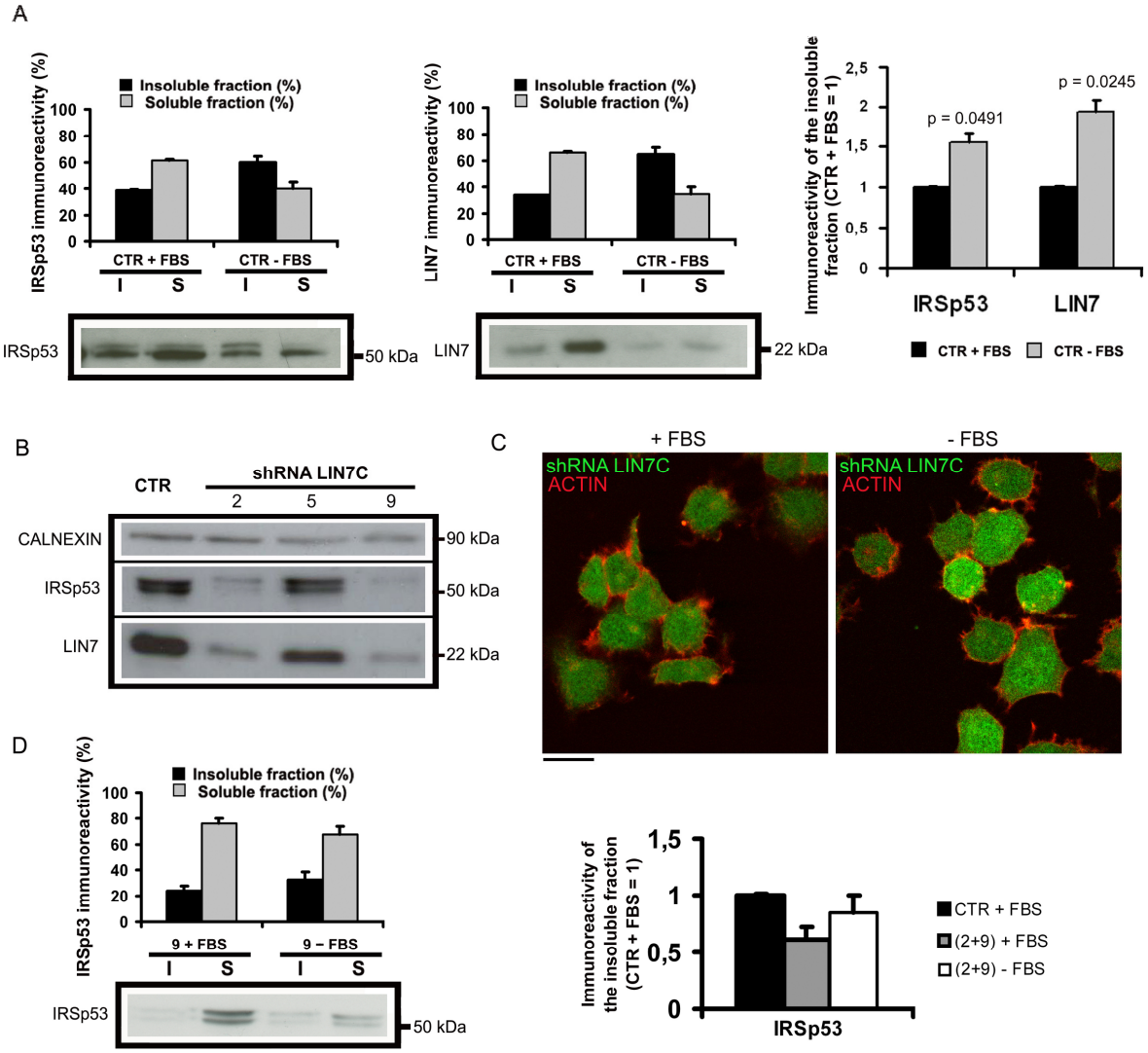

Figure 6

LIN7 increases Triton X-100 detergent insolubility of IRSp53 in differentiated N2A cells. **(A)** Western blot analysis of the amount of IRSp53 and LIN7 in Triton X-100-insoluble (I) and -soluble (S) fractions. Undifferentiated N2A cells (CTR+FBS) or differentiated in serum-free meidium (CTR-FBS) for 48 h were extracted in 0.5% Triton X-100 for 10 min at 0°C. Equivalent volumes of the fractions were separated by 11% SDS-PAGE. Representative immunoblots and densitometric quantification (expressed as a percentage of the total I+S immunoreactivity) of two independent experiments are presented. The histogram on the right shows the values obtained by measuring the percentage of immunoreactivity in the insoluble fractions compared with that of CTR+FBS (CTR+FBS=1). Data are means ± s.e.m. and P-values (t-test) are indicated. **(B)** Western blot analysis of the level of expression of LIN7 and IRSp53 in the selected (2, 5 and 9) N2A clones specifically knocked down for LIN7C protein expression by shRNA 1; Calnexin was probed as a loading control. (C) Confocal laser analysis of shRNA LIN7C clone 9 in undifferentiated (+FBS) or differentiated (–FBS) culture conditions. Scale bar: 15 µm. **(D)** Western blot analysis of the amount of IRSp53 in Triton X-100-insoluble (I)

and -soluble (S) fractions from undifferentiated (+FBS) or differentiated (–FBS) N2A cells stably silenced for LIN7C. A representative immunoblot and the densitometric quantification (expressed as the percentage of the total I+S immunoreactivity) of two independent experiments performed with clone 9 are shown. The histogram on the right shows the results (means ± s.e.m.) of two independent experiments, each one performed with both clones 2 and 9. Data were obtained by measuring the percentage of immunoreactivity in the insoluble fractions of clones 2 and 9 (2+9) compared with the percentage of immunoreactivity in the insoluble fraction of CTR+FBS (CTR+FBS=1).

To demonstrate that IRSp53 detergent insolubility depends on LIN7, we characterised three independent N2A clones (2, 5 and 9) stably silenced for LIN7C with shRNA 1 (Fig. 6B). It is of note that the total level of downregulation of IRSp53 was directly proportional to that of LIN7, suggesting that LIN7 protects IRSp53 from degradation. More importantly, a nearly complete absence of neurites (Fig. 6C) and of IRSp53 redistribution in Triton X-100-insoluble fractions (Fig. 6D) was found in silenced cell lines even after 48 h serum-starvation. The defective neuritogenesis observed in these cells coincided with that obtained in transiently silenced cells, where the expression of IRSp53 was unchanged (see Fig. 4B), further corroborating the requirement of the LIN7:IRSp53 complex for neuritogenesis.

4.4 Discussion

By coupling membrane deformation to actin filament polymerisation, IRSp53 has emerged as one of the key proteins in promoting PM protrusions (filopodia) considered to be precursors of neurites and polarised structures such as synapses (Ziv and Smith, 1996; Dent et al.,

2007). We have previously shown that LIN7 regulates epithelial polarity through its binding and recruitment of IRSp53 to tight junctional PM domains (Massari et al., 2009), and here, we have tested whether LIN7 regulates the formation of IRSp53-dependent filopodia and neurites.
Our findings indicate that LIN7 plays a positive regulatory role on the filopodium- and neurite-promoting activity of IRSp53, and that this regulation depends on both protein-protein association domains of LIN7: the PDZ domain for binding to the last C-terminal residues of IRSp53, and the L27 domain for association with PM protein complexes.

We found that full-length LIN7 regulates IRSp53 activity by preventing the formation of actin-deficient abnormal protrusions and by sustaining the extension of F-actin-rich protrusions in NSC34 cells. These findings were confirmed by live-cell imaging experiments in differentiated N2A cells, collectively indicating that static protrusions induced by the overexpression of IRSp53 were abolished in cells overexpressing the L27-IRSp53 chimera, and that virtually all the protrusions in cells overexpressing the L27-IRSp53 chimera were dynamic and thus bona fide identified as filopodia. Moreover, downregulation of LIN7C by shRNA definitively demonstrate the strict requirement of LIN7C isoform in the formation of filopodia and neurites induced by IRSp53, as overexpression of IRSp53 completely failed to induce any protrusions in N2A silenced for LIN7.

LIN7 association with IRSp53 rather than its simple presence was required to control IRSp53 activity, and this is clearly indicated by the

fact that LIN7 is not able to prevent the formation of actin-deficient protrusions induced by the expression of the IRSp53Δ5 mutant lacking the interaction motif for LIN7. The additional finding that protrusions unstained or poorly labelled by phalloidin, and thus floppy, are formed in cells expressing either unbalanced levels of IRSp53 and LIN7 or the IRSp53Δ5 mutant, further suggests that the two proteins must operate as a tightly regulated complex for the proper formation of actin-proficient cellular protrusions. In line with these findings, IRSp53 and LIN7 colocalize at the tips of actin-filled protrusions, whereas IRSp53 is uniformly distributed along those actin-deficient. Notably, LIN7 localisation at the tips depends also on the L27 domain, that not only mediates LIN7 membrane association, but is also necessary and sufficient to direct to the tips the otherwise uniformly distributed IRSp53Δ5 (chimera L27-IRSp53Δ5). Finally, LIN7 lacking the L27 domain, but maintaining the PDZ domain sequesters IRSp53 in the cytoplasm, thus preventing the formation of actin-deficient protrusions. Conversely, LIN7ΔL27 is not able to retain IRSp53Δ5 in the cytoplasm and to inhibit the formation of actin-deficient protrusions. The essential role for LIN7 association with IRSp53 is further supported by functional interference studies (using RNAi-based downregulation of LIN7C) and structure-function rescue experiments, which collectively argue that the association between LIN7 and IRSp53 is necessary for neuritogenesis. Again, both the L27 and PDZ domains of LIN7 are required to rescue neuritogenesis in N2A cells silenced for LIN7C, the major isoform in these cells, as demonstrated by transient and stable downregulation

experiments. These data further suggest that LIN7, through recruitment of IRSp53 to PM complexes, is a critical early molecular determinant in the formation of these protrusions.

Our data, showing that the L27 domain of LIN7 is necessary and sufficient to localise IRSp53 to protrusion tips in NSC34 cells and to promote filopodia and neurites in N2A cells, suggest that interactors of the L27 domains play a crucial role in IRSp53 membrane recruitment. IRSp53 may exist in an auto-inhibited state in the cytoplasm, and IRSp53 dimers may become active on PM through binding to activated Rho-GTPases (Krugmann et al., 2001). The surface recruitment of IRSp53 is therefore a first crucial step in filopodium extension from the cell periphery, and the L27 domain of LIN7 may accomplish this function.
The L27 domains form heterodimers to achieve their biological functions and to correctly assemble protein complexes and prevent promiscuous binding (Feng et al., 2004; Funke et al., 2005; Shin et al., 2006). Partners of the L27 domain of LIN7 are MAGUK proteins, and multimerisation of these proteins via their L27 domains may be required to link Rho family small GTPases with IRSp53, thus stabilising IRSp53 in its active dimeric form, with its I-BAR and SH3 domains respectively competent for membrane curvature and concentration, at the tips of emergent protrusions, of downstream effectors involved in initiation and bundling of actin filaments. For instance, LIN7 may recruit IRSp53 in the PAR3/PAR6/atypical PKC (protein kinase C) complex that through the guanine nucleotide exchange factor Tiam1 control cell-cell junction

assembly in epithelia and neurons (Shin et al., 2006), neurite elongation and axon or dendrite fate (Yoshimura et al., 2006).

In agreement with a role for LIN7 in increasing the association of IRSp53 to actin filaments, cells silenced for LIN7 fail to differentiate and to increase the amount of IRSp53 found in the detergent-insoluble fraction. Moreover, a decreased amount of IRSp53 was found in cell lines stably silenced for LIN7, suggesting that LIN7-mediated recruitment in Triton X-100-insoluble complexes may not only activate but also protect IRSp53 from downregulation.

Collectively our data strengthen the crucial importance of LIN7 for IRSp53 function. However, the removal of LIN7 had no effects on filopodia and neurite formation induced by either mDia2 or mDia1, since both formins, when individually overexpressed in LIN7-silenced cells, were sufficient to restore completely neuritogenesis. The results obtained by the ectopic expression of mDia1 in LIN7-silenced neuronal cells were particularly surprising, as mDia1 was recently shown to be an important SH3 domain partner of IRSp53 in forming filopodia (Goh et al., 2012). However, it must be pointed out that more than one independent pathway for filopodium and therefore neurite formation exist (Mattila et al., 2008). Our data are consistent with this notion, indicating that a LIN7-IRSp53 pathway may act independently of mDia1 and mDia2. In neuronal N2A cells, the LIN7-IRSp53 pathway may co-exist with the Rif-mDia1/mDia2 pathway and with the one dependent on IRSp53 and mDia1 (see Fig. 7). Notably, the latter pathway has been demonstrated in a

neuroblastoma cell line strictly related to N2A, although no data are available concerning the possibility that the IRSp53-mDia1 pathway may also regulate neuritogenesis. Further experiments will be required to elucidate the nature of these pathways and to understand the LIN7 functions in filopodia and neurite formation.

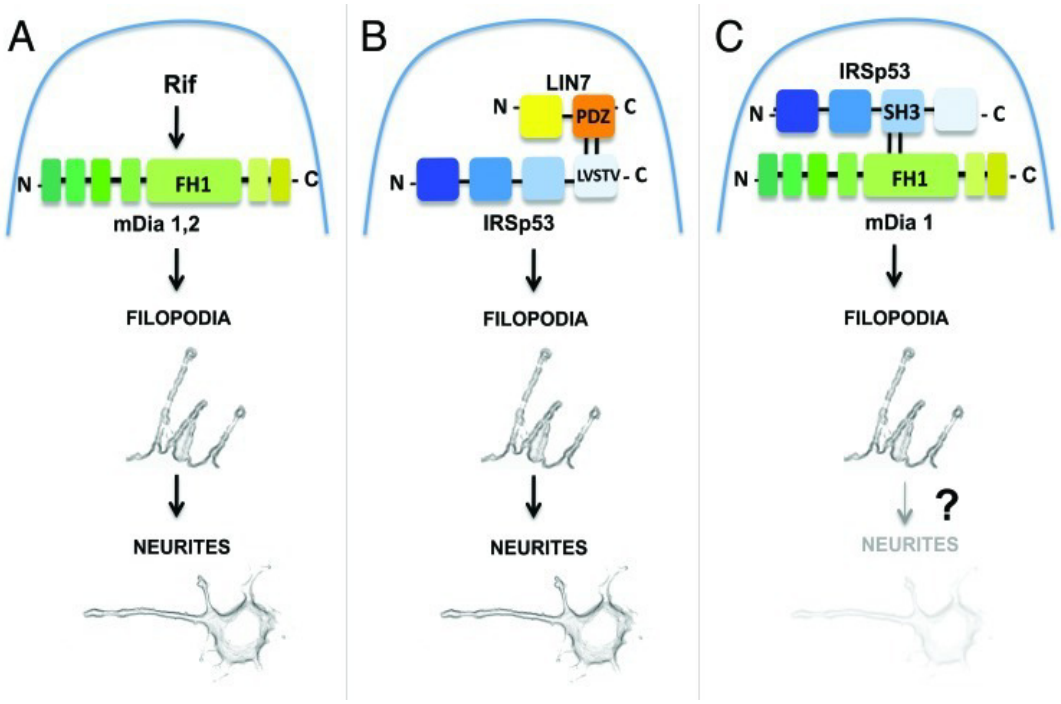

Figure 7. A model describing parallel pathways for the formation of filopodia and neurites. **(A)** mDia1,2-dependent pathway (Goh et al., 2011). Activation of mDia1 or mDia2-mediated by the Rho GTPase Rif induces filopodia formation and neuritogenesis; **(B)** LIN7-IRSp53-dependent pathway. Binding between the class I PDZ domain of LIN7 and the PDZ target motif (LVSTV) of IRSp53 induces the formation of filopodia and neurites; **(C)** IRSp53-mDia1-dependent pathway (Goh et al., 2012). Binding of mDia1 to the SH3 domain of IRSp53 induces the formation of filopodia. No data are available concerning a role of this pathway in neuritogenesis. Domains for protein-protein interaction are indicated.

To conclude, our data identify in LIN7 a novel regulator of IRSp53 that is critical to spatially restrict the LIN7:IRSp53 complex to the plasma membrane for filopodium and neurite initiation, and to further promote the stabilisation of these actin-rich structures. Moreover, underlying the key role of the IRSp53-LIN7 association in neuritogenesis, our results suggest that neurodevelopmental disorders, such as human attention-deficit/hyperactivity disorder (ADHD), recently associated with polymorphisms of LIN7 or IRSp53 or altered expression of LIN7 in humans (Lanktree et al., 2008; Ribasés et al., 2009; Zucker et al., 2010; Shinawi et al., 2011) may be due to unbalanced alterations in the expression of LIN7 and/or IRSp53 or to mutations that prevent their interaction.

CHAPTER 5

LIN7 and IRSp53 possible involvement in the generation of SOD1-induced lamellipodia

5.1 Brief introduction

A wide variety of neurological disorders of the central and peripheral nervous system are characterized by a slowly evolving distal to proximal axonal degeneration, a process termed 'dying back' degeneration (Fischer et al. 2003; Dadon-Nachum, 2011). Given the importance of the cytoskeleton in maintaining axon integrity, signalling pathways that lead to destabilization of microtubules, actin, or interactions between the two cytoskeletal systems could be involved in axonal defects. However, few signalling mechanisms regulating such processes have been investigated thoroughly, with the exception of a pathway involving the Rho family of small GTPase proteins: altered Rho GTPases signalling impairs normal dendritic and axonal formation, and mutations in regulators and effectors of Rho-GTPases have been associated with diseases affecting the nervous system (Nadif Kasri and Van Aelst 2008). By facilitating the reorganization of the cytoskeleton, appropriate levels of the Rac1 Rho GTPases are required to promote and maintain a normal neuronal morphology. In line with these functions, Rac1 has been considered a common target in many neurodegenearative diseases, including amyotrophic lateral sclerosis (ALS). Several genes found to be mutated in both familiar and sporadic ALS have in fact been linked to Rac1. For example, the protein encoded by the ALS2 gene, Alsin, acts as a GEF for Rac1, and in neurons induces neurite outgrowth by stimulating the Rac1- p21 activated kinase (PAK) signalling pathway (Nadif Kasri and Van Aelst 2008). Moreover, ALS is characterized by

aggregates containing ubiquitinated TAR DNA binding protein (TDP-43), a protein that regulates mammalian spinogenesis through translational repression of Rac1 (Majumder et al., 2011) and that has been found mutated in some cases of familial and sporadic ALS (Sreedharan et al, 2008). Mutations in the copper/zinc superoxide dismutase 1 (SOD1) gene account for 20% of familial ALS cases (Rosen et al.,1994) and 2% of sporadic cases. SOD1 was the first gene whose mutations were linked to ALS, and its identification allowed the generation of mouse models which recapitulate most features of ALS pathology. In glial cells, a direct interaction between SOD1 and Rac1 has been documented to control GTP hydrolysis by Rac1 in a redox–dependent manner. Such regulation appeared to be lost in cells expressing SOD1 mutants, leading to enhanced Rac1 and NADPH oxidase (Nox) activation (Harraz et al., 2008). Rac1, however, is most widely known for its crucial involvement in the regulation and organization of the actin cytoskeleton, especially at the level of lamellipodia, which are actin-based membranous projections that usually appear on the moving edge of a cell (Bisi et al., 2013). In differentiating cultured primary neurons, in particular, activation of Rac1 is associated with neurite outgrowth and growth cone turning in response to attractive cues (Blanchoin et al., 2014). Thus, if SOD1 could control Rac1 activity also in neuronal cells, modifications in the levels of SOD1 could in theory impact on neuronal morphology. To explore this hypothesis, we analyzed the effects of the overexpression of SOD1 (either WT or its G93A mutant) on membrane morphology and differentiation rate of neuronal-like N2A cells, similarly to what we did to

demonstrate the role of LIN7 and IRSp53 in filopodia and neurite extension. The preliminary data we obtained will be briefly discussed below.

5.2 Results

5.2.1 Overexpression of SOD1 or SOD1^{G93A} induces the extension of lamellipodia in both undifferentiated or differentiated N2A cells

Given Rac1 involvement in the regulation of the actin cytoskeleton, especially inside the lamellipodium, we tested whether overexpression of SOD1 could induce the formation of membrane protrusions in neuronal cells. To answer this question, we ectopically expressed untagged SOD1 or SOD1^{G93A} in N2A cells. This neuroblastoma cell line was chosen as a model because their differentiation state can be readily regulated by the levels of serum in the medium (Wu et al., 1998). When undifferentiated (+ FBS), N2A cells have either a spherical or fibroblast-like morphology, and cells extend lamellipodia and filopodia in order to sense and sample the surrounding environment. When cultured in differentiating conditions (-FBS), N2A cells start emitting neurites, and lamellipodia formation is usually restricted to the growth cone of such neurites. To evaluate the effects of the overexpression of SOD1 on N2A membrane dynamics, 24 hours after transfection cells were cultured for additional 24-48 hours in undifferentiating (15% FBS) or differentiating (-FBS) conditions.

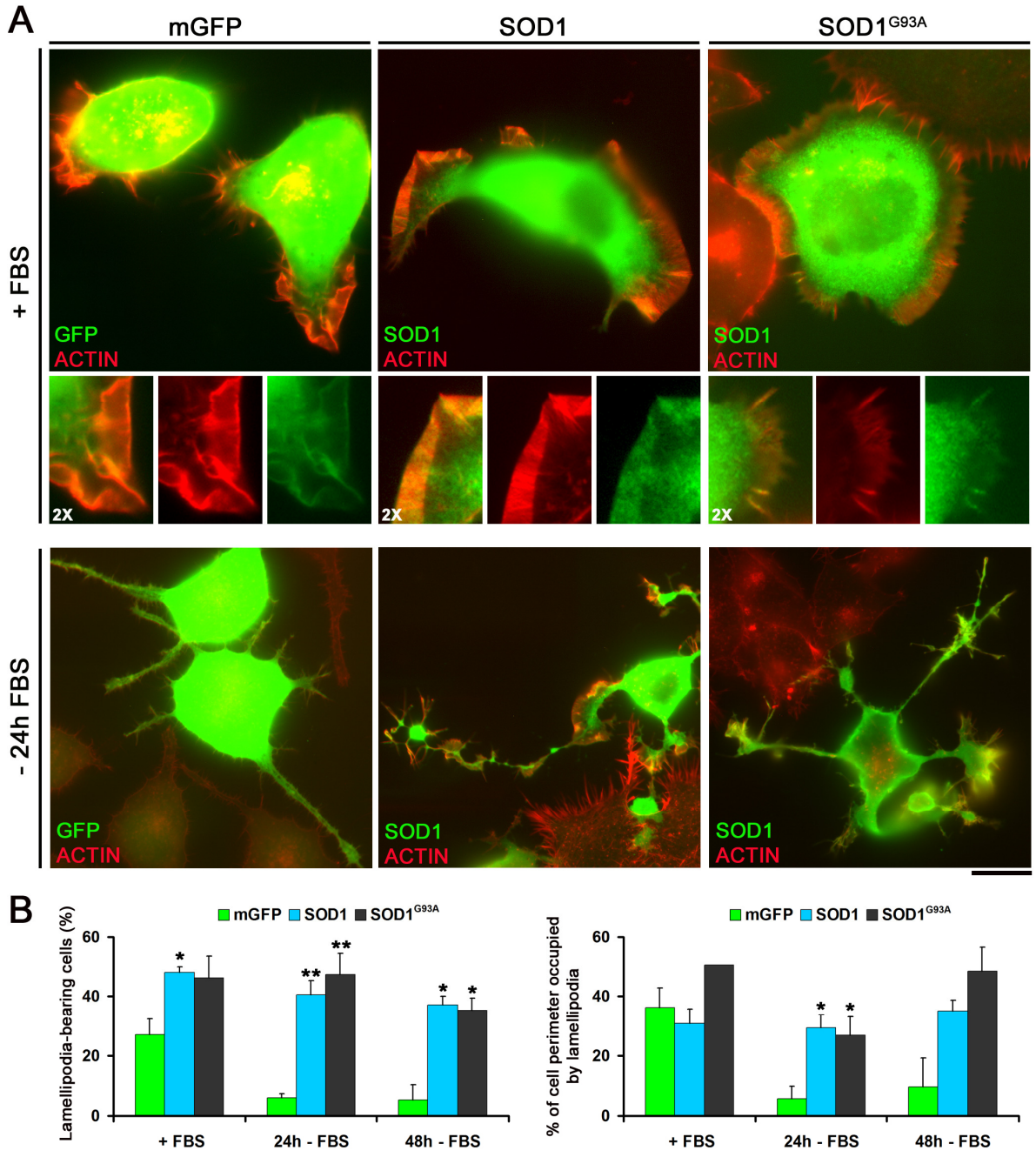

Figure 8

Figure 8: Overexpression of SOD1 or SOD1^{G93A} induces the extension of lamellipodia in both undifferentiated or differentiated N2A cells. (A) Wide-field microscopy of N2A cells transfected with mGFP, SOD1 or SOD1^{G93A}. Twenty-four hours after transfection the culture medium was changed with fresh medium containing either 15% FBS (+ FBS) or no serum (-FBS) and cells were cultured for additional 24-48 hours. Cells were then fixed and stained with anti-SOD1 (green) or Phalloidin to visualize F-actin (red). A 2X individual staining magnification is shown. Scale bar; 10 µm. **(B)** The histograms represent quantifications of the percentage of cells bearing lamellipodia (*n*>120 cells

from 3 independent experiments) and the mean percentage of cell perimeter occupied by lamellipodia (*n*>20 cells from 2 independent experiments). Data are presented as the mean ± s.e.m. *P*-values (*t*-test): ***P*<0.05, ****P*<0.01 and *****P*<0.001.

The analysis of undifferentiated cells and their corresponding quantifications (Fig. 8 A,B), indicate an increase in the percentage of lamellipodia-bearing cells in SOD1-transfected cells compared to control cells, which were transfected with a GFP fused to a PM localisation signal (mGFP). On the contrary, the average number of filopodia per 100 µm of PM did not increase significantly in SOD1-transfected cells compared to control (not shown). Upon serum deprivation the percentage of lamellipodia-bearing cells dropped to under 10% in mGFP transfected cells, while it remained to ~ 40% in SOD1-transfected cells. Moreover, in differentiated SOD1-overexpressing N2A cells, the extension of lamellipodia was not restricted to the growth cone, as lamellipodia could also be detected along neurite shafts. It is interesting to note that no significant differences could be seen between the overexpression of WT SOD1 and $SOD1^{G93A}$, either because the mutation did not impair the lamellipodia-inducing activity of SOD1, or because the experimental conditions were not appropriate to reveal dysfunctions of the mutant.

5.2.2 IRSp53 and LIN7 are involved in SOD1-induced, Rac1-dependent lamellipodia extension in N2A cells

In order to demonstrate Rac1 involvement in SOD1-induced lamellipodia, we co-transfected N2A cells with SOD1 (either WT or G93A) and a

dominant negative mutant of Rac1, HA-Rac1-N17. Twenty-four hours after transfection cells were fixed and scored for the presence of lamellipodia.

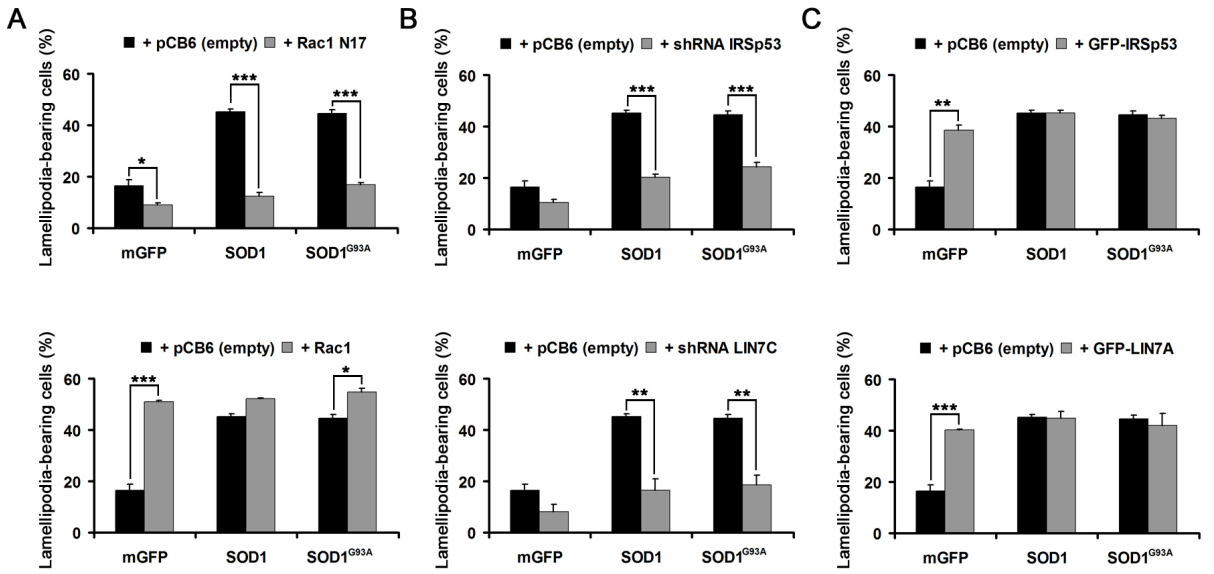

Figure 9

Figure 9: IRSp53 and LIN7 are involved in SOD1-induced, Rac1-dependent lamellipodia extension in N2A cells. (A-C) Histograms representing quantifications of the percentage of lamellipodia-bearing cells 24 (A,C) or 48 hours (B) after co-transfection with the indicated cDNAs. Data are presented as the mean ± s.e.m. *P*-values (*t*-test): **P*<0.05, ***P*<0.01 and ****P*<0.001. Significance between mGFP and SOD1: ***; significance between mGFP and $SOD1^{G93A}$: ***.

The expression of Rac1-N17 clearly impaired lamellipodia formation both in control mGFP-transfected cells and in cells transfected with SOD1 isoforms, as demonstrated by the dramatic decrease in the percentage of lamellipodia-bearing cells (Fig. 9A). We further analyzed the lamellipodia-inducing capacity of SOD1 compared to that of WT Rac1, as well as the effect of their co-transfection. We found that in cells overexpressing Rac1, either alone or in combination with the SOD1

isoforms, the percentage of cells bearing lamellipodia was slightly but significantly higher than in cells overexpressing the SOD1 isoforms alone. Most importantly, however, the co-expression of Rac1 with the SOD1 isoforms did not have an additive effect on lamellipodia formation compared to the overexpression of Rac1 alone, once again suggesting that the effects of SOD1 overexpression depend on the activation of the Rac1 pathway for lamellipodia formation (Fig. 9A).

Many proteins have been demonstrated to participate in Rac1 pathway for lamellipodia formation (Bisi et al., 2013). Among these proteins, IRSp53 activity has been demonstrated to be essential for lamellipodia formation during haptotaxis, which is the ability of a migrating cell to sense ECM gradients on the substrate (Wu et al., 2012). Having already demonstrated the importance of IRSp53 and its binding partner LIN7 in filopodia and neurite formation, we wondered whether these two proteins may participate also in SOD1-induced, Rac1-dependent lamellipodia formation. To explore this hypothesis, we analyzed the percentage of lamellipodia-bearing cells in N2A cells co-transfected with SOD1 (WT or G93A) and a shRNA against either LIN7 or IRSp53. Downregulation of either LIN7 or IRSp53 was able to decrease in the percentage of lamellipodia-bearing cells both in control and SOD1-transfected cells, although not to the extent of that obtained by Rac1 inhibition (Fig. 9B), suggesting either an incomplete downregulation of the two proteins, or that a Rac1-mediated pathway that is independent of IRSp53 and LIN7 activity do exist in these cells. To further confirm the involvement of IRSp53 and LIN7 in lamellipodia formation, we analyzed

the effect of the co-expression of either LIN7 or IRSp53 with SOD1 isoforms. We found that, although IRSp53 and LIN7 overexpression did induce a significant increase in the percentage of lamellipodia-bearing cells compared to control, their co-expression with SOD1 did not have any additive effect on lamellipodia formation (Fig. 9C), once again suggesting that the three proteins work in the same pathway.

5.2.3 SOD1 overexpression induces neurite outgrowth in undifferentiated N2A cells

In differentiating neuronal cells lamellipodia and filopodia are required for the first steps of differentiation, when the cell has to initiate and subsequently elongate neurites in specific directions. Given that the overexpression of SOD1 was able to induce lamellipodia extension in more than 40% of transfected cells both in undifferentiating and differentiating conditions, we investigated whether the overexpression of SOD1 (either WT or G93A) could induce neurite outgrowth in N2A cells grown in 15% FBS, as well as the effect of SOD1 overexpression upon serum starvation.

Figure 10: SOD1 overexpression induces neurite outgrowth in undifferentiated N2A cells. (A) Wide-field microscopy of N2A cells transfected with mGFP, SOD1 or $SOD1^{G93A}$ and cultured in either 15% FBS (+ FBS) or no serum (-FBS for additional 24-48 hours before fixation. The Adobe Photoshop filter emboss was applied. Scale bar: 20 µm. **(B)** A representative image of N2A cells in various stages of differentiations, before and after skeletonization with ImageJ. **(C)** Graphs representing quantifications of the percentage of cells bearing lamellipodia (left) and the ratio between differentiated and undifferentiated cells (left) under different culture conditions (40 cells per experiment, from at least 2 independent experiments). Data are presented as the mean ± s.e.m. P-values (t-test): **P*<0.05, ***P*<0.01 and ****P*<0.001.

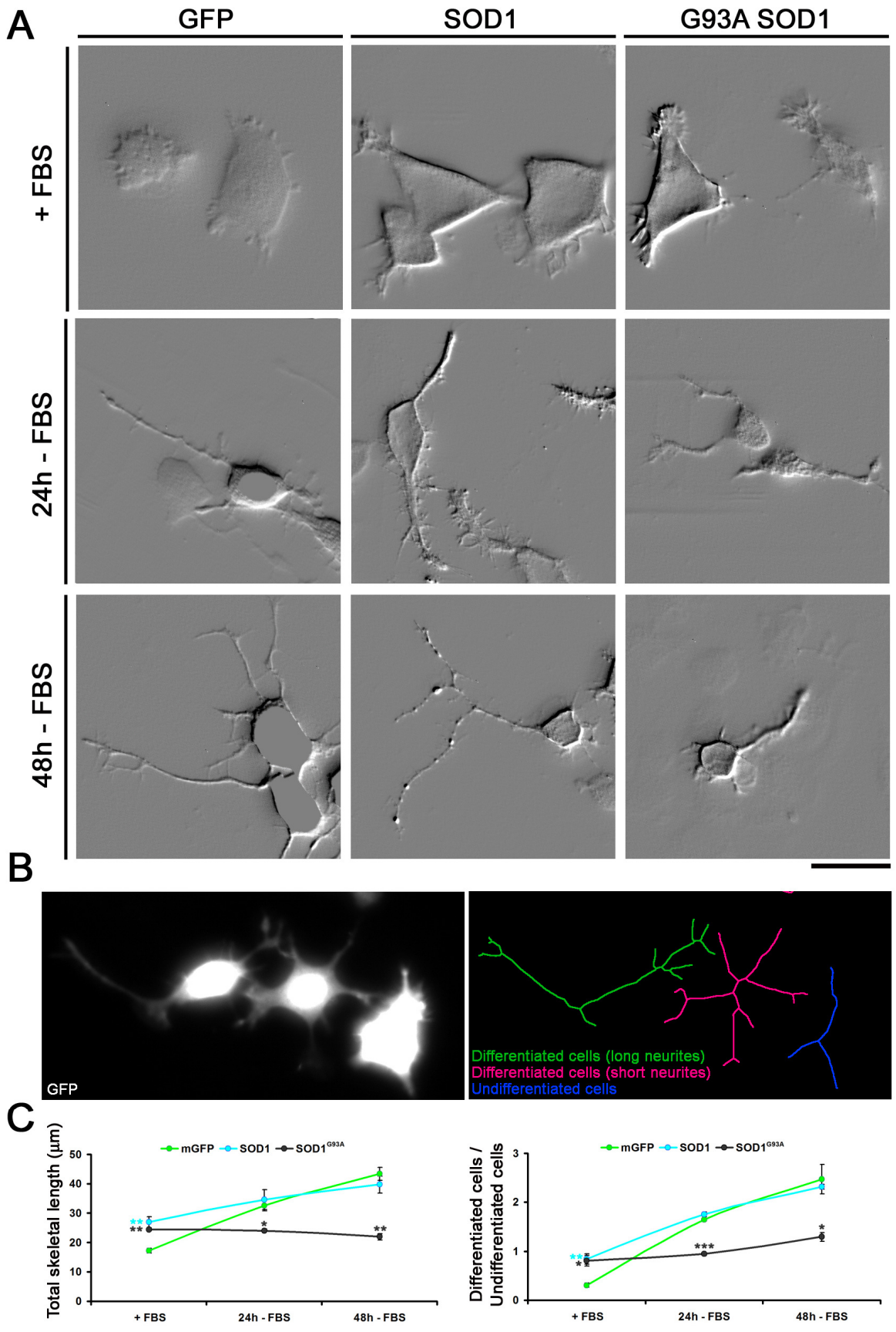
A
GFP
SOD1
G93A SOD1
+ FBS
24h - FBS
48h - FBS
B
GFP
Differentiated cells (long neurites)
Differentiated cells (short neurites)
Undifferentiated cells
C
Total skeletal length (µm)
mGFP
SOD1
SOD1G93A
+ FBS
24h - FBS
48h - FBS
Differentiated cells / Undifferentiated cells

Figure 10

To this end, N2A cells were transfected with mGFP or with cDNAs encoding for either SOD1 or $SOD1^{G93A}$, and 24 h after transfection the cells were further cultured either in 15% FBS for 24 hours or in serum-free medium for 24-48 hours. To assess neuronal differentiation, we quantified the ratio between differentiated (with long or short neurites) and undifferentiated (round) cells, as well as their total skeletal length (see Fig. 10B for a representative image).

In undifferentiating conditions (+ FBS), the overexpression of SOD1 isoforms induced a significant increase of both parameters, in agreement with the hypothesis that an increase in membrane dynamics has a positive effect on neuronal differentiation (Fig 10 A,C).

When differentiation was induced by serum deprivation, WT SOD1-expressing cells started to differentiate at the same rate of mGFP-transfected cells, indicating that the overexpression of SOD1 is neither able to exert a positive effect on neurite outgrowth in differentiating conditions, nor to inhibit it. The overexpression of $SOD1^{G93A}$, on the other hand, did exert a negative effect on N2A differentiation upon serum starvation (Fig 10 A,C). A possible explanation for this result is that the longer transfection times (up to 72 hours) used in these experiments to follow neuritogenesis, as well as the stress caused by culturing in the serum free medium might have uncovered $SOD1^{G93A}$-induced cell toxicity, otherwise unnoticed in the previous experiments.

These preliminary data seem to support a role for SOD1-Rac1 interaction also in neuronal cells. Further data resulting form this study may possibly uncover a differential regulation of Rac1 exerted by mutant SOD1

compared to the WT, and would characterize Rac1 as a key molecule in the pathogenesis of ALS, thus identifying its pathway as a novel therapeutic target in ALS, and suggesting that other regulators of this Rho GTPase, such as IRSp53 and LIN7 themselves, might be good candidates in the quest to broaden the genetic spectrum of this disease. On this respect, it is important to note that alterations in the levels of IRSp53 or LIN7 have also been reported in other neurodegenerative diseases such as Huntington's Corea (Zucker et al., 2010) and Alzheimer disease (Zhou et al., 2013).

CHAPTER 6

LIN7 and IRSp53 participate in the regulation of mitochondrial morphology in HeLa cells

6.1 Summary

Eukaryotic cells strictly regulate the overall morphology of their mitochondrial network thanks to the existence of protein complexes able to assemble on the mitochondrial membranes and to control fission and fusion events.

Recently, we found that endogenous LIN7 and IRSp53 localized in punctuate structures along mitochondria, a fact that prompted us to further investigate the possible effects of modifications in the expression levels of IRSp53/LIN7 on mitochondrial morphology. We found that, upon overexpression of LIN7 and/or IRSp53, mitochondria morphology was altered, with a significant increase in the percentage of cells showing a less interconnected mitochondrial network compared to GFP-transfected control cells, a phenotype that was blocked by co-expression of the K38A dominant negative mutant of the fission protein Drp1. Downregulation of endogenous LIN7 and/or IRSp53 by shRNA, on the other hand, increased the amount of cells with highly fused mitochondria. Mitochondria hyperfusion in the downregulated cells was associated with an increased resistance to NaN_3-induced mitochondrial fragmentation, and by the appearance of cells with aberrantly shaped and often multi-lobed nuclei, a phenotype that we also found in Drp1 K38A-expressing cells, and has already been reported to be caused by defective mitochondrial fragmentation during mitosis. Our data strongly

suggest a Drp1-dependent function of LIN7 and IRSp53 on mitochondrial division apparatus.

Taken together, our data unravel a role of the IRSp53-LIN7 complex on membrane dynamics that is not restricted to the plasma membrane alone, as we previously thought, but may also apply to other cellular mechanisms that heavily rely on membrane deformation, as the data on mitochondrial morphology have demonstrated.

6.2 Brief introduction

Within the cell environment mitochondria are organized in an integrated ever-changing network, whose overall morphology at any specific time-point can be considered as the result of a continuous flux between two extreme states: a reticular network of fused mitochondria and a fragmented state. The balance between these two situations is controlled by proteins involved in fission and fusion events, whose work is tightly regulated in response to physiological and environmental conditions (Rafelski et al., 2013).

The regulation of mitochondrial fusion and fission is controlled by the coordinated action of a series of well-conserved GTPases (Chan, 2012). Fusion of the outer mitochondrial membrane is mediated by the GTPases Mfn 1 and 2, which are able to form complexes in *trans* between adjacent mitochondria and pull the juxtaposing membranes together with a SNARE-like mechanism (Santel and Fuller, 2001; Hoppins et al., 2007;

Chen et al.,2003). A third GTPase, OPA1, localizes to the inner mitochondrial membrane, where it facilitates its fusion in a mechanism not dissimilar from that of Mitofusins (Hoppins et al., 2007; Alexander et al., 2000). Mitochondrial fission, on the other hand, is driven by the cytosolic GTPase DRP1 (Bleazard et al., 1999), whose recruitment to mitochondria in mammalian cells depends on integral outer mitochondrial membrane (OMM) proteins acting as its receptors (Loson et al., 2012). Upon recruitment to a mitochondrion, DRP1 monomers will assemble around it into extended helices, which will then constrict in order to sever both the outer and inner mitochondrial membrane (IMM) (Youle and Karbowski 2005, Ingerman et al., 2005).

Structural analysis of the Drp1 ring, however, estimated its maximum diameter to be around 30–50 nm, thus smaller than the diameter of the mitochondrion, suggesting that some other pre-constriction factors may be needed before Drp1 can assemble around mitochondria (Smirnova et al., 2001; Ingerman et al., 2005).

More recently, it was suggested that actin polymerization mediated by INF2, a formin associated to the endoplasmic reticulum (ER), might provide the pushing force that constricts mitochondria to a diameter consistent with that of the Drp1 ring (Korobova et al., 2013). Further evidence of a role of actin polymerization in membrane fission was provided in a recent paper in which myosin II-mediated constriction of actin filaments was demonstrated to provide further mechanical force for membrane deformation (Korobova et al., 2014; Pon et al., 2014). Furthermore, the possible existence of additional factors controlling pre-

constriction have been suggested by Hatch and colleagues (Hatch et al., 2014). In respect to that, proteins able to induce changes in membranes shape and curvature are largely recognized as major determinants in processes that heavily rely on membrane deformation, such as mitochondrial fission itself. Among such proteins, of particular interest is IRSp53. Such protein, in fact, possesses both an inverted BAR domain, which is able to bind to membranes rich in PtdIns(4,5)P_2 and push them into negatively curved structures, and a SH3 domain for the interaction with various actin regulators. The co-existence of such domains in the same protein enables IRSp53 to couple membrane deformation with actin dynamics, making it a possible candidate also in mitochondrial dynamics.

Localization of IRSp53 on mitochondria has never been reported, but Rosivatz and colleagues demonstrated that PtdIns(4,5)P_2 is also present on the OMM (Rosivatz et al., 2010). Moreover, IRSp53 downstream effector WAVE1 has already been reported to localizes to the OMM (Danial et al., 2003) and has been proposed to control depolarization-induced mitochondrial movement into dendritic spines (Sung et al., 2008). Therefore, we speculated that IRSp53, and possibly its partner LIN7, may localize to and exert a role on mitochondria, a hypothesis that we evaluated in HeLa cells.

6.3 Results

6.3.1 LIN7 and IRSp53 localize to mitochondria in HeLa cells

To investigate our hypothesis, we performed immunofluorecence localization experiments in HeLa cells, a widely used model to study mitochondria thanks to their broad cytoplasm, in which mitochondrial morphology is easier to detect. In these cells, staining with either anti-LIN7 or anti-IRSp53 antibodies revealed a fine punctuate staining, that sometimes appeared to be somehow aligned. To evaluate whether at least a fraction of these puncta could possibly localize on mitochondria, subconfluent HeLa cells were stained with the viable cell dye Texas Red-conjugated Mitotracker before fixation and staining with anti-LIN7 or anti-IRSp53 antibodies (Fig. 11 A,B). In agreement with our hypothesis, most of the puncta recognized by either LIN7 or IRSp53 were aligned on Mitotracker-positive structures, as demonstrated by the plot profile graphs and by the ~ 60% colocalization of both proteins with a mitochondrial marker obtained by calculating Manders' Colocalization Coefficient (MCC). As these puncta appeared to be in some cases regularly distributed along the mitochondria tubules, we analyzed the mean distance between adjacent signal peaks, which we calculated to be ~ 1 µm for both proteins, thus suggesting that the two proteins may colocalize also on mitochondria (Fig. 11 B). The mitochondrial localization of LIN7 and IRSp53 by immunofluorecence experiments isn't a peculiarity of Hela cells, as their colocalization with mitochondrial

markers was confirmed also in neuronal-like N2A cells and in subconfluent epithelial MDCK cells (data not shown).

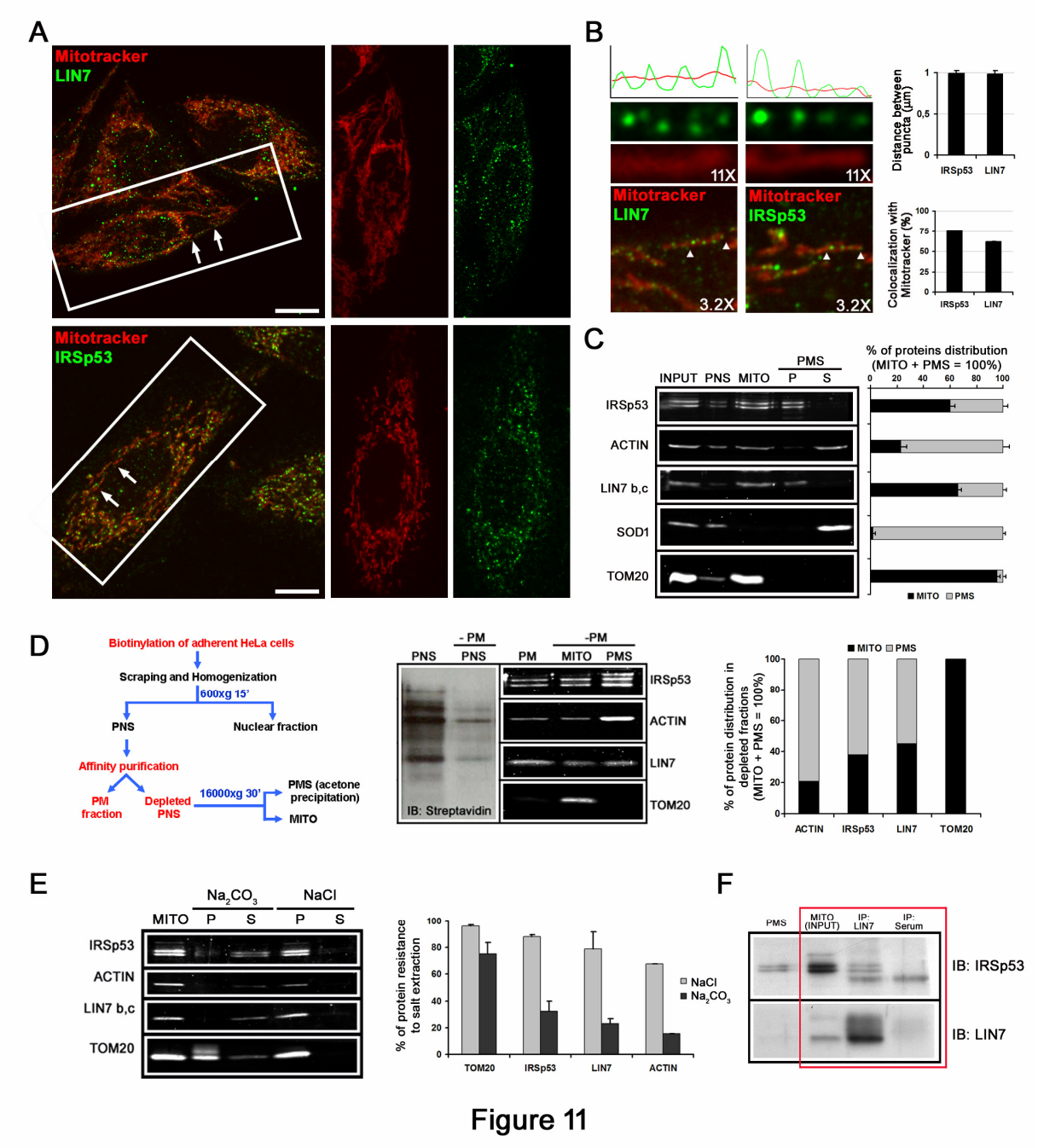

Figure 11

Figure 11: LIN7 and IRSp53 localize to mitochondria in HeLa cells. The subcellular localization of IRSp53 and LIN7 was investigated by immunocytochemistry (A-B) or Western blot (C-F). **(A,B)** Subconfluent HeLa cells stained with Texas Red-conjugated Mitotracker (red) and either anti-LIN7 or anti-IRSp53 antibodies (green). **(A)** Merged images and individual stainings of the boxed cells are shown. Arrows indicate the

location of the area magnified in B. Scale bars: 10 µm. **(B)** Arrowheads in the merged images show the mitochondria further magnified in the individual staining images ad used to generate plot profiles. The reported magnifications refer to the original images in (A). The histograms represent the mean distance between IRSp53/LIN7 puncta along mitochondria measured in ~ 200 µm of mitochondrial network and the percentage of colocalization between LIN7/IRSp53 and a mitochondrial marker obtained by calculating Manders' colocalization coefficient (MCC), respectively. (C) A representative Western blot analysis showing the subcellular distribution of IRSp53 and LIN7 compared to markers of mitochondria (TOM20) and cytosol (SOD1, ACTIN). Equal volumes of mitochondrial (MITO) and post-mitochondrial supernatant (PMS, further subdivided into a membranous **P**ellet fraction and an acetone-precipitated **S**oluble fraction) fractions, or 2% of the INPUT and post-nuclear supernatant (PNS) lysates, were separated using 11% SDS-page, blotted onto nitrocellulose and probed with the indicated antibodies. Proteins distribution in the MITO and PMS fractions (expressed as a percentage of the total MITO+PMS immunoreactivity from at least five independent experiments) is shown. **(D)** Left: schematic representation of the protocol used to deplete the PNS from biotinylated surface proteins and plasma membrane (PM)-associated proteins (left). Middle: Western blot analysis of a PM depletion experiment: equal volumes of the PM, MITO and PMS fractions, or 2% of the non-depleted and depleted PNS, were separated using 11% SDS, blotted, and probed with the indicated antibodies or peroxidase-conjugated streptavidin, respectively. The graph showing proteins distribution in the depleted MITO and PMS fractions (expressed as a percentage of the total MITO+PMS immunoreactivity) is shown on the right. **(E)** Western blot analysis of IRSp53 and LIN7 association with the MITO fraction under salt extraction conditions. Equal amounts of MITO pellets were treated with 0.5 M NaCl or 0.2 M Na_2CO_3 and the resulting pellet (P) and supernatant (S) fractions were probed for the indicated proteins. The percentage of proteins resistant to salt extraction (expressed as a percentage of the total P+S immunoreactivity calculated from two different experiments) is shown in the histogram. **(F)** Co-immunoprecipitation of IRSp53 with LIN7 from the MITO fraction. The MITO fraction obtained from three 100 mm Petri dishes of HeLa cells grown to 80% confluence was immunoprecipitated with anti-LIN7 antibodies (IP: LIN7) or preimmune IgG (IP: Serum). The presence of IRSp53 in the immunocomplexes was determined by immunoprobing the nitrocellulose membranes with anti-IRSp53 antibodies (IB: IRSp53), while immunoprecipitation of LIN7 was verified by using anti-LIN7 antibodies (IB: LIN7).

To further confirm the mitochondrial localization of LIN7 and IRSp53 we went on to perform cell fractionation experiments in subconfluent Hela cells. Confirming the immunoflorecence experiments, we found that ~ 55 % of IRSp53/LIN7 signal recovered in the post-nuclear supernatant (PNS)

co-fractionated in a crude mitochondrial fraction (MITO) with the OMM marker TOM20. What was even more surprising is the fact that virtually no soluble, cytosolic signal for both IRSp53 and LIN7 could be detected (Fig. 11 C). Upon ultracentrifugation of the post mitochondrial supernatant (PMS), in fact, signals for LIN7 and IRSp53 could be detected only in the pellet (P), which is known to contain smaller organelles and PM residues. This evidence underlies the high degree of affinity of IRSp53 and LIN7 for cell membranes.

Possible contaminations of the crude mitochondrial fraction by soluble proteins or smaller organelles were verified by the absence of any signal for the soluble protein SOD1 or for the β1 subunit of the Na, K-ATPase (not shown). As both IRSp53 and LIN7 are known to localize to the plasma membrane (PM), the possibility that the signal for IRSp53 and LIN7 in the MITO fraction was only an artifact due to PM contamination also had to be excluded. Because specific PM markers are missing in Hela cells, to solve this problem we decided to add a PM depletion step in our fractionation protocol. To do so, we biotinylated subconfluent HeLa cells with impermeant Sulpho NHS-LC-biotin before lysis and, by means of a streptavidin magnetic beads isolation protocol, the biotinylated PM proteins were used to deplete the PNS from the sheets of plasma membrane to whom such proteins were attached (Zhao Y.et al., 2004; see materials and methods and Fig. 11 D for a schematic representation). The streptavidin beads efficiently retained biotinylated proteins (PNS depletion >85%), and proteins associated to the PM such as LIN7, IRSp53 and actin could also be recovered in the PM fraction. Most importantly, a

consistent amount of LIN7 and IRSp53 was still present in the mitochondrial fraction, despite the almost complete depletion of surface biotinylated proteins (Fig. 11 D). These results further indicate a true mitochondrial association of LIN7 and IRSp53 and exclude that their signals in the crude mitochondrial fraction is due to contamination of PM.

Once sure of this, we sought to better characterize LIN7 and IRSp53 localization on mitochondria by salt-extraction experiments. As washing of the MITO pellet with carbonate, but not NaCl, was able to detach LIN7 and IRSp53 from the pellet itself, it is possible to conclude that both IRSp53 and LIN7 are peripheral proteins tightly associated to the OMM (Fig. 11 E).

To conclude our localization experiments, we performed an immunoprecipitation experiment, using either the anti-LIN7 antibody or a rabbit preimmune serum, on a solubilized MITO fraction obtained from subconfluent HeLa cells. The anti-LIN7 antibody, but not the pre-immune serum, was able to immunoprecipitate IRSp53 doublet, thus strongly indicating LIN7-IRSp53 association also on the OMM.

6.3.2 Overexpression of LIN7 and/or IRSp53 induces mitochondrial fragmentation in HeLa cells

The morphology of the mitochondrial network changes constantly within a given cell, and is the result of two highly regulated activities:

mitochondrial network remodelling and motility (Palmer et al., 2011; van der Bliek et al., 2013). It is widely reported in literature that altering the equilibrium of these two processes, for example by modifying the expression levels of proteins involved in either fusion or fission, can have huge effects on the overall morphology of the mitochondrial network and, consequently, on cell physiology itself (Mozdy and Shaw, 2003; Osteryoung and Nunnari, 2003). In order to unravel the possible role of LIN7 and IRSp53 localization on mitochondria, we started by analyzing whether their transient overexpression in HeLa cells might have any effect on mitochondria morphology and/or localization inside the cytoplasm.

Figure 12: Overexpression of LIN7 and/or IRSp53 induces mitochondrial fragmentation in HeLa cells. (A) Laser confocal microscopy of HeLa cells transfected with GFP-IRSp53 (green) ans stained with Texas Red-conjugated Mitotracker (red). Magnifications of the boxed areas are shown on the right. The diffuse green signal in those magnifications was partially removed by using the 'subtract background' function from ImageJ. The plot profile represents signal distribution along the magnified mitochondrion whose position in the image is indicated by arrowheads. Scale bar: 10 µm. **(B)** Four cartoon cells representing the typical morphology of transfected cells belonging to a certain category are shown along with a table that summarizes the main mitochondrial features of each category. **(C)** Laser confocal microscopy of HeLa cells transfected with the pSUPER empty vector (encoding for GFP), or double tranfected with GFP-LIN7 and a pCB6 empty vector, GFP-IRSp53 and a pCB6 empty vector, or GFP-IRSp53 and GFP-LIN7. Transfected cells are outlined by the green dotted lines. The RGB original images are presented in the insets (3X smaller). The histogram represents the scoring of mitochondrial network morphologies for each transfectant (n>120 cells from 3 independent experiments). **(D)** A magnified region of interest (ROI) cropped from each image shown in C is presented, along with its false-coloured mask generated with ImageJ as described in Materials and Methods. The box and whiskers plot and the histogram represent the distribution of the average mitochondrial length and the mean longest mitochondrion calculated from at least 25 ROIs (from at least 3 independent experiments) similar to those presented in this figure. Data are presented as the mean ± s.e.m. P-values (t-test): *P<0.05, **P<0.01 and ***P<0.001.

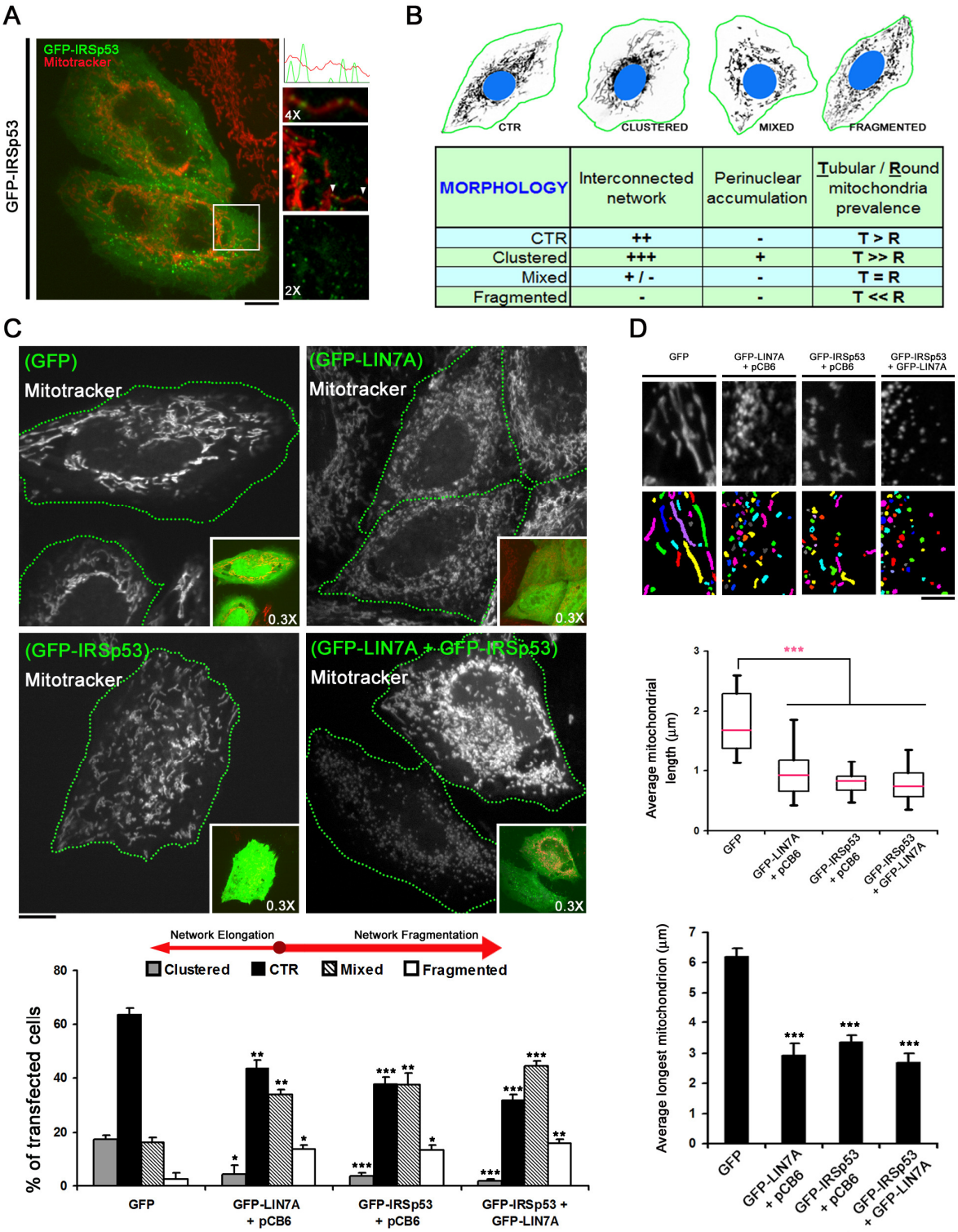
A
GFP-IRSp53
Mitotracker
GFP-IRSp53
4X
2X
B
CTR
CLUSTERED
MIXED
FRAGMENTED
MORPHOLOGY | Interconnected network | Perinuclear accumulation | Tubular / Round mitochondria prevalence
CTR | ++ | - | T > R
Clustered | +++ | + | T >> R
Mixed | + / - | - | T = R
Fragmented | - | - | T << R
C
(GFP)
Mitotracker
(GFP-LIN7A)
Mitotracker
(GFP-IRSp53)
Mitotracker
(GFP-LIN7A + GFP-IRSp53)
Mitotracker
0.3X
Network Elongation
Network Fragmentation
Clustered
CTR
Mixed
Fragmented
% of transfected cells
GFP
GFP-LIN7A + pCB6
GFP-IRSp53 + pCB6
GFP-IRSp53 + GFP-LIN7A
D
GFP
GFP-LIN7A + pCB6
GFP-IRSp53 + pCB6
GFP-IRSp53 + GFP-LIN7A
Average mitochondrial length (µm)
Average longest mitochondrion (µm)

Figure 12

To this purpose, HeLa cells where transfected on two consecutive days with either LIN7, IRSp53 or both, and 48 hours after the first transfection cells where stained with Texas Red-conjugated Mitotracker and fixed so that their mitochondrial morphology could be assessed. First of all, we analyzed by confocal imaging whether the GFP-tagged overexpressed constructs could be detected on mitochondria. The signal of GFP-IRSp53 was largely diffused in the cytoplasm with a slight PM enrichment detectable in most cells, but puncta aligned along Mitotracker-positive mitochondria could be detected in some cells (Fig 12 A). On the contrary, GFP-LIN7 puncta along Mitotracker-positive structures were never observed, perhaps due to its lower mitochondrial association or higher overexpression masking the association.

To evaluate possible effects of IRSp53 and/or LIN7 on mitochondrial morphology, cells were subdivided into four categories as follows: CTR = extended network of tubular mitochondria, distributed all through the cytoplasm; CLUSTERED = highly interconnected mitochondria, often accumulated in the perinuclear area of the cell; MIXED = the mitochondrial network is partially lost in favor of smaller, often misshaped, individual mitochondria; FRAGMENTED = the mitochondrial network is mostly fragmented into dot-like organelles (Fig. 12 B) (Loson et al. 2012, Smirnova et al., 2011). By applying this morphology scoring method to transfected cells, we were able to find that overexpression of LIN7 and/or IRSp53 caused a significant increase in the percentage of cells showing a less interconnected mitochondrial network compared to GFP-transfected control cells. . The mitochondrial morphology resulted

similarly altered by changing the expression levels of either one or both proteins, thus suggesting that they form a functional complex in mitochondria. Such observations were confirmed by the analysis of mitochondrial length parameters conducted with ImageJ on random regions of interest (ROIs) selected in the cells periphery of transfected cells, where mitochondria outlines can be readily resolved. A two-fold highly significant decrease in both the average mitochondrial length and average longest mitochondrion per ROI was measured in cells overexpressing LIN7 and/or IRSp53 compared with the GFP transfected cells.

It is interesting to note that overexpression of two deleted IRSp53 constructs, the myc-IRSp53Δ5 construct deleted of the specific domain for LIN7 association and the myc-IRSp53ΔSH3 construct deleted of the specific domain for interaction with actin regulators (Crespi et al., 2012) failed to induce mitochondrial fragmentation (data not shown), indicating that both IRSp53 capacity to induce actin polymerization through interaction with its partners and IRSp53 association with LIN7 are required for the induction of mitochondrial fragmentation, further suggesting a role for the IRSp53-LIN7 complex in regulating mitochondrial dynamics.

6.3.3 Downregulation of LIN7 and/or IRSp53 induces mitochondrial network elongation in HeLa cells

Given the results obtained by overexpression of either LIN7, IRSp53 or both, we investigated whether their downregulation would have an

opposite effect on mitochondrial network morphology, as positive results would not only strengthen our observations, but also rule out the possibility that data obtained by overexpression were only artifacts due to any kind of toxicity mechanisms. To this end, we transiently transfected HeLa cells with shRNA constructs against IRSp53 (Disanza et al., 2006) and LIN7C, the most abundantly expressed LIN7 isoform in HeLa cells according to the Human Protein Atlas.

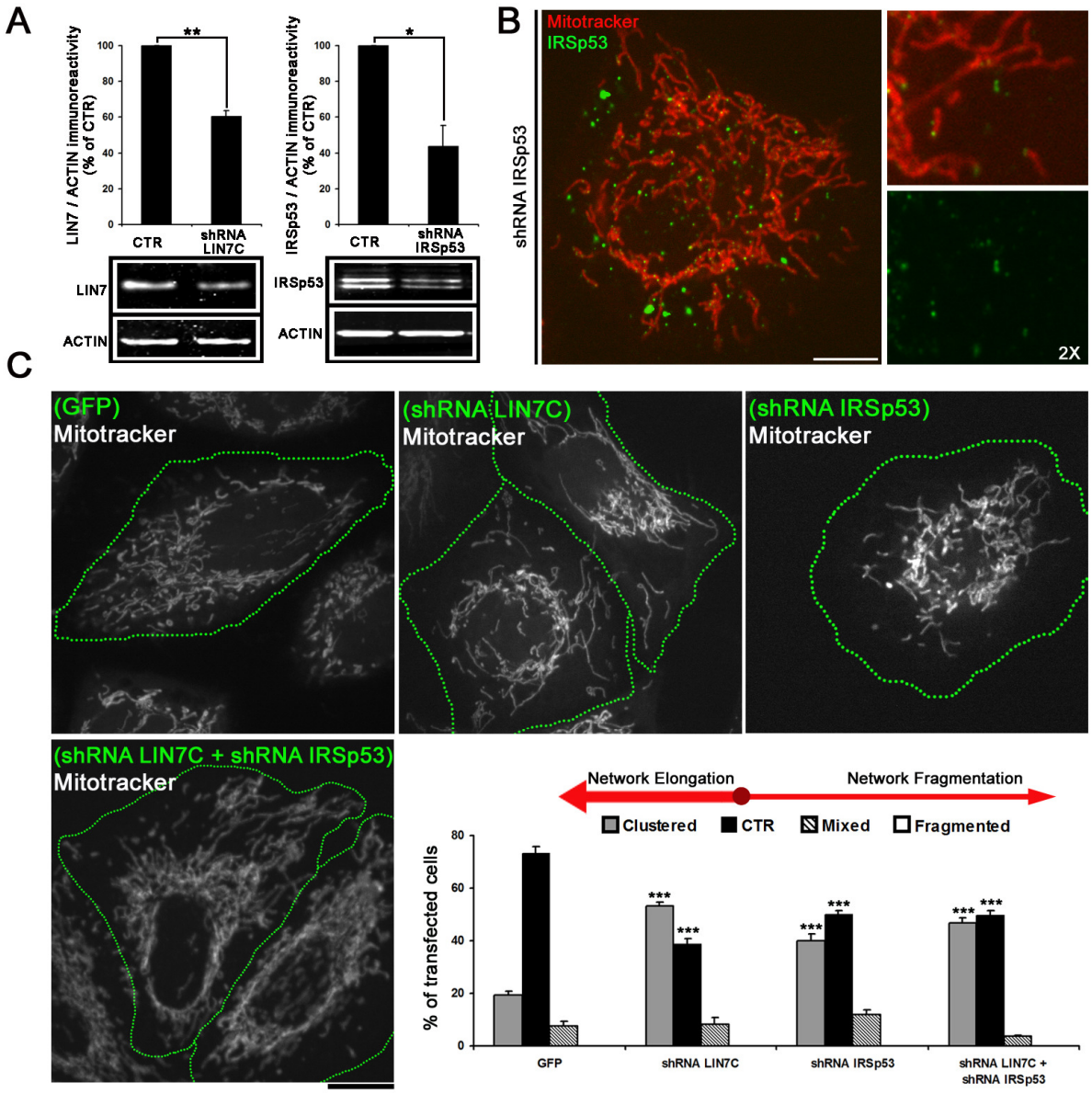

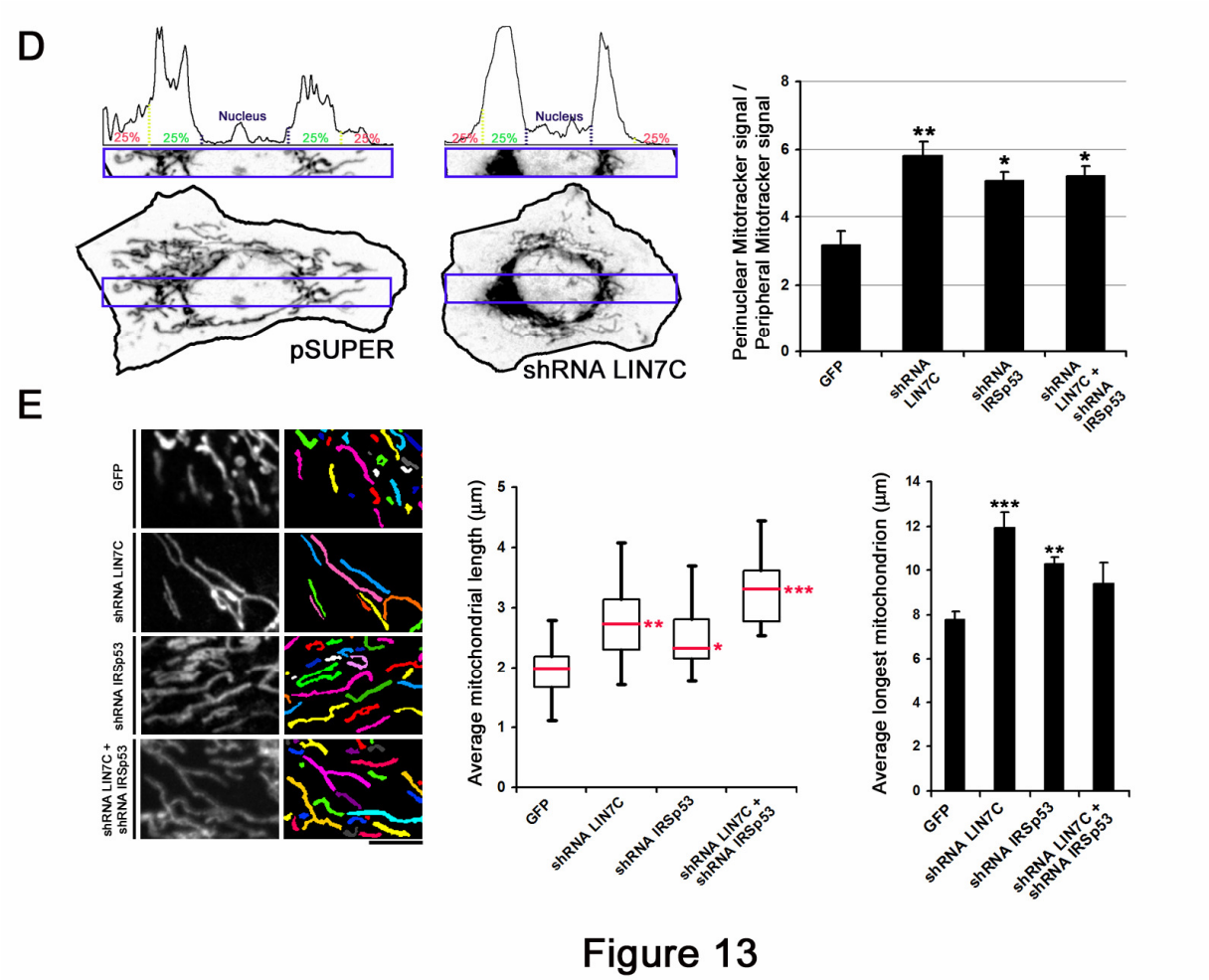

Figure 13

Figure 13: Downregulation of LIN7 and/or IRSp53 induces mitochondrial network elongation in HeLa cells. (A) Two representative Western blots showing downregulation of LIN7C and IRSp53 in HeLa cells transiently transfected with shRNA LIN7C and shRNA IRSp53, respectively The histograms representing the percentage of LIN7/IRSp53 in silenced cells normalized to ACTIN and compared with control was obtained by densitometric quantification of two independent experiments. **(B)** Laser confocal microscopy of a HeLa cell transfected with the shRNA against IRSp53 and stained with Texas Red-conjugated Mitotracker (red) and the anti-IRSp53 antibody (green). A 2X individual staining magnification is shown. Scale Bar: 10 µm. **(C)** Laser confocal microscopy of HeLa cells transfected with the pSUPER empty vector (encoding for GFP), shRNA LIN7C, or double transfected with shRNA IRSp53 and the pSUPER empty vector or shRNAs for both IRSp53 and LIN7. Transfected cells are outlined by the green dotted lines. The histogram represents the scoring of mitochondrial network morphologies for each transfectant (*n*>120 cells from 3 independent experiments). **(D)** A graphical representation, and corresponding quantification, showing different mitochondrial distribution inside either a GFP- or shRNA LIN7C- transfected cells and the resulting densitometry plots. **(E)** A magnified region of interest (ROI) cropped from each image shown in C is presented along with

its false-coloured mask generated with ImageJ as described in Materials and Methods. The box and whiskers plot and the histogram represent the distribution of the average mitochondrial length and the mean longest mitochondrion calculated from at least 25 ROIs (from at least 3 independent experiments) similar to those presented in this figure. Data are presented as the mean ± s.e.m of at least three independent experiments. *P*-values (*t*-test): **P*<0.05, ***P*<0.01 and ****P*<0.001.

A 30-40% reduction in the expression levels of both LIN7 and IRSp53 bands was observed by Western Blot analysis in HeLa cells lysed 48-72 hours after transfection with either shRNA LIN7C or shRNA IRSp53, respectively (Fig. 13 A). Reduction in IRSp53-positive puncta density along mitochondria of cells downregulated for IRSp53 was also observed by confocal imaging (Fig. 13B).

In agreement with our hypothesis, we found that downregulation of either LIN7C, IRSp53 or both increased the percentage of cells bearing a more elongated, tangled mitochondrial network morphology (Fig 13 C). In those cells, mitochondria also often appeared to be clustered in the perinuclear region of the cell, as demonstrated by the two-fold increase in the Mitotracker signal ratio between the perinuclear area and the cell periphery calculated by densitometric analysis (Fig. 13 D). This clusterization could easily be explained by the fact that the longer mitochondria are, the harder it is to transport and spread them in the cytoplasm. The elongation phenotype observed in LIN7C and/or IRSp53 downregulated cells is consistent with published data obtained by silencing proteins involved in mitochondrial fission (Karbowski et al 2004; Gandre-Babbe and van der Bliek 2008, Otera et al., 2010, Loson et al 2013).

The increase in mitochondrial network elongation observed in downregulated cells by morphometric analysis was once again confirmed by the measurement of mitochondrial length parameters. A significant increase in both average mitochondrial length and average longest mitochondrion per ROI was observed in LIN7 and/or IRSp53 downregulated cells, compared to GFP-transfected controls (Fig. 13 E). It is important to note that the measurements we obtained, especially in the case of the longest mitochondrion parameter, are probably slightly underestimating of the actual mitochondrial length change, as some of the mitochondria in downregulated cells became too long to fit our ROIs, with one extremity being obscured in the perinuclear region.

6.3.4 Functional consequences of altered expression of LIN7 and/or IRSp53 in Drp1-mediated mitochondrial fission

The results we obtained with either overexpression or downregulation of LIN7 and/or IRSp53 are all consistent with a possible role for the two proteins in mitochondrial fission. Thus, to test whether LIN7 and IRSp53 effect on mitochondrial morphology could be due to an enhanced activity of the Drp1-mediated mitochondrial fission pathway, we co-expressed GFP-LIN7A or GFP-IRSp53 with a dominant-negative mutant of Drp1, in which substitution of lysine 38 for an alanine in the GTPase domain causes a disruption in its enzymatic activity. Such cells displayed an interconnected network of mitochondria identical to that of cells expressing the DN alone, thus indicating that IRSp53- and LIN7-mediated mitochondrial fission is dependent on Drp1 activity, and suggesting that

both proteins may enhance mitochondria fission by acting upstream of Drp1 (Fig. 14 A).

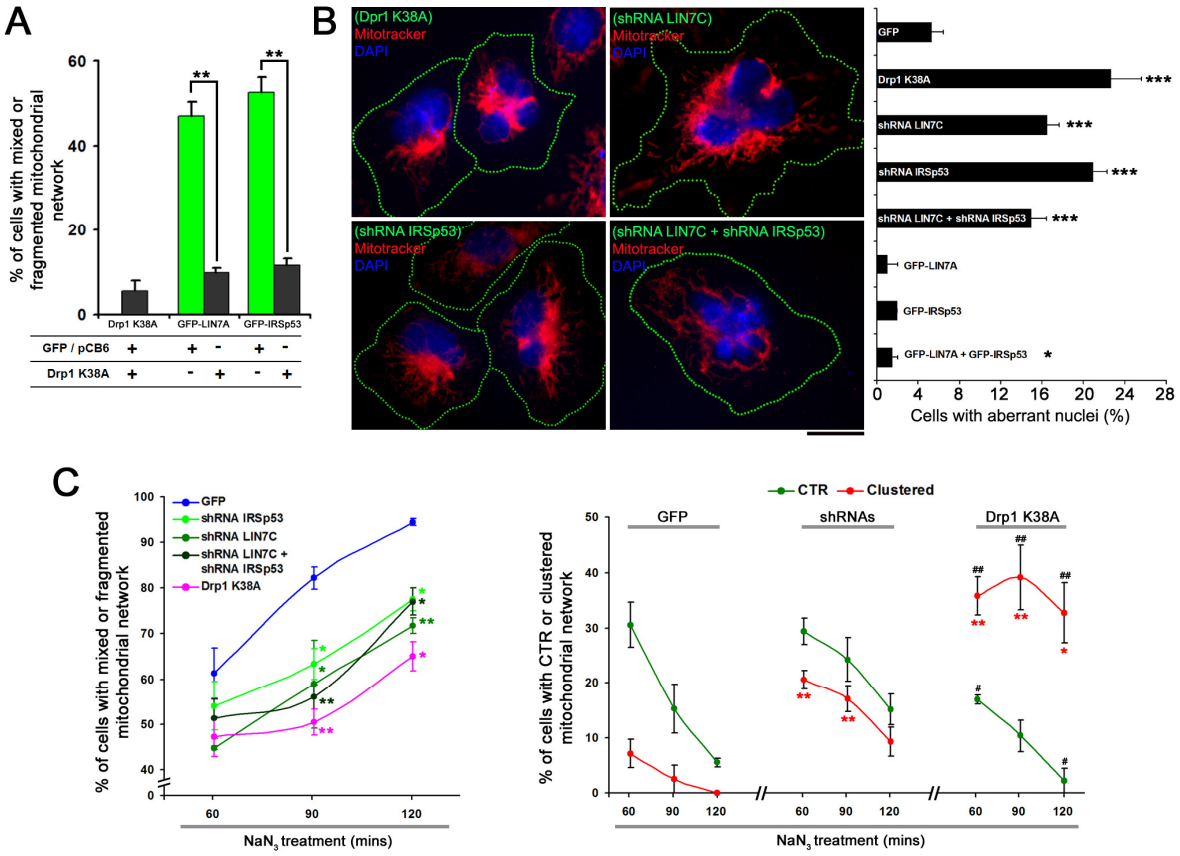

Figure 14

Figure 14: Functional consequences of altered expression of LIN7 and/or IRSp53 in Drp1-mediated mitochondrial fission. (A) Histogram representing the percentage of cells with a Mixed or Fragmenten mitochondrial morphology (*n*>80 cells from 2 independent experiments) after transfection with the indicated constructs. **(B)** Wide-field microscopy of HeLa cells transfected with shRNA LIN7C or double-transfected with HA-Drp1 K38A + GFP, shRNA IRSp53 + GFP or shRNA LIN7 + shRNA IRSp53. Transfected cells are outlined by the green dotted lines. Nuclei were stained with DAPI (blue), and mitochondria with Texas Red-conjugated Mitotracker (red). The histogram represents the % of transfected cells bearing abnormal, often multi-lobed shaped nuclei (n> 120 cells from 3 experiments). **(C)** Two time-course graphs showing the effect of treatment with NaN_3 on HeLa cells tranfected with GFP, the shRNAs against either IRSp53 or LIN7C (or both), or HA-Drp1 K38A + GFP. Cells were treated with 30 mM NaN_3 for the indicated times before fixation with 4% paraformaldehyde and staining with an

antibody against TOM20. Transfected cells were then scored for their mitochondrial network morphologies. The graph on the left shows the increase in the percentage of cells bearing either a mixed or fragmented mitochondrial network morphology over time (n> 80 cells from 2 experiments). Multicoloured asterisks represents the significance between GFP-transfected cells and the other transfectants. The graph on the right shows the decrease in the percentage of cells with a CTR (green lines) or Clustered (red lines) network morphology over time. As the data obtained with the various shRNA combinations were similar, those data were summarized in the 'shRNAs' section of the graph. Red asterisks represent the significance with respect to GFP-transfected cells, while black pounds represent significance between shRNAs- and Drp1 K38A-transfected cells. Data are presented as the mean ± s.e.m. *P*-values (*t*-test): ***P*<0.05, ****P*<0.01 and *****P*<0.001.

Next, we went on to analyze whether we could find any other morphological commonalities between DN Drp1-transfected cells and cells downregulated for IRSp53 and/or LIN7. Drp1-mediated mitochondrial fission is of pivotal importance in many aspects of cell physiology, including at mitosis, where mitochondria fragmentation ensures equal segregation of mitochondria during cell division (Chen et al., 2009). In respect to this, recent papers have in fact shown that inhibition of the fission protein Drp1 causes a delay in G2/M cell cycle progression, coupled with the appearance of cells that are multinucleated or bear abnormally shaped nuclei surrounded by aggregated mitochondria, a phenotype that can be explained by a disruption in cytokinesis progression (Westrate et al., 2014; Qian et al., 2012). Indeed, we measured an increased number of cells showing abnormally-shaped nuclei surrounded by aggregated mitochondria in cells either expressing the Drp1 K38A dominant negative mutant or downregulated for LIN7, IRSp53, or both. On the contrary, a decrease in

aberrant nuclei compared to GFP-expressing cells was observed in cells overexpressing LIN7 and/or IRSp53 (Fig. 14 B). This observation further corroborates our hypothesis that LIN7 and IRSp53 may exert a role in Drp1-mediated fission.

Lastly, having unraveled some similarities between LIN7/IRSp53 downregulation and Drp1 inhibition, we decided to compare the effects of NaN_3-induced mitochondria fragmentation in cells transfected with either the shRNAs against LIN7C/IRSp53 or with DN Drp1. NaN_3 is a an inhibitor of complex IV of the electron transport chain that slows electron transport flux and lowers mitochondrial membrane potential. As mitochondria that lose their membrane potential are unable to fuse back into the mitochondrial network (Twig et al. 2008), treatments with depolarizing compounds, such as NaN_3, will result in the inhibition of fusion and consequent unopposed Drp1-mediated fission (De Vos et al., 2005). As such, treatment with a depolarizing drug can unmask possible defects in the fission machinery in the form of an increased resistance to fragmentation compared to control. Therefore, we treated transiently transfected HeLa cells with 30 mM NaN_3 for 60-120 minutes before fixation and staining with an antibody against TOM20 to detect mitochondrial morphology. Cells expressing the Drp1 DN or silenced for LIN7 and/or IRSp53 displayed higher resistance than GFP-expressing cells to mitochondrial fragmentation (Fig. 14 C, left). After 120 minutes of NaN_3 treatment, in fact, 100% of the control GFP transfected cells exhibited fragmented or mixed morphology, whereas approximately 40% of the cells downregulated for LIN7/IRsp53 or expressing the

dominant negative mutant Drp1 were still protected from fission. However, the behavior of shRNAs transfected cells in response to NaN_3 was partially dissimilar to that of Drp1 K38A transfected cells. Among DN Drp1 transfected cells, in fact, it was possible to identify a subset of cells with a clustered morphology (~30%-35%) that seemed to be totally resistant to mitochondrial fragmentation, even after 120 minutes of NaN_3 treatment. Conversely, in shRNAs transfected cells the percentage of cells showing either a clustered or CTR mitochondrial morphology gradually decreased, albeit at a slower pace compared to GFP-expressing control cells (Fig. 14 C, right), suggesting that fission in the silenced cells is attenuated, but can still occur, probably through Drp1-mediated pathways independent on LIN7 and IRSp53.

6.4 Discussion

Mitochondrial fission is a strictly regulated process which depends on the activity of Drp1, a GTPase protein able to assemble around mitochondria in a helical shape that, upon GTP hydrolysis, will constrict and sever the organelle itself (Youle and Karbowski 2005, Ingerman et al., 2005). It has however been suggested that, for Drp1 to be able to assemble around a mitochondrion, a Drp1-independent pre-constriction step must occur on that mitochondrion, as the maximum diameter of the Drp1 ring was calculated by structural analysis to be smaller than the mitochondrial diameter (Smirnova et al., 2001; Ingerman et al., 2005). So far, actin polymerization mediated by the formin INF2 and myosin II-

mediated constriction of actin filaments have both been suggested to exert their positive role on mitochondrial fission by providing a pushing force that constricts mitochondria to a diameter consistent with that of the Drp1 ring (Korobova et al., 2013; Korobova et al., 2014; Pon et al., 2014). This models are somewhat similar to the ones proposed for leading-edge extension or the initial steps of endocytosis, where actin polymerization provide the mechanical force necessary to bend the PM.

It is widely known that the aforementioned processes strictly depend not only on actin polymerization, but also on the activity of proteins able to induce PM curvature, such as the BAR and I-BAR domain-containing proteins. Being mitochondrial fission a process that heavily relies on membrane deformation, it is conceivable that membrane-deforming proteins might exert a role. A possible candidate for such role could be IRSp53, an I-BAR and SH3 domains-containing protein able to both deform membranes into negatively curved structures and interact with various actin regulators. Indeed, we found that both IRSp53 and its PDZ-binding motif partner LIN7 localize in punctuate structures on the OMM in subconfluent HeLa cells, as revealed by immunofluorescence staining and biochemical fractionation experiments. Colocalization of the two proteins on mitochondria was suggested by their similar distribution on mitochondria, i.e. in distinct puncta spaced by 1 μm, and by their co-immunoprecipitation from crude mitochondrial fractions.

Alterations in the expression levels of both proteins, either alone or in combination, affected the mitochondrial network morphology, with their overexpression inducing mitochondrial network fragmentation and

their downregulation causing network elongation and clusterization in the perinuclear area of the cell. The increase in mitochondrial fragmentation observed upon overexpression of LIN7 and/or IRSp53 is dependent on Drp1, as expression of the dominant negative mutant Drp1 K38A completely abolished LIN7- and IRSp53-mediated fission. This results strongly suggest that the IRSp53-LIN7 complex enhances mitochondria fission by acting upstream of Drp1.

It is important to note, however, that downregulation of LIN7 and/or IRSp53 does not inhibit mitochondrial fission to the same extent as the disruption of Drp1 activity, as clustered/fused mitochondria were observed in 40-50% of cells downregulated for LIN7/IRSp53, compared to almost 90% in cells transfected with DN Drp1. This result could be explained by a lower level of expression or transfection efficiency of the shRNAs. Alternatively, LIN7 and IRSp53 may act as regulators whose impairment does attenuate, but not prevent, Drp1-mediated fission. The latest explanation is supported by the results obtained upon treatment with the fission-inducing drug NaN_3, in which fragmentation was slowed down but not abrogated in IRSp53 and LIN7 downregulated cells. Our results favor a possible role for LIN7 and IRSp53 in facilitating Drp1-mediated fission of mitochondria, but also point out that other proteins may partially substitute them.

IRSp53 and LIN7 localize to mitochondria not only in HeLa cells, but also in other cell types, such as neuronal-like N2A cells and subconfluent MDCK cells. In the latter cell type, mitochondrial localization of IRSp53

and LIN7 is lost when cells reach confluence and start to polarize (Massari et al., 2009) in favor of their localization at the junctional level. It is conceivable that IRSp53-LIN7 mediated fission may be required only in MDCK cells that are still proliferating, and thus in need to ensure mitochondrial inheritance to the daughter cells. When cells switch from proliferation to differentiation, IRSp53 and LIN7 function may be more needed at the junctional level rather than on mitochondria, as senescent cells usually display longer mitochondria (Lee et al., 2007).

Collectively, our data suggest that LIN7 and IRSp53 may have a role on Drp1-mediated fission, perhaps by participating in the generation of pre-constriction sites on mitochondria. The IRSp53-LIN7 complex may either act in concert with or be an alternative mechanism to INF2 and Myosin II pathways for mitochondria pre-constriction that have already been described in literature (Korobova et al., 2013; Korobova et al., 2014). By possessing both an I-BAR domain and a SH3 domain for the interaction with actin regulators, IRSp53 may enhance pre-constriction both by pushing the OMM forward and by enhancing actin polymerization. In this model, LIN7 may have a role in controlling/stabilizing IRSp53 localization to mitochondria, as suggested by the fact that staining of cells downregulated for LIN7C with the anti-IRSp53 antibody revealed how a subset of those cells displayed a decrease in the number and intensity IRSp53-positive puncta along mitochondria (preliminary observations made in both MDCK and HeLa cells; data not shown). Moreover, LIN7 binding partner CASK has recently been found to be localized on mitochondria (Mukherjee et al., 2014), further corroborating

the hypothesis that LIN7 may stabilize IRSp53 localization to mitochondria through interaction with its L27 binding partners.

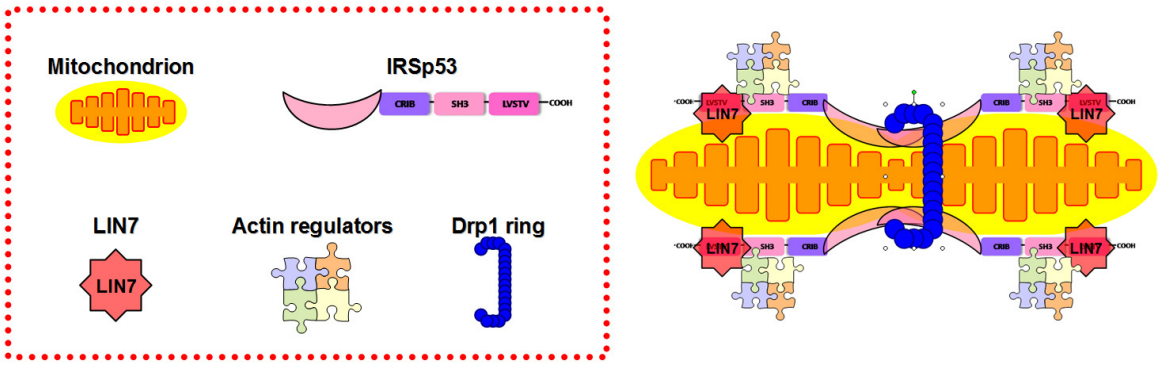

Figure 15

Figure 15: Schematic representation of the possible mechanism of IRSp53-LIN7-mediated pre-constriction of the mitochondrion.

A second possibility we cannot rule out is that the IRSp53-LIN7 complex may have a secondary effect on mitochondrial fission by enhancing mitochondrial trafficking along microtubules. It is in fact known that mitochondrial transport rates and directionality affect mitochondrial morphology (Bowes et al., 2008; Liu et al., 2009), and LIN7 has already been proposed to participate in the trafficking of vesicles containing neurotransmitters receptors along microtubules tracks (Setou et al., 2000). The LIN7-mediated recruitment of IRSp53 at specific mitochondrial sites may therefore contribute to the regulation of mitochondrial morphology either directly, by participating to the Drp1 fission pathway, or through mitochondrial trafficking along microtubules.

In conclusion, our data unravel a role of the IRSp53-LIN7 complex on membrane dynamics that is not restricted to the PM alone, as we previously thought, but may also apply to other cellular mechanisms that heavily rely on membrane deformation, such as mitochondrial morphology itself.

CHAPTER 7

Concluding remarks

7. Concluding remarks

In this study we investigated the role of the IRSp53:LIN7 complex in cellular mechanisms that heavily rely on membrane deformation, such as the formation of filopodia and neurites, or mitochondrial fission. By means of morphological and biochemical experiments, we first of all investigated the role of IRSp53-LIN7 association on filopodia and neurites formation in neuronal-like N2A and NSC34 cells. The data we obtained indicate that LIN7 plays a positive regulatory role on the filopodium- and neurite-promoting activity of IRSp53, and that this regulation depends on both protein-protein association domains of LIN7: the PDZ domain for binding to the last C-terminal residues of IRSp53, and the L27 domain for association with plasma membrane protein complexes. Our results also provided further evidence that neuritogenesis depends on actin-stabilised filopodia.

To investigate the possible role of the complex on other membranous compartments, we performed morphological and localization experiments in HeLa cells, and found that both endogenous LIN7 and IRSp53 localized in punctuate structures along mitochondria, where they seem to exert a role in Drp1-dependent mitochondrial fission. Downregulation of LIN7 and/or IRSp53 induced mitochondria hyperfusion and the appearance of cells with aberrantly shaped and often multi-lobed nuclei, a secondary defect caused by defective mitochondrial fragmentation during mitosis.

Collectively, our data support a crucial role of LIN7 for IRSp53 function, and suggest three different mechanisms by which LIN7 may exert a facilitating role on IRSp53 function.

1. Differential binding of IRSp53 with either LIN7 or other interactors may have a role in controlling/stabilizing IRSp53 localization to its various targets. This hypothesis is supported by the localization experiments conducted in NSC34 cells with the different mutants of IRSp53 and LIN7 (see Fig. 1), in which we saw that the PDZ-binding motif of IRSp53 is essential to guarantee IRSp53 enrichment at the filopodium tip, and that a mutant of LIN7 lacking the L27 domain was able to sequester overexpressed IRSp53 in the cytosol. Moreover, downregulation of LIN7 in HeLa cells seems to partially disrupt IRSp53 localization to mitochondria (preliminary data, not shown), strengthening the hypothesis that binding to LIN7 may regulate and stabilize IRSp53 localization in various compartments.

2. It is known that, when not bound to a Rho GTPase, IRSp53 is present in the cytosol in a closed, self-inhibited conformation, in which the CRIB domain binds to the SH3 domain, thus preventing the latter from binding its effectors (Kast et al., 2014). IRSp53 dimers may become active on membranes through binding to activated Rho-GTPases (Krugmann et al., 2001). Therefore, LIN7-mediated recruitment of IRSp53 to its target may also exert a secondary effect of favouring IRSp53 activation. Moreover, stable

binding of IRSp53 with its partners may inhibit IRSp53 deactivation by generating steric hindrance.

3. LIN7-mediated recruitment of IRSp53 into large protein complexes may not only activate but also protect IRSp53 from degradation. This third hypothesis is supported by the fact that when we generated stable N2A cell clones downregulated for LIN7, we found a concomitant downregulation of IRSp53 that was directly proportional to that of LIN7 (see Fig. 6 B).

It is important to note that the level of activation and the differential localization of the IRSp53-LIN7 complex to its various protein and membrane targets may be cell-specific, and may also strongly depend on the level of differentiation of a certain cell type. For example, although we were able to detect a mitochondrial localization of LIN7 and IRSp53 in MDCK cells by immunofluorecence experiments (data not shown), in fully polarized MDCK cells their localization seems to be restricted to cell junctions (Massari et al., 2009).

An important point raised by the fact that the IRSp53-LIN7 complex regulates membrane dynamics in various membrane compartments, and that their relative role on such compartments may change in different cell conditions, is whether the inhibition of neurite outgrowth reported in N2A cells downregulated for LIN7 (see Figure 5) could be more due to inhibition of plasma membrane dynamics or to defects in mitochondrial fragmentation, as both processes have been liked to neuronal differentiation (Dent et al., 2007; Ishihara et al., 2009).

What we think is that the decrease in plasma membrane dynamics caused by the disruption of the IRSp53-LIN7 complex may be the primary cause of inhibition of neurite outgrowth, while disruption of mitochondrial fragmentation, by impairing mitochondrial transport inside neurites to support their growth, might be a secondary cause of neurite resorbtion or collapse.

Finally, as defects of both neurites outgrowth and mitochondrial dynamics have been reported to be involved in the pathogenesis of neurodevelopmental and/or neurological diseases, our data collectively suggest that unbalanced alterations in the expression of LIN7 or IRSp53 or mutations that prevent their interaction may play a role in such diseases.

To conclude, our data unravel a complex role of the IRSp53-LIN7 complex on membrane dynamics that is not restricted to the plasma membrane alone, but also applies to intracellular organelles that heavily rely on membrane deformation. This notion is strongly supported not only by data on mitochondrial morphology, but also by the fact that virtually 100% of the endogenous IRSp53 and LIN7 is bound either to the PM, the mitochondria or smaller intracellular organelles, at least in HeLa cells (see Fig. 11 C). As some of the proteins involved in mitochondrial fission have already been demonstrated to play a similar role on peroxisomes (van der Bliek et al., 2013), it is feasible that such organelles might be another target of the complex.

Further studies will be needed to define the spectrum of action of the IRSp53-LIN7 complex inside the cell.

CHAPTER 8

Materials and Methods

8.1 Molecular biology

Molecular biology techniques were used for the preparation of shRNA constructs. The experiments were performed either according to Maniatis protocols or, when commercial kits were used, according to the manufacturer's protocol. shRNA plasmids were generated by using the pSUPER.gfp/neo RNAi system (OligoEngine, Inc., Seattle, WA) as vector.

8.1.1 Design and annealing of the oligo inserts

The oligo inserts required for the insertion in the pSUPER.gfp/neo RNAi system were designed according to the manufacturer's protocol. The 19-nucleotides long sequences derived from the messenger RNA transcript of mouse or human LIN7C were selected based on the absence of any homology to other genes expressed in the cell lines in which silencing would be performed. The chosen sequences for mouse LIN7C were 5′GGGAAGGTTAAATTAGTCG-3′ (shRNA1), and 5′-CGGATAATTCCAGGTGGAA-3′ (shRNA2). The sequence chosen from human LIN7C was 5′-GGCTACTGTTGCTGCATTT-3'. The forward and reverse oligo inserts were synthesised by Sigma Aldrich (Sigma Aldrich, St Louis, MO). The oligos were then dissolved in sterile, nuclease-free water to a concentration of 3 mg/ml. The annealing reaction was assembled by dissolving 1 µl of each oligo in 48 µl of annealing buffer (100 mM NaCl, 50 mM Hepes pH 7.4). The mixture was annealed in a Thermal Cycler programmed as follows:

- Denaturation step: 90°C for 4 minutes.
- Annealing: 70°C for 10 minutes.
- Final hold: step-cool to 37°C for 15-20 minutes, then to room temperature (RT).

8.1.2 Restriction enzyme digestion of the pSUPER vector

Restriction endonucleases are bacterially derived enzymes that recognize specific sequences within double-stranded DNA. They can be divided into three groups (type I-III), and the restriction endonucleases used in molecular cloning belong to the type II class. These enzymes generally recognize an inverted repeat palindrome sequence and cut DNA in that sequence. The DNA double strand will be cut symmetrically within the palindrome and, depending on the enzyme, the cut will generate a DNA fragment with either blunt or sticky ends. Blunt DNA ends are universally compatible with other blunt-ended DNAs. Sticky ends, on the other hand, will ligate only to a complementary region of sticky DNA.

Each restriction enzyme requires optimal reaction conditions: the most important parameters to be taken into consideration are the temperature of incubation and the buffer composition. Generally, restriction enzymes used in molecular biology can be divided into three groups, according to the characteristics of the buffer: a) those that work best at high ionic strength (100 mM NaCl, 50 mM Tris HCl pH 7.5, 10 mM $MgCl_2$ and 1 mM DTT); b) those that prefer medium ionic strenth (50 mM NaCl, 10 mM Tris HCl pH 7.5, 10 mM $MgCl_2$ and 1 mM DTT) and c) those

that have a preference for low ionic strength buffers (10 mM Tris HCl pH 7.5, 10 mM $MgCl_2$ and 1 mM DTT).

Digestion of the pSUPER vector with restriction enzymes was carried out in a total volume of 20 µl as follows:

- 1 µg of DNA was mixed with sterile water to a final volume of 18 µl
- 2 µl of the appropriate digestion buffer was added
- 1 U of XhoI enzyme was added and, after mixing, the tube was incubated at the appropriate temperature for 60 minutes.
- 1 U of BglII was then added to the mixture, and digestion was carried out for additional 2 hours.

After the incubation, cleavage of the plasmid was checked by agarose gel electorophoresis.

8.1.3 Agarose gel electrophoresis

Agarose gel electrophoresis is the standard method used to separate, identify and purify DNA fragments. DNA bands in the gel are detected by intercalation within the DNA double strand of the fluorescent dye ethidium bromide (EtBr). The electrophoretic migration rate of DNA through agarose gels depends on the molecular size of DNA, agarose concentration, DNA conformation and the current applied. Agarose gels electrophoresis is performed in Tris-acetate buffer (TAE: 40 mM Tris actetate and 2 mM EDTA).

To prepare agarose gels, the appropriate amount of powder agarose must be dissolved in the correct volume of TAE, and 0.5 µg/ml of EtBr

must be added to the cooling agarose solution before solidification into appropriately shaped plates.

The DNA samples must be mixed with loading buffer (30% glycerol and 0.025% bromophenol) before loading onto the gel. Once the electrophoretic run is completed, the DNA bands can be detected by excitation of the intercalated EtBr with an ultraviolet (UV) light.

8.1.4 Purification of DNA fragments from agarose bands

In order to purify the cleaved pSUPER vector from the undigested circular plasmids, the digested plasmid solution was loaded onto a 1% agarose gel, and the electrophoretic band corresponding to the linear vector was excised from the agarose gel with a clean and sharp scalpel. The DNA fragment was then extracted from agarose and purified using the QIAEX II Gel Extraction Kit (QIAGEN, Venlo, Netherlands), according to the manufacturer's protocol.

8.1.5 Ligation of the annealed oligos into the pSUPER vector

Ligation between two DNA fragments is achieved by the generation of a covalent bond between the 5'-phosphate and the 3' hydroxyl group of two adjacent nucleotides. The ligase most commonly used in molecular biology is the ligase from the T4 bacteriophage, simply referred to as T4 ligase. This enzyme can ligate both blunt- and sticky-ended DNA fragments. The ligation reaction was carried out in a total volume of 10 µl as follows: 15 mg of linearized pSUPER vector was mixed with a threefold molar excess (compared to the plasmid) of annealed oligos, in

a proper amount of ligation buffer (50 mM Tris HCl pH 7.4, 10 mM $MgCl_2$, 10 mM DTT, 0.5 mM spermidine, 2 mM ATP, 2.5 mM hexamine cobalt chloride and 20 µg/ml BSA). A proper amount of T4 ligase was then added to the mixture, and the reaction was allowed to occur at 19°C overnight. In the morning, the enzyme was inactivated by heating the mix to 60°C for 20 minutes before being transformed into 100 µl of competent bacterial cells.

8.1.6 Preparation of competent bacteria

For plasmidic DNA amplification, competent E. coli bacteria (strain DH5α) were used in this study. The following protocol was used to obtain competent DH5α cells. Briefly, one colony of non-competent DH5α bacteria was inoculated into 2 ml of LB medium (1% Bacto-tryptone, 0.5% Bacto-yeast extract and 1% NaCl) and grown into an orbital shaking incubator at 37°C overnight. Half of that culture was then inoculated into 100 ml of LB medium and grown to OD_{600} ~ 0.4. The 100 ml culture was then chilled on ice for 10 minutes before centrifugation at 2500 rpm for 20 minutes. The bacterial pellet was resuspended in 20 ml of 0.1 M $CaCl_2$ and left in ice for 1 hour. Fifteen % glycerol was then added to the solution, which was subdivided into 0.5 ml aliquots before freezing in liquid nitrogen and storage at -80°C.

8.1.7 Transformation of plasmid DNA into competent E.coli

Bacterial cells transformation is the process that allows insertion of plasmid DNA into competent bacteria. The process is as follows: 1-10 ng of DNA plasmid (or 10 µl of a ligation reaction) are added to 100 µl of competent bacteria in a tube, which is then kept in ice for 30 minutes. The tube is then transferred into a water bath preheated to 42°C for 45 seconds, and put back in ice for 1 minute. 900 µl of LB medium is added to the mix, and the tube is incubated in a orbital shaking incubator for 1 hour, to allow the expression of the antibiotic resistance encoded on the plasmids. 300 µl of the bacterial mixture is then spread onto a selective plate of LB-Agar (1.5% Bacto-Agar, 1% Bacto-tryptone, 0.5% Bacto-yeast extract, 1% NaCl and 1 mg/ml of the appropriate antibiotic). The plate is left to grow overnight into a 37°C heater to allow the appearance of visible colonies of transformed bacteria.

8.1.8 Plasmidic DNA extraction

Different procedures are available for isolating DNA plasmids amplified from bacterial colonies. Those procedures usually differ for the quantity of plasmidic DNA that can be yielded.

8.1.8.1 Small-scale isolation of plasmid DNA (MINI prep)

This technique usually yields enough DNA for the analysis by restriction enzymes, and is particularly suitable for the initial analyses needed to validate a newly ligated plasmid. The protocol used is the following:

- one colony of transformed DH5α bacteria is inoculated into 2 ml of LB medium containing the appropriate antibody and grown overnight into an orbital shaking incubator set to 37°C.
- In the morning, 1.5 ml of the culture is centrifuged in a 2 ml sterile eppendorf tube for 5 minutes.
- The bacterial pellet is then resuspended in 100 µl of Solution 1 (50 mM glucose, 25 mM Tris HCl pH 8 and 10 mM EDTA)
- 200 µl of Solution 2 (1% SDS and 0.2 N NaOH) is added to the tube, which is mixed gently by inverting
- 150 µl of Solution 3 (5 M potassium acetate and 11,5% glacial acetic acid) is added to the tube, and the solution is vigorously mixed by vortexing for 10 seconds.
- After being kept in ice for 5 minutes, the tube is centrifuged for 5 minutes to obtain a supernatant containing the plasmidic DNA
- To achieve DNA precipitation, an equal volume of isopropanol must be added to the tube, which is then kept at RT for 2 minutes
- The tube is centrifuged at RT for 15 minutes to pellet DNA
- The DNA pellet is washed with 150 µl of 70% cold ethanol and centrifuged again
- The DNA pallet is then air-dried and resuspended in 50 µl of TE (10 mM Tris HCl pH 7.6 and 1 mM EDTA) containing 100 µg/ml RNAse-

8.1.8.2 Large-scale isolation of plasmid DNA (MIDI prep)

Large-scale isolation of plasmid DNAs was performed using the QIAGEN Plasmid *Plus* MIDI kit II Gel Extraction Kit (QIAGEN), according to the manufacturer's protocol.

8.1.8 Constructs

Generation and subcloning of mouse LIN7A, human IRSp53 constructs and chimeras have been previously described (Massari et al., 2009). The GFP-mDia1, GFP-mDia2 and GFP-IRSp53 cDNAs used in this paper have been described elsewhere (Yang et al., 2009). RFP-pLifeAct (Ibidi GmbH, Martinsried, München, Germany) was used to visualise filopodial F-actin in live cell imaging experiments, and a GFP construct fused to a membrane localisation sequence (mGFP) was a kind gift from Dr Nica Borgese (Ronchi et al., 2008).

The cDNA encoding for SOD1 and $SOD1^{G93A}$ have been described elsewhere (Tortarolo et al., 2004). The constructs encoding for HA-RAC1 and HA-RAC1-N17 were a kind gift of Dr. Giorgio Scita. The shRNA against mouse IRSp53 was purchased from Sigma Aldrich.

Generation of a shRNA against human IRSp53 was described in Disanza et al., 2006. The cDNA encoding for HA-Drp1 K38A was a kind gift of Dr Alexander van der Bliek, and its generation was described in Smirnova et al., 2001. The pCB6 vector was purchased from Addgene (Cambridge, MA).

8.2 Cell Biology

8.2.1 Cells

8.2.1.1 NSC34 cells

This murine motoneuron-neuroblastoma hybrid cell line was generated in 1992 in Neil R. Cashman's lab by fusing neuroblastoma N18TG2 cells with primary motoneurons from E12-14 mice (Cashman et al., 1992). This cell line possesses some morphological and physiological features that are typical of primary motoneurons, such as the capacity to extend neurites and to generate action potentials. In this study, NSC34 cells were grown in DMEM (Euroclone, Milan, Italy) with 5% Foetal bovine serum (FBS) (Euroclone), 1 mM pyruvate (Sigma Aldrich), 1 mM glutamine and antibiotics (Sigma Aldrich).

Cells were transfected using Lipofectamine 2000 (Invitrogen, Carlsbad, CA), following the manufacturer's protocol. For co-transfections 1:1 cDNAs ratio were used.

8.2.1.2 N2A cells

This cell line was obtained by R.J. Klebe and F.H. Ruddle (Klebe and Ruddle, 1969) from the mouse tumour line C1300 (Jackson laboratory, Bar Harbor, Maine), which was isolated form a spinal cord spontaneous tumour of an albino mouse, strain A. The tumour derived from cells of

the sympathetic nervous system. N2A cells have the capacity to outgrow neurites in response to various stimuli, such as serum starvation or treatment with ionomycin, retinoic acid or arachidonic acid (Wu et al., 1997).

N2A cells were grown in DMEM (Euroclone) supplemented with 1% L-glutamine (Sigma Aldrich), 1% penicillin–streptomycin (Sigma Aldrich), and 10% FBS (Euroclone), and were transfected with Polyethylenimine (PolyScience, Eppelheim, Germany) according to the manufacturers' protocol.

The N2A cell lines stably expressing shRNA LIN7C were selected on the basis of growth in the antibiotic G418 (0.5 mg/ml; Sigma Aldrich), and the expression of the construct was assessed by fluorescence microscopy and Western blotting.

8.2.1.3 HeLa cells

HeLa cells represent the oldest and most commonly used human cell line. This line was derived from cervical cancer cells taken from Henrietta Lacks, a patient who eventually died of her cancer on October 4, 1951. The cells from Henrietta's tumour were isolated by George Gey (Gey et al., 1952), who named the line HeLa, after the initial letters of Henrietta Lacks' name. The isolation of HeLa cells represented an enormous boon to medical and biological research, and since then HeLa cells have been used in more than 60,000 scientific articles (as of 2009).

HeLa cells were grown in DMEM (Euroclone) supplemented with 1% L-glutamine (Sigma Aldrich), 1% penicillin–streptomycin (Sigma Aldrich), and 10% FBS (Euroclone).

Transfections: cDNAs and shRNAs were transiently transfected in HeLa cells using Polyethylenimine (PolyScience) according to the manufacturers' protocol. For overexpression experiments, cells were transfected on two consecutive days and fixed 48 hours after the first transfection. Cells transfected with shRNA LIN7C were transfected once and fixed after 48 hours. Cells co-transfected with shRNA IRSp53 + GFP or shRNA IRSp53 + shRNA LIN7C were transfected on two consecutive days and fixed 72 hours after the first transfection. pSUPER-transfected control cells were either transfected once (for comparison with shRNAs transfected cells, data in Fig. 13) or twice (for comparison in overexpression experiments, data in Fig. 12) with no significant difference on mitochondrial network morphology or mitochondrial length.

All cell lines were cultured in a 37°C incubator containing 5% CO_2

8.2.2 Antibodies

In this study, antibodies were used in both biochemical and immunofluorescence experiments to detect specific proteins. Both protocols rely on a first 2 hours long incubation with a primary antibody and a second, 1 hour long incubation with a secondary antibody, which is conjugated to either a fluorophore (for immunofluorescence

experiments and Western blot detection by the Odissey system) or peroxidase (for conventional Western blot experiments).

Primary antibodies are immunoglobulins raised against an antigenic target of interest (a protein, peptide, carbohydrate or other small molecules), and are typically unconjugated. Primary antibodies recognize and bind with high affinity and specificity unique epitopes across a broad spectrum of molecules, and are available as high specificity monoclonal antibodies or as polyclonal antibodies. The primary antibodies used in this study are listed below.

Commercial primary antibodies were:

- mouse monoclonal anti-myc (Santa Cruz Biotechnology, Dallas, TX), anti-actin (Sigma Aldrich) and anti-GFP (MBL, Medical and Biological Laboratories Co., Japan);
- sheep polyclonal anti-cytochrome C (Sigma Aldrich) an anti-SOD1 (Calbiochem, Billerica, MA);
- rabbit polyclonal anti-SOD1 (Enzo LifeSciences, Farmingdale, NY), anti-TOM20 (Santa Cruz Biotechnology) and anti-Calnexin (Stressgen, San Diego, CA),

The polyclonal rabbit anti-LIN7 antiserum was raised against the histidine-LIN7A fusion protein (Massari et al., 2009). The polyclonal rabbit anti-IRSp53 was a kind gift from Dr E. Kim (Korea Advanced Institute of Science and Technology) (Choi et al., 2005).

8.2.3 Immunofluorescence

After being grown and transfected as described, the cells were either used for live-cell imaging (see below) or fixed for 20 min in 4% paraformaldehyde and permeabilized with 0.5% Triton X-100. Immunostaining with primary antibodies was followed by incubation with FITC/CY5/488/CY3/Rodamine anti-rabbit/mouse antibodies (Jackson ImmunoResearch Laboratories, West Grove, PA, USA). Rhodamine-labelled phalloidin (Cytoskeleton, Denver, CO) was used to detect filamentous actin. To detect mitochondria, cells were incubated for 30 minutes with 500 nM Texas Red conjugated Mitotracker CMX Ros (Molecular Probes, Invitrogen) dissolved in growth medium before fixation. The confocal images were acquired using either a Bio-Rad MRC-1024 confocal microscope (Nikon, Yurakucho, Tokyo, Japan) or an Axiovert 200 M (Zeiss, Oberkochen, Germany) confocal system equipped with spinning-disc (PerkinElmer LifeScience, Waltham, MA).

8.2.4 Live-cell imaging

For live-cell imaging experiments, N2A cells were co-transfected with GFP tagged IRSp53 constructs (IRSp53 and L27-IRSp53) or with mGFP as a control and RFP-pLifeAct. Twenty-four hours after transfection, cells were serum-starved for additional 16 h and then placed in an environmentally controlled chamber with 5% CO_2 at 37°C, using an Axiovert 200 M (Zeiss) confocal system equipped with spinning-disc (PerkinElmer LifeScience). A 100× objective and the 488/561 nm laser lines were used for acquisition of GFP fusion proteins or RFP-LifeAct,

respectively. Images were collected every 20 s for a period of 10 min; thirty still images of each recording session were analysed for the emergence and retraction of protrusions. The unbranched, dynamic, actin-containing protrusions with a mean length of 3.44±0.36 μm and half-life of 173±1 s were defined as filopodia; the branched and unbranched protrusions, poorly stained with phalloidin, unchanging their length and position from time zero to the end of the analysis (5 min), were respectively defined branched and linear static protrusions. For each transfectant a total of at least 400 μm of PM from 10 different cells obtained in two separate experiments were analysed. Image analysis was performed with the Volocity High-Performance Imaging System (PerkinElmer LifeScience). To measure lifetime: sixty protrusions from ten different cells obtained from two separate experiments were recorded. The number of frames from the point of emergence of individual filopodia to their complete loss was determined and multiplied by 20 s to achieve the lifetime. To determine the mean number of filopodia in 100 μm PM: for each transfectant we analysed a total of at least 400 μm of PM from ten different cells obtained in two separate experiments, and the total number of filopodia that protruded or retracted in the selected region of the membrane during the 5 min time-lapse were quantified.

8.2.5 SDS-PAGE and Western blot

SDS-PAGE, sodium dodecyl sulphate poliacrylamide gel elecrophoresis, is a widely used technique in biochemistry to separate proteins according

to their electrophoretic mobility. The electrophoretic mobility of a given protein is a function of the length of the polypeptide chain, as well as higher-order protein folding, post-translational modification and other factors. Besides the addition of SDS, proteins may optionally be briefly heated to near boiling in the presence of a reducing agent, such as mercaptoethanol (β-mercaptoethanol), to further denature the proteins by reducing disulfide linkages, thus preventing tertiary protein folding and breaking up quaternary protein structures (oligomers formation). This method is known as 'reducing SDS-PAGE', ad is the most commonly used form of SDS-PAGE.

In this sudy, cell lysates were mixed with 2X SDS solubilization buffer (300 mM TrisHCl pH 8.9, 5% SDS, 20% glycerol, 1.4 M 2-Mercaptoethanol) and heated at 100°C for 2 min before being loaded onto a 10 or 11% SDS–PAGE. Separated proteins were then transferred onto nitrocellulose membranes (GE Healthcare Bio-Sciences AB, Uppsala, Sweden). Blots were probed with the indicated primary antibodies followed by secondary antibodies conjugated to either peroxidase or infrared dyes. The method used will be specified below.

8.2.6 Co-immunoprecipitation from whole cell lysates

Co-immunoprecipitation is a technique used to isolate intact protein complexes with the goal of identifying protein-protein interactions as well as novel members of protein complexes. To demonstrate IRSp53-LIN7 interaction, N2A cells grown to 90% confluence in 100 mm dishes were harvested in 1.5 ml of ice-cold lysis buffer (25 mM Tris-HCl pH 7.5,

100 mM NaCl, 5 mM EDTA, 0.5% Triton X-100, 1 mM DTT, PMSF and a cocktail of protease inhibitors) for 30 min at 4°C. The lysates were then spun at 14,000 *g* for 20 min at 4°C. For input samples, 40 µl of the cell lysate were mixed with 2× SDS samples loading buffer and heated at 100°C for 5 min. For affinity precipitation, 700 µl of lysate were incubated with 25 µl bead volume of protein-A–Sepharose (Sigma Aldrch) cross linked to anti-LIN7 antibodies or preimmune IgG at 4°C for 2 h. The immunocomplexes, washed and released from the beads by boiling the samples in SDS solubilisation buffer, and 20 µl of the input sample (3% of the total) were loaded onto a 10% SDS–PAGE, and transferred onto nitrocellulose membranes (GE Healthcare). The blots were probed with the indicated primary antibodies, followed by peroxidase conjugated with mouse IgG or anti-rabbit IgG, light chain specific (Jackson ImmunoResearch Laboratories) and proteins were visualised by ECL (GE Healthcare). Signal intensity was quantified by densitometry using NIH ImageJ 1.59 software.

8.2.7 Triton X-100 cytoskeleton extraction

Detergent extraction experiments were carried out as described (Blikstad and Carlsson, 1982). Briefly, cells were treated for 10 min at 0°C using extraction buffer (0.5% Triton X-100, 100 mM NaF, 50 mM KCl, 2 mM $MgCl_2$, 1 mM EGTA, 10 mM KPO_4, pH 7.5, 0.5 M sucrose) supplemented with PMSF (phenylmethylsulfonyl fluoride) and protease cocktail inhibitor (Sigma Aldrich) to block the partial depolymerisation of actin seen in other buffers. The supernatant (detergent-soluble fraction

containing the G-actin fraction) was taken for immunoblotting. Cell matrix pellets containing F-actin fractions were scraped in the same extraction buffer of the supernatant with a rubber policeman, and both fractions were solubilised with the same volume of SDS solubilization buffer. Equal volumes of each fraction were probed by immunoblotting on an 11% SDS-PAGE with the indicated antibodies, followed by peroxidase conjugated secondary antibodies.

8.2.8 Subcellular fractionation

HeLa cells grown to 90% confluence were scraped in PBS and collected by centrifugation. Cells were then resuspended in Homogenization buffer (buffer H) (1 mM TrisHCl pH 7.4, 15 mM KCl, 30 mM NaCl, 1 mM EDTA, PMSF and a cocktail of protease inhibitors) for 15' in ice and homogenized for approximately 3-4 minutes on ice using a tight-fitting Teflon pestle attached to a Stuart SS30 stirrer (Bibby Scientific, Stone, Staffordshire, UK) set to 600–1,000 rpm. The homogenate was then centrifuged at 600 g for 15' at 4°C to pellet nuclei and unbroken cells. The post-nuclear supernatant (PNS) obtained was further centrifuged at 16,000 g for 30' at 4°C to obtain a crude mitochondrial pellet (MITO), which was washed once with fresh buffer H and pelleted again at 16,000 g for 25'. Smaller organelles were pelleted from the Post-mitochondrial supernatant (PMS) at 130,000 g for 1 hour using a Beckman Optima TL ultracentrifuge (Beckman Coulter, Brea, CA). The supernatant, containing cytosolic proteins, was then precipitated in 4 volumes of ice cold acetone at –20°C for at least 1 hour followed by centrifugation at

16,000 g for 20 minutes. All the pellets obtained were resuspended in the same volume of buffer H and mixed with 2X SDS solubilization buffer and heated at 100°C for 2 min.

Equal volumes of the subcellular fractions, or 2% of the INPUT and PNS fractions were separated by SDS-PAGE and transferred onto nitrocellulose membranes (GE Healthcare). The blots were probed using the appropriate primary antibodies, followed by infrared-conjugated anti-rabbit IgG IRDye 800CW or anti-mouse IgG 680RD (LI-COR Bioscience, Lincoln, NE) as secondary reagents. Blots were scanned with the Odyssey CLx Infrared Imaging System (LI-COR Bioscience), and the bands were quantified with Image Studio software (LI-COR Bioscience).

8.2.9 PM depletion experiments.

Three 100 mm Petri dishes of HeLa cells grown to 80% confluence were incubated with 0.5 mg/ml EZ-Link Sulfo-NHS-LC-Biotin (Thermo Scientific Pierce, Rockford, IL) at 4°C for 40 minutes (the biotin-containing medium was changed once during the incubation time). To quench the reaction, cells were incubated with 50 mM Glycine pH 8 for 10 minutes at 4°C. Cells were then scraped, homogenized and centrifuged as described for the subcellular fractionation protocol to obtain a PNS. Such PNS (roughly 1 ml) was incubated with 400 µl of magnetic streptavidin beads (Streptavidin Mag Sepharose, GE Healthcare) at 4°C for 2 hrs. The beads were collected using a magnetic plate and boiled in 100 µl of SDS solubilisation buffer to obtain a plasma membrane (PM) fraction.

MITO and PMS fractions were obtained from the depleted PNS as described in the subcellular fractionation protocol. To quantify the decrease in the content of biotinilated proteins in the depleted PNS, equal amounts of PNS and depleted PNS were blotted and probed with peroxidase-conjugated streptavidin (Jackson ImmunoResearch Laboratories) and visualised by ECL (GE Healthcare). Signal intensity was quantified by densitometry using NIH ImageJ 1.59 software.

8.2.10 Immunoprecipitation from the MITO fraction

The MITO fraction obtained from three 100 mm Petri dishes of HeLa cells grown to 80% confluence was resuspended in 200 µl of ice-cold IP buffer (25 mM Tris-HCl pH 7.5, 100 mM NaCl, 5 mM EDTA, 0.5% Triton X-100, 1 mM DTT, PMSF and a cocktail of protease inhibitors) and affinity precipitated with 25 µl bead volume of protein-A–Sepharose (Sigma Aldrich) cross-linked to anti-LIN7 antibodies or preimmune IgG at 4°C for 2 h. The immunocomplexes were washed and released from the beads by boiling the samples in SDS solubilisation buffer. Samples were blotted and probed with the indicated primary antibodies, followed by peroxidase-conjugated anti-rabbit IgG, light chain specific (Jackson ImmunoResearch Laboratories) and visualization by ECL.

8.2.11 Image analysis

8.2.11.1 On N2A and NSC34 cells

Morphological phenotypes in NSC34 cells were quantified using the following definitions. Actin-filled protrusions: thin elongated structures (average length between 5-10 μm and width of 0.5-1 μm) positively stained by labelled phalloidin for their entire length. Actin-deficient protrusions: protrusions corresponding to both linear and branched structures emerging from the plasma membrane not stained for their entire length with labelled phalloidin.

Quantification of the signals was evaluated by using ImageJ plot profile. To count cell protrusions, the Adobe Photoshop software filters 'trace contour' and 'find edges' were sequentially applied at the outlined protrusions above described, and the average total number of actin-filled and actin-deficient protrusions was obtained by manual counting in at least 20 different cells (6 mm of total plasma membrane) for each transfectant.

For neurite quantification, after 48 h serum-starvation, cells were fixed in 4% paraformaldehyde for 20 min at 37°C, and viewed with a Zeiss Axioplan inverted phase-contrast microscope (40× objective) connected with an AxioCam HRm CCD camera. Neurites were defined as processes with a length of at least a cell body diameter, and this definition in no

way attributes any functional value to these structures and is purely a reflection of morphological similarity to neurites.

For quantification of the total skeletal length, wide field images of transfected N2A cells were modified with ImageJ as follows: the cells' outlines were drawn using the polygon selection tool and filled with white. The black and white masks obtained were then skeletonized, and the length of the resulting skeletons was measured with the magic wand tool.

8.2.11.2 On HeLa cells

Quantification of the distance between IRSp53/LIN7 puncta on mitochondria was carried out by measuring the mean distance among signal peaks generated with ImageJ plot profile (a representative plot profile for both IRSp53 and LIN7 is shown in Fig. 11B). At least 200 µm of mitochondrial network from 10 cells was quantified for both IRSp53 and LIN7. The percentage of colocalization between IRSp53/LIN7 and a mitochondrial marker was obtained by calculating the Manders' colocalization coefficient (MCC) in at least 10 cells using ImageJ plugin JACoP (Bolte and Cordelieres, 2006).

Subdivision of transfected HeLa cells in four groups according to their mitochondrial morphology was carried out using the following definitions: CTR: extended network of tubular mitochondria, distributed all through the cytoplasm; CLUSTERED: highly interconnected

mitochondria, often accumulated in the perinuclear area of the cell; MIXED: the mitochondrial network is partially lost in favour of smaller, often misshaped, individual mitochondria; FRAGMENTED: the mitochondrial network is mostly fragmented into dot-like organelles. Data are the mean of at least 3 independent experiments, and at least 40 cells from each experiments were evaluated.

The diffuse green signal in GFP-IRSp53 transfected cells shown in Fig. 12A was removed from the image by using the 'subtract background' function from ImageJ.

The representative cartoon cells shown in Fig. 12B were obtained by modifying confocal images of transfected HeLa cells with Adobe Photoshop (Adobe Systems, San Jose, CA) as follows: black mitochondria were obtained by inverting the greyscale signal of the Mitotracker, while the cell boundary was drawn by outlining the signal of the transfectants (generally GFP) with the brush tool. The blue-filled oval (drawn with the ellipse tool) indicates the position of the nucleus.

To quantify mitochondrial length in transfected HeLa cells, regions of interest (ROIs) were selected in the cells periphery, where mitochondria outlines can be readily resolved. Such ROIs were modified with ImageJ as follows: the background signal was lowered by using the subtract background function (rolling ball radius set to 2). The remaining signal was contrast enhanced and despeckled with the homonymous ImageJ tools. To obtain a binary image of white mitochondria on a black

background, the threshold tool was then manually adjusted on each ROI, and the resulting masks were manually examined and modified to ensure that the binary mitochondrial shapes obtained were true to the original images (representative binary ROI images are shown in false colours in Fig. 12 and 13). To measure mitochondrial length, the skeletonize tool was applied to each ROI, and the mitochondria skeletons obtained were measured with the 'analyze skeleton' plugin (Arganda-Carreras et al., 2010). For branched mitochondria, the longest shortest path was measured). At least 25 cells for each transfectant from at least three independent experiments were examined.

To evaluate the degree of mitochondria clusterization in downregulated cells compared to control, we measured the Mitotracker signal ratio between the perinuclear area of the cell and the cell periphery as follows: for each cell analyzed, the greyscale Mitotracker signal was 'inverted' and the cell boundary drawn by outlining the signal of the transfectant with the Adobe Photoshop 'brush tool'. Using ImageJ, a rectangle ROI long as the cell's longest axis and 40 pixels tall was drawn over the image, crossing the nucleus. Such ROI was then used to generate and quantify a densitometry plot, which was in turn used to quantify the Mitotracker signal in the perinuclear and peripheral areas of the cell and to calculate the ratio.

8.2.12 Statistical analysis

All quantitative data are presented as mean ± s.e.m. Each quartile value used to draw the box and whiskers plots represents itself the mean of at least three independent experiments. Multiple comparisons among groups were carried out by Student's *t*-test using Prism software (GraphPad PrismTM software), $*P<0.05$, $**P<0.01$ and $***P<0.001$.

CHAPTER 9

References

8. References

Alexander C, Votruba M, Pesch UE, Thiselton DL, Mayer S, Moore A, Rodriguez M, Kellner U, Leo-Kottler B, Auburger G, Bhattacharya SS, Wissinger B. *OPA1, encoding a dynamin-related GTPase, is mutated in autosomal dominant optic atrophy linked to chromosome 3q28.* Nat Genet. 2000 Oct;26(2):211-5.

Ahmed, S., Goh, W. I. and Bu, W. (2010). I-*BAR domains, IRSp53 and filopodium formation.* Semin. Cell Dev. Biol. 21, 350–356.

Archer SL. *Mitochondrial dynamics--mitochondrial fission and fusion in human diseases.* N Engl J Med. 2013 Dec 5;369(23):2236-51.

Arganda-Carreras I, Fernández-González R, Muñoz-Barrutia A, Ortiz-De-Solorzano C. *3D reconstruction of histological sections: Application to mammary gland tissue.* Microsc Res Tech. 2010 Oct;73(11):1019-29.

Arimura N, Kaibuchi K. *Key regulators in neuronal polarity.* Neuron. 22;48(6):881-4, 2005. Review.

Arimura N, Kaibuchi K. *Neuronal polarity: from extracellular signals to intracellular mechanisms.* Nat Rev Neurosci. 8(3):194-205, 2007. Review.

Barnes AP and Polleux F. *Establishment of axon-dendrite polarity in developing neurons.* F. Annu Rev Neurosci., 32:347-81, 2009. Review.

Berg JS and Cheney RE. *Myosin-X is an unconventional myosin that undergoes intrafilopodial motility. Nat Cell Biol., 4(3):246-50, 2002.*

Berg JS, Derfler BH, Pennisi CM, Corey DP and Cheney RE. *Myosin-X, a novel myosin with pleckstrin homology domains, associates with regions of dynamic actin.* J Cell Sci., 113 Pt 19:3439-51, 2000.

Biederman J, Petty C, Fried R, Fontanella J, Doyle AE, Seidman LJ, Faraone SV. *Impact of psychometrically defined deficits of executive functioning in adults with attention deficit hyperactivity disorder.* Am J Psychiatry. 163(10):1730-8, 2006.

Bisi S, Disanza A, Malinverno C, Frittoli E, Palamidessi A, Scita G. *Membrane and actin dynamics interplay at lamellipodia leading edge.* Curr Opin Cell Biol. 2013 Oct;25(5):565-73.

Blanchoin L, Boujemaa-Paterski R, Sykes C, Plastino J. *Actin dynamics, architecture, and mechanics in cell motility.* Physiol Rev. 2014 Jan;94(1):235-63.

Bleazard W, McCaffery JM, King EJ, Bale S, Mozdy A, et al. (1999) *The dynamin-related GTPase Dnm1 regulates mitochondrial fission in yeast.* Nat Cell Biol 1: 298–304.

Blikstad, I. and Carlsson, L. (1982). *On the dynamics of the microfilament system in HeLa cells.* J. Cell Biol. 93, 122–128.

Block J, Breitsprecher D, Kühn S, Winterhoff M, Kage F, Geffers R, Duwe P, Rohn JL, Baum B, Brakebusch C, Geyer M, Stradal TE, Faix J, Rottner K. *FMNL2 drives actin-based protrusion and migration downstream of Cdc42*. Curr Biol. 2012 Jun 5;22(11):1005-12.

Block, J., Stradal, T. E., Hänisch, J., Geffers, R., Köstler, S. A., Urban, E., Small, J. V., Rottner, K. and Faix, J. (2008). *Filopodia formation induced by active mDia2/Drf3.* J. Microsc. 231, 506–517.

Bolte, S. and Cordelieres, F. P. (2006). *A guided tour into subcellular colocalization analysis in light microscopy*. J. Microsc. 224, 213-232.

Bowes T, Gupta RS. *Novel mitochondrial extensions provide evidence for a link between microtubule-directed movement and mitochondrial fission.* Biochem Biophys Res Commun. 2008 Nov 7;376(1):40-5.

Bryant DM and Mostov KE. *From cells to organs: building polarized tissue.* Nat Rev Mol Cell Biol., 9(11):887-901, 2008. Review.

Cashman, N. R., Durham, H. D., Blusztajn, J. K., Oda, K., Tabira, T., Shaw, I. T., Dahrouge, S. and Antel, J. P. (1992). *Neuroblastoma x spinal cord (NSC) hybrid cell lines resemble developing motor neurons*. Dev. Dyn. 194, 209–221.

Chan DC. *Mitochondrial fusion and fission in mammals*. Annu Rev Cell Dev Biol. 2006;22:79-99.

Chan DC. *Fusion and fission: interlinked processes critical for mitochondrial health.* Annu Rev Genet. 2012;46:265-87.

Chen H, Detmer SA, Ewald AJ, Griffin EE, Fraser SE, Chan DC. *Mitofusins Mfn1 and Mfn2 coordinately regulate mitochondrial fusion and are essential for embryonic development.* J Cell Biol. 2003 Jan 20;160(2):189-200.

Chiurazzi P, Neri G, Oostra BA. *Understanding the biological underpinnings of fragile X syndrome*. Curr Opin Pediatr. 15(6):559-66, 2003. Review.

Chen H, Chan DC. *Mitochondrial dynamics--fusion, fission, movement, and mitophagy--in neurodegenerative diseases*. Hum Mol Genet. 2009 Oct 15;18(R2):R169-76.

Cho DH, Nakamura T, Fang J, Cieplak P, Godzik A, Gu Z, Lipton SA. *S-nitrosylation of Drp1 mediates beta-amyloid-related mitochondrial fission and neuronal injury.* Science. 2009 Apr 3;324(5923):102-5.

Choi J, Ko J, Racz B, Burette A, Lee JR, Kim S, Na M, Lee HW, Kim K, Weinberg RJ and Kim E. *Regulation of dendritic spine morphogenesis by insulin receptor substrate 53, a downstream effector of Rac1 and Cdc42 small GTPases*. J Neurosci., 25(4):869-79, 2005.

Choi SY, Huang P, Jenkins GM, Chan DC, Schiller J, Frohman MA. *A common lipid links Mfn-mediated mitochondrial fusion and SNARE-regulated exocytosis.* Nat Cell Biol. 2006 Nov;8(11):1255-62.

Chou AM, Sem KP1, Wright GD, Sudhaharan T, Ahmed S. *Dynamin1 Is a Novel Target for IRSp53 Protein and Works with Mammalian Enabled (Mena) Protein and Eps8 to Regulate Filopodial Dynamics*. J Biol Chem. 2014 Aug 29;289(35):24383-96.

Cohen D, Fernandez D, Lázaro-Diéguez F, Müsch A. *The serine/threonine kinase Par1b regulates epithelial lumen polarity via IRSp53-mediated cell-ECM signaling.* J Cell Biol. 2011 Feb 7;192(3):525-40.

Craig AM, Banker G. *Neuronal polarity*. Annu Rev Neurosci. 1994;17:267-310. Review.

Crespi A, Ferrari I, Lonati P, Disanza A, Fornasari D, Scita G, Padovano V, Pietrini G. *LIN7 regulates the filopodium- and neurite-promoting activity of IRSp53.* J Cell Sci. 2012 Oct 1;125(Pt 19):4543-54.

Dadon-Nachum M, Melamed E, Offen D. *The "dying-back" phenomenon of motor neurons in ALS.* J Mol Neurosci. 2011 Mar;43(3):470-7.

Danial NN, Gramm CF, Scorrano L, Zhang CY, Krauss S, Ranger AM, Datta SR, Greenberg ME, Licklider LJ, Lowell BB, Gygi SP, Korsmeyer SJ. *BAD and glucokinase reside in a mitochondrial complex that integrates glycolysis and apoptosis*. Nature. 2003 Aug 21;424(6951):952-6.

Davies VJ1, Hollins AJ, Piechota MJ, Yip W, Davies JR, White KE, Nicols PP, Boulton ME, Votruba M. *Opa1 deficiency in a mouse model of autosomal dominant optic atrophy impairs mitochondrial morphology, optic nerve structure and visual function.* Hum Mol Genet. 2007 Jun 1;16(11):1307-18.

De Vos KJ, Allan VJ, Grierson AJ, Sheetz MP. *Mitochondrial function and actin regulate dynamin-related protein 1-dependent mitochondrial fission*. Curr Biol. 2005 Apr 12;15(7):678-83.

Delettre C, Lenaers G, Griffoin JM, Gigarel N, Lorenzo C, Belenguer P, Pelloquin L, Grosgeorge J, Turc-Carel C, Perret E, Astarie-Dequeker C, Lasquellec L, Arnaud B, Ducommun B, Kaplan J, Hamel CP. *Nuclear gene OPA1, encoding a mitochondrial dynamin-related protein, is mutated in dominant optic atrophy.* Nat Genet. 2000 Oct;26(2):207-10.

Dent EW, Kwiatkowski AV, Mebane LM, Philippar U, Barzik M, Rubinson DA, Gupton S, Van Veen JE, Furman C, Zhang J, Alberts AS, Mori S and Gertler FB. *Filopodia are required for cortical neurite initiation.* Nat Cell Biol., 9(12):1347-59, 2007.

Detmer SA, Chan DC. *Functions and dysfunctions of mitochondrial dynamics.* Nat Rev Mol Cell Biol. 2007 Nov;8(11):870-9. Review.

Disanza A, Mantoani S, Hertzog M, Gerboth S, Frittoli E, Steffen A, Berhoerster K, Kreienkamp HJ, Milanesi F, Di Fiore PP, Ciliberto A, Stradal TE, Scita G. *Regulation of cell shape by Cdc42 is mediated by the synergic actin-bundling activity of the Eps8-IRSp53 complex*. Nat Cell Biol. 2006 Dec;8(12):1337-47.

Drubin DG and Nelson WJ. *Origins of cell polarity.* Cell., 9;84(3):335-44, 1996. Review.

Etienne-Manneville S, Hall A. *Rho GTPases in cell biology*. Nature. 2002 Dec 12;420(6916):629-35.

Faix, J. and Grosse, R. (2006). *Staying in shape with formins.* Dev. Cell 10, 693–706.

Faix, J. and Rottner, K. (2006). *The making of filopodia*. Curr. Opin. Cell Biol. 18, 18–25.

Farsad K, Ringstad N, Takei K, Floyd SR, Rose K, De Camilli P. *Generation of high curvature membranes mediated by direct endophilin bilayer interactions*. J Cell Biol. 2001 Oct 15;155(2):193-200.

Feng, W., Long, J. F., Fan, J. S., Suetake, T. and Zhang, M. (2004). *The tetrameric L27 domain complex as an organization platform for supramolecular assemblies.* Nat. Struct. Mol. Biol. 11, 475–480.

Ferrari I, Crespi A, Scita G, Pietrini G. *LIN7-IRSp53: A novel pathway for filopodia and neurite formation?* Commun Integr Biol. 2012 Nov 1;5(6):631-3.

Fiala JC, Spacek J and Harris KM. *Dendritic spine pathology: cause or consequence of neurological disorders?* Brain Res Brain Res Rev., 39(1):29-54, 2002. Review.

Fischer LR, Culver DG, Tennant P, Davis AA, Wang M, Castellano-Sanchez A, Khan J, Polak MA, Glass JD. *Amyotrophic lateral sclerosis is a distal axonopathy: evidence in mice and man.* Exp Neurol. 2004 Feb;185(2):232-40.

Fujiwara T, Mammoto A, Kim Y, Takai Y. *Rho small G-protein-dependent binding of mDia to an Src homology 3 domain-containing IRSp53/BAIAP2.* Biochem Biophys Res Commun. 2000 May 19;271(3):626-9.

Funato Y, Terabayashi T, Suenaga N, Seiki M, Takenawa T, Miki H. *IRSp53/Eps8 complex is important for positive regulation of Rac and cancer cell motility/invasiveness*. Cancer Res. 2004 Aug 1;64(15):5237-44.

Funke, L., Dakoji, S. and Bredt, D. S. (2005). *Membrane-associated guanylate kinases regulate adhesion and plasticity at cell junctions.* Annu. Rev. Biochem. 74, 219–245.

Futó K, Bódis E, Machesky LM, Nyitrai M, Visegrády B. *Membrane binding properties of IRSp53-missing in metastasis domain (IMD) protein.* Biochim Biophys Acta. 2013 Nov;1831(11):1651-5.

Galluzzi L, Kepp O, Kroemer G. *Mitochondria: master regulators of danger signalling.* Nat Rev Mol Cell Biol. *2012 Dec;13(12):780-8.*

Gandre-Babbe S, van der Bliek AM. The novel tail-anchored membrane protein Mff controls mitochondrial and peroxisomal fission in mammalian cells. Mol Biol Cell. 2008 Jun;19(6):2402-12.

Gey GO, Coffman WD and Kubicek MT. *TISSUE CULTURE STUDIES OF THE PROLIFERATIVE CAPACITY OF CERVICAL CARCINOMA AND NORMAL EPITHELIUM.* Cancer Res 1952;12:243-312.

Gilbert, M. and Fulton, A. B. (1985). *The specificity and stability of the triton-extracted cytoskeletal framework of gerbil fibroma cells.* J. Cell Sci. 73, 335–345.

Goh WI, Lim KB, Sudhaharan T, Sem KP, Bu W, Chou AM, Ahmed S. *mDia1 and WAVE2 proteins interact directly with IRSp53 in filopodia and are involved in filopodium formation.* J Biol Chem. 2012 Feb 10;287(7):4702-14.

Goh, W. I., Sudhaharan, T., Lim, K. B., Sem, K. P., Lau, C. L. and Ahmed, S. (2011). *Rif-mDia1 interaction is involved in filopodium formation independent of Cdc42 and Rac effectors.* J. Biol. Chem. 286, 13681–13694.

Goley ED and Welch MD. *The ARP2/3 complex: an actin nucleator comes of age.* Nat Rev Mol Cell Biol., 7(10):713-26, 2006. Review.

Goodrich LV. *The plane facts of PCP in the CNS.* Neuron., 9;60(1):9-16, 2008. Review.

Govek EE, Newey SE, Van Aelst L. *The role of the Rho GTPases in neuronal development.* Genes Dev., 1;19(1):1-49, 2005. Review.

Guo X, Macleod GT, Wellington A, Hu F, Panchumarthi S, Schoenfield M, Marin L, Charlton MP, Atwood HL, Zinsmaier KE. The *GTPase dMiro is required for axonal transport of mitochondria to Drosophila synapses.* Neuron. 2005 Aug 4;47(3):379-93.

Harraz MM, Marden JJ, Zhou W, Zhang Y, Williams A, Sharov VS, Nelson K, Luo M, Paulson H, Schöneich C, Engelhardt JF. *SOD1 mutations*

disrupt redox-sensitive Rac regulation of NADPH oxidase in a familial ALS model. J Clin Invest. 2008 Feb;118(2):659-70.

Hata Y, Butz S and Sudhof TC. *CASK: a novel Dlg/PSD95 homolog with an N-terminal calmodulin-dependent protein kinase domain identified by interaction with neurexins*. J. Neurosci., 16:2488-2494, 1996.

Hatch AL, Gurel PS, Higgs HN. *Novel roles for actin in mitochondrial fission*. J Cell Sci. 2014 Sep 12. pii: jcs.153791.

Heasman SJ and Ridley AJ. *Mammalian Rho GTPases: new insights into their functions from in vivo studies.* Nat Rev Mol Cell Biol., 9(9):690-701, 2008. Review.

Heiman MG, Shaham S. *Twigs into branches: how a filopodium becomes a dendrite.* Curr Opin Neurobiol., 20(1):86-91, 2010. Review.

Hoppins S, Lackner L, Nunnari J (2007) *The machines that divide and fuse mitochondria.* Annu Rev Biochem 76: 751–780.

Hori K, Konno D, Maruoka H and Sobue K. *MALS is a binding partner of IRSp53 at cell-cell contacts*. FEBS Lett., 554(1-2):30-4, 2003.

Hsueh YP, Yang FC, Kharazia V, Naisbitt S, Cohen AR, Weinberg RJ and Sheng M. *Direct interaction of CASK/LIN-2 and syndecan heparan sulfate proteoglycan and their overlapping distribution in neuronal synapses.* J Cell Biol. Jul 13;142(1):139- 51, 1998.

Iden S and Collard JG. *Crosstalk between small GTPases and polarity proteins in cell polarization*. Nat Rev Mol Cell Biol., 9(11):846-59, 2008. Review.

Ingerman E, Perkins EM, Marino M, Mears JA, McCaffery JM, Hinshaw JE, Nunnari J. *Dnm1 forms spirals that are structurally tailored to fit mitochondria.* J Cell Biol. 2005 Sep 26;170(7):1021-7.

Ishihara N, Fujita Y, Oka T, Mihara K. *Regulation of mitochondrial morphology through proteolytic cleavage of OPA1.* EMBO J. 2006 Jul 12;25(13):2966-77.

Ishihara N, Nomura M, Jofuku A, Kato H, Suzuki SO, Masuda K, Otera H, Nakanishi Y, Nonaka I, Goto Y, Taguchi N, Morinaga H, Maeda M, Takayanagi R, Yokota S, Mihara K. *Mitochondrial fission factor Drp1 is essential for embryonic development and synapse formation in mice.* Nat Cell Biol. 2009 Aug;11(8):958-66.

Ismail AM, Padrick SB, Chen B, Umetani J, Rosen MK. *The WAVE regulatory complex is inhibited*. Nat Struct Mol Biol. 2009 May;16(5):561-3.

Jayashankar V, Rafelski SM. *Integrating mitochondrial organization and dynamics with cellular architecture.* Curr Opin Cell Biol. 2014 Feb;26:34-40. Review.

Jang KJ, Kim MS, Feltrin D, Jeon NL, Suh KY, Pertz O. *Two distinct filopodia populations at the growth cone allow to sense nanotopographical extracellular matrix cues to guide neurite outgrowth.* PLoS One., 30;5(12):e15966, 2010.

Jo K, Derin R, Li M and Bredt DS. *Characterization of MALS/Velis-1, -2 and - 3: a family of mammalian LIN-7 homologues enriched at brain synepses in association with the post-synaptic density-95/NMDA receptor post-synaptic complex*. J. Neurosci., 19:4189-4199, 1999.

Kaech SM, Whitfield CW and Kim SK. *The LIN-2/LIN-7/LIN-10 complex mediates basolateral membrane localization of the C. elegans EGF receptor LET-23 in vulval epithelial cells.* Cell, 94:761-771, 1998.

Karbowski M, Jeong SY, Youle RJ. *Endophilin B1 is required for the maintenance of mitochondrial morphology.* J Cell Biol. 2004 Sep 27;166(7):1027-39.

Kast DJ, Yang C, Disanza A, Boczkowska M, Madasu Y, Scita G, Svitkina T, Dominguez R. *Mechanism of IRSp53 inhibition and combinatorial activation by Cdc42 and downstream effectors*. Nat Struct Mol Biol. 2014 Apr;21(4):413-22.

Kim MH, Choi J, Yang J, Chung W, Kim JH, Paik SK, Kim K, Han S, Won H, Bae YS, Cho SH, Seo J, Bae YC, Choi SY and Kim E. *Enhanced NMDA receptor-mediated synaptic transmission, enhanced long-term potentiation, and impaired learning and memory in mice lacking IRSp53*. J Neurosci., 4;29(5):1586-95, 2009.

Klebe, R. J. and Ruddle, F. H. (1969). *Neuroblastoma: Cell culture analysis of a differentiating stem cell system.* J. Cell Biol. 43, 69A.

Korobova F, Gauvin TJ, Higgs HN. *A role for myosin II in mammalian mitochondrial fission.* Curr Biol. 2014 Feb 17;24(4):409-14.

Korobova F, Ramabhadran V, Higgs HN: *An actin-dependent step in mitochondrial fission mediated by the ER-associated formin INF2*. Science 2013, 339:464-467.

Kornau H, Schenker LT, Kennedy MB and Seeburg PH. *Domain interaction between NMDA receptor subunits and the post-synaptic density protein PSD-95*. Science, 269:1737-1740, 1995.

Koshiba T, Detmer SA, Kaiser JT, Chen H, McCaffery JM, Chan DC. *Structural basis of mitochondrial tethering by mitofusin complexes.* Science. 2004 Aug 6;305(5685):858-62.

Krugmann S, Jordens I, Gevaert K, Driessens M, Vandekerckhove J, Hall A. *Cdc42 induces filopodia by promoting the formation of an IRSp53:Mena complex.* Curr Biol. 2001 Oct 30;11(21):1645-55.

Lanktree M, Squassina A, Krinsky M, Strauss J, Jain U, Macciardi F, Kennedy JL, Muglia P. *Association study of brain-derived neurotrophic factor (BDNF) and LIN-7 homolog (LIN-7) genes with adult attention-deficit/hyperactivity disorder.* Am J Med Genet B Neuropsychiatr Genet., 5;147B(6):945-51, 2008.

Lee YG, Macoska JA, Korenchuk S and Pienta KJ. *MIM, a potential metastasis suppressor gene in bladder cancer.* Neoplasia, 4(4):291-4, 2002.

Lee YJ, Jeong SY, Karbowski M, Smith CL, Youle RJ. *Roles of the mammalian mitochondrial fission and fusion mediators Fis1, Drp1, and Opa1 in apoptosis.* Mol Biol Cell. 2004 Nov;15(11):5001-11.

Lee S, Jeong SY, Lim WC, Kim S, Park YY, Sun X, Youle RJ, Cho H. *Mitochondrial fission and fusion mediators, hFis1 and OPA1, modulate cellular senescence.* J Biol Chem. 2007 Aug 3;282(31):22977-83.

Legesse-Miller A1, Massol RH, Kirchhausen T. *Constriction and Dnm1p recruitment are distinct processes in mitochondrial fission.* Mol Biol Cell. 2003 May;14(5):1953-63. Epub 2003 Feb 6.

Legros F, Lombès A, Frachon P, Rojo M. *Mitochondrial fusion in human cells is efficient, requires the inner membrane potential, and is mediated by mitofusins.* Mol Biol Cell. 2002 Dec;13(12):4343-54.

Li Y, Karnak D, Demeler B, Margolis B, Lavie A. *Structural basis for L27 domain-mediated assembly of signaling and cell polarity complexes.* EMBO J., 21;23(14):2723-33, 2004.

Lim KB, Bu W, Goh WI, Koh E, Ong SH, Pawson T, Sudhaharan T, Ahmed S. *The Cdc42 effector IRSp53 generates filopodia by coupling membrane protrusion with actin dynamics*. J Biol Chem. 2008 Jul 18;283(29):20454-72.

Liu X, Weaver D, Shirihai O, Hajnóczky G. *Mitochondrial 'kiss-and-run': interplay between mitochondrial motility and fusion-fission dynamics*. EMBO J. 2009 Oct 21;28(20):3074-89.

Losón OC, Song Z, Chen H, Chan DC. *Fis1, Mff, MiD49, and MiD51 mediate Drp1 recruitment in mitochondrial fission*. Mol Biol Cell. 2013 Mar;24(5):659-67.

Lowery LA, Van Vactor D. *The trip of the tip: understanding the growth cone machinery.* Nat Rev Mol Cell Biol., 10(5):332-43, 2009. Review.

Majumder P, Chen YT, Bose JK, Wu CC, Cheng WC, Cheng SJ, Fang YH, Chen YL, Tsai KJ, Lien CC, Shen CK. *TDP-43 regulates the mammalian spinogenesis through translational repression of Rac1.* Acta Neuropathol. 2012 Aug;124(2):231-45.

Massari S, Perego C, Padovano V, D'Amico A, Raimondi A, Francolini M, Pietrini G. *LIN7 mediates the recruitment of IRSp53 to tight junctions*. Traffic. 2009 Feb;10(2):246-57.

Mattila PK, Lappalainen P. *Filopodia: molecular architecture and cellular functions.* Nat Rev Mol Cell Biol., 9(6):446-54, 2008. Review.

Mattila PK, Pykäläinen A, Saarikangas J, Paavilainen VO, Vihinen H, Jokitalo E, Lappalainen P. *Missing-in-metastasis and IRSp53 deform PI(4,5)P2-rich membranes by an inverse BAR domain-like mechanism*. J Cell Biol. 2007 Mar 26;176(7):953-64.

Miki H, Yamaguchi H, Suetsugu S, Takenawa T. *IRSp53 is an essential intermediate between Rac and WAVE in the regulation of membrane ruffling.* Nature. 2000 Dec 7;408(6813):732-5.

Millard TH, Bompard G, Heung MY, Dafforn TR, Scott DJ, Machesky LM and Fütterer K. *Structural basis of filopodia formation induced by the IRSp53/MIM homology domain of human IRSp53.* EMBO J. 26;24(2):240-50, 2005.

Miyahara A, Okamura-Oho Y, Miyashita T, Hoshika A, Yamada M. *Genomic structure and alternative splicing of the insulin receptor tyrosine kinase substrate of 53-kDa protein*. J Hum Genet., 48(8):410-4, 2003.

Mozdy AD, Shaw JM. *A fuzzy mitochondrial fusion apparatus comes into focus.* Nat Rev Mol Cell Biol. 2003 Jun;4(6):468-78.

Mukherjee K, Slawson JB, Christmann BL, Griffith LC. *Neuron-specific protein interactions of Drosophila CASK-β are revealed by mass spectrometry*. Front Mol Neurosci. 2014 Jun 30;7:58.

Nadif Kasri N, Van Aelst L. *Rho-linked genes and neurological disorders*. Pflugers Arch. 2008 Feb;455(5):787-97. Epub 2007 Nov 15.

Neff RA 3rd, Gomez-Varela D, Fernandes CC, Berg DK. *Postsynaptic scaffolds for nicotinic receptors on neurons.* Acta Pharmacol Sin. 2009 Jun;30(6):694-701.

Newey SE, Velamoor V, Govek EE and Van Aelst L. *Rho GTPases, dendritic structure, and mental retardation.* J Neurobiol., 64(1):58-74, 2005. Review.

Niethammer M, Kim E and Sheng M. *Interaction between the C-terminus of NMDA receptor subunits and multiple members of the PSD-95 family of membrane- associated guanylate kinases.* J. Neurosci., 16:2157-2163, 1996.

Okamoto K, Shaw JM. *Mitochondrial morphology and dynamics in yeast and multicellular eukaryotes*. Annu Rev Genet. 2005;39:503-36. Review.

Okamura–Oho, Y., Miyashita, T. and Yamada, M. (2001). *Distinctive tissue distribution and phosphorylation of IRSp53 isoforms.* Biochem. Biophys. Res. Commun. 289, 957–960.

Olsen O, Moore KA, Fukata M, Kazuta T, Trinidad JC, Kauer FW, Streuli M, Misawa H, Burlingame AL, Nicoll RA, Bredt DS. *Neurotransmitter release regulated by a MALS-liprin-alpha presynaptic complex*. J Cell Biol., 26;170(7):1127-34, 2005.

Olsen O, Moore KA, Nicoll RA and Bredt DS. *Synaptic transmission regulated by a presynaptic MALS/Liprin-alpha protein complex*. Curr Opin Cell Biol., 18(2):223-7, 2006. Review.

Osteryoung KW, Nunnari J. *The division of endosymbiotic organelles. Science.* 2003 Dec 5;302(5651):1698-704.

Otera H, Ishihara N, Mihara K. *New insights into the function and regulation of mitochondrial fission.* Biochim Biophys Acta. 2013 May;1833(5):1256-68.

Otera H, Wang C, Cleland MM, Setoguchi K, Yokota S, Youle RJ, Mihara K. *Mff is an essential factor for mitochondrial recruitment of Drp1 during mitochondrial fission in mammalian cells.* J Cell Biol. 2010 Dec 13;191(6):1141-58.

Palmer CS, Osellame LD, Stojanovski D, Ryan MT. *The regulation of mitochondrial morphology: intricate mechanisms and dynamic machinery.* Cell Signal. 2011 Oct;23(10):1534-45.

Parone PA, Da Cruz S, Tondera D, Mattenberger Y, James DI, Maechler P, Barja F, Martinou JC. *Preventing mitochondrial fission impairs mitochondrial function and leads to loss of mitochondrial DNA*. PLoS One. 2008 Sep 22;3(9):e3257.

Paschou P, Feng Y, Pakstis AJ, Speed WC, DeMille MM, Kidd JR, Jaghori B, Kurlan R, Pauls DL, Sandor P, Barr CL, Kidd KK. *Indications of linkage and association of Gilles de la Tourette syndrome in two independent family samples: 17q25 is a putative susceptibility region.* Am J Hum Genet. 2004 Oct;75(4):545-60.

Perego C, Vanoni C, Bossi M, Massari S, Basudev H, Longhi R and Pietrini G. *The GLT-1 and GLAST glutamate transporters are expressed on morphologically distinct astrocytes and regulated by neuronal activity in primary hippocampal cocultures*. J. Neurochem., 75:1076-1084, 2000.

Perego C, Vanoni C, Massari S, Raimondi A, Pola S, Cattaneo MG, Francolini M, Vicentini LM and Pietrini G. *Invasive behaviour of glioblastoma cell lines is associated with altered organisation of the cadherin-catenin adhesion system.* J. Cell Science, 115:3331-3340, 2002.

Perego C, Vanoni C, Villa A, Longhi R, Kaech SM, Frohli E, Hajnal A, Kim SK and Pietrini G. *PDZ-mediated interactions retain the epithelial GABA transporter on the basolateral surface of polarized epithelial cells.* EMBO J., 18:2384-2393, 1999.

Poelmans G, Pauls DL, Buitelaar JK, Franke B. *Integrated genome-wide association study findings: identification of a neurodevelopmental network for attention deficit hyperactivity disorder.* Am J Psychiatry., 168(4):365-77., 2011. Review.

Pon LA. *Mitochondrial fission: rings around the organelle.* Curr Biol. 2013 Apr 8;23(7):R279-81.

Qian W, Choi S, Gibson GA, Watkins SC, Bakkenist CJ, Van Houten B. *Mitochondrial hyperfusion induced by loss of the fission protein Drp1 causes ATM-dependent G2/M arrest and aneuploidy through DNA replication stress.* J Cell Sci. 2012 Dec 1;125(Pt 23):5745-57.

Quintana A, Schwindling C, Wenning AS, Becherer U, Rettig J, Schwarz EC, Hoth M. *T cell activation requires mitochondrial translocation to the immunological synapse*. Proc Natl Acad Sci U S A. 2007 Sep 4;104(36):14418-23.

Rafelski SM. *Mitochondrial network morphology: building an integrative, geometrical view.* BMC Biol. 2013 Jun 24;11:71. Review.

Ribasés M, Bosch R, Hervás A, Ramos-Quiroga JA, Sánchez-Mora C, Bielsa A, Gastaminza X, Guijarro-Domingo S, Nogueira M, Gómez-Barros N, Kreiker S, Gross-Lesch S, Jacob CP, Lesch KP, Reif A, Johansson S, Plessen KJ, Knappskog PM, Haavik J, Estivill X, Casas M, Bayés M, Cormand B. *Case-control study of six genes asymmetrically expressed in*

the two cerebral hemispheres: association of BAIAP2 with attention-deficit/hyperactivity disorder. Biol Psychiatry., 15;66(10):926-34, 2009.

Robens JM, Yeow-Fong L, Ng E, Hall C, Manser E. *Regulation of IRSp53-dependent filopodial dynamics by antagonism between 14-3-3 binding and SH3-mediated localization.* Mol Cell Biol.,30(3):829-44, 2010.

Rogelj B, Mitchell JC, Miller CC, McLoughlin DM. *The X11/Mint family of adaptor proteins.* Brain Res Rev. 2006 Sep;52(2):305-15.

Rojo M, Legros F, Chateau D, Lombès A. *Membrane topology and mitochondrial targeting of mitofusins, ubiquitous mammalian homologs of the transmembrane GTPase Fzo.* J Cell Sci. 2002 Apr 15;115(Pt 8):1663-74.

Roman T, Rohde LA, Hutz MH. *A role for neurotransmission and neurodevelopment in attention-deficit/hyperactivity disorder.* Genome Med., 19;1(11):107, 2009.

Romanello V, Sandri M. *Mitochondrial biogenesis and fragmentation as regulators of protein degradation in striated muscles.* J Mol Cell Cardiol. 2013 Feb;55:64-72. Review.

Rommelse NN, Franke B, Geurts HM, Hartman CA, Buitelaar JK. *Shared heritability of attention-deficit/hyperactivity disorder and autism spectrum disorder*. Eur Child Adolesc Psychiatry., 19(3):281-95, 2010. Review.

Ronchi, P., Colombo, S., Francolini, M. and Borgese, N. (2008). *Transmembrane domain-dependent partitioning of membrane proteins within the endoplasmic reticulum*. J. Cell Biol. 181, 105–118.

Rosen DR, Sapp P, O'Regan J, McKenna-Yasek D, Schlumpf KS, Haines JL, Gusella JF, Horvitz HR, Brown RH Jr. *Genetic linkage analysis of*

familial amyotrophic lateral sclerosis using human chromosome 21 microsatellite DNA markers. Am J Med Genet. 1994 May 15;51(1):61-9.

Rosivatz E1, Woscholski R. *Removal or masking of phosphatidylinositol(4,5)bisphosphate from the outer mitochondrial membrane causes mitochondrial fragmentation.* Cell Signal. 2011 Feb;23(2):478-86.

Sala C, Cambianica I and Rossi F. *Molecular mechanisms of dendritic spine development and maintenance*. Acta Neurobiol Exp (Wars), 68(2):289-304, 2008. Review.

Santel A, Fuller MT. *Control of mitochondrial morphology by a human mitofusin.* J Cell Sci. 2001 Mar;114(Pt 5):867-74.

Sawallisch C, Berhörster K, Disanza A, Mantoani S, Kintscher M, Stoenica L, Dityatev A, Sieber S, Kindler S, Morellini F, Schweizer M, Boeckers TM, Korte M, Scita G and Kreienkamp HJ. *The insulin receptor substrate of 53 kDa (IRSp53) limits hippocampal synaptic plasticity*. J Biol Chem., 3;284(14):9225-36, 2009.

Schultz J, Hoffmuller U, Krause G, Ashurst J, Macias MJ, Schmieder P, Schneider-Mergener J and Oschkinat H. *Specific interactions between the syntrophin PDZ domain and voltage-gated sodium channels.* Nat. Struct. Biol., 5, 19-24, 1998.

Scita G, Confalonieri S, Lappalainen P and Suetsugu S. *IRSp53: crossing the road of membrane and actin dynamics in the formation of membrane protrusions.* Trends Cell Biol., 18(2):52-60, 2008.

Sekino Y, Kojima N and Shirao T. *Role of actin cytoskeleton in dendritic spine morphogenesis*. Neurochem Int., 51(2-4):92-104, 2007. Review.

Serafini T. *An old friend in a new home: cadherins at the synapse.* Trends Neurosci., 20(8):322-3, 1997. Review.

Setou M, Nakagawa T, Seog DH, Hirokawa N. *Kinesin superfamily motor protein KIF17 and mLin-10 in NMDA receptor-containing vesicle transport.* Science. 2000 Jun 9;288(5472):1796-802.

Sheng M and Sala C. *PDZ domains and the organization of supramolecular complexes.* Annu Rev Neurosci., 24:1-29, 2001. Review.

Shin, K., Fogg, V. C. and Margolis, B. (2006). *Tight junctions and cell polarity. Annu. Rev.* Cell Dev. Biol. 22, 207–235.

Shinawi M, Sahoo T, Maranda B, Skinner SA, Skinner C, Chinault C, Zascavage R, Peters SU, Patel A, Stevenson RE, Beaudet AL. *11p14.1 microdeletions associated with ADHD, autism, developmental delay, and obesity.* Am J Med Genet A., 155A(6):1272-80. doi: 10.1002/ajmg.a.33878, 2011.

Simske JS, Kaech SM, Harp SA and Kim SK. *LET-23 receptor localization by the cell junction protein LIN-7 during C. elegans vulval induction.* Cell, 85:195-204, 1996.

Smirnova E, Griparic L, Shurland DL, van der Bliek AM. *Dynamin-related protein Drp1 is required for mitochondrial division in mammalian cells*. Mol Biol Cell. 2001 Aug;12(8):2245-56.

Soltau M, Berhörster K, Kindler S, Buck F, Richter D and Kreienkamp HJ. *Insulin receptor substrate of 53 kDa links postsynaptic shank to PSD-95.* J Neurochem., 90(3):659-65, 2004.

Song W, Chen J, Petrilli A, Liot G, Klinglmayr E, Zhou Y, Poquiz P, Tjong J, Pouladi MA, Hayden MR, Masliah E, Ellisman M, Rouiller I, Schwarzenbacher R, Bossy B, Perkins G, Bossy-Wetzel E. *Mutant huntingtin binds the mitochondrial fission GTPase dynamin-related protein-1 and increases its enzymatic activity.* Nat Med. 2011 Mar;17(3):377-82.

Songyang Z, Fanning AS, Fu C, Xu J, Marfatia SM, Chishti AH, Crompton A, Chan AC, Anderson JM and Cantley LC. *Recognition of unique carboxyl- terminal motifs by distinct PDZ domains.* Science, 275:73-77, 1997

Spencer TJ. *Pharmacology of adult ADHD with stimulants.* CNS Spectr., 12(4 Suppl 6):8-11, 2007.

Sreedharan J1, Blair IP, Tripathi VB, Hu X, Vance C, Rogelj B, Ackerley S, Durnall JC, Williams KL, Buratti E, Baralle F, de Belleroche J, Mitchell JD, Leigh PN, Al-Chalabi A, Miller CC, Nicholson G, Shaw CE. *TDP-43 mutations in familial and sporadic amyotrophic lateral sclerosis.* Science. 2008 Mar 21;319(5870):1668-72.

Stowers RS, Megeath LJ, Górska-Andrzejak J, Meinertzhagen IA, Schwarz TL. *Axonal transport of mitochondria to synapses depends on milton, a novel Drosophila protein.* Neuron. 2002 Dec 19;36(6):1063-77.

Straight SW, Pieczynski JN, Whiteman EL, Liu CJ, Margolis B. *Mammalian lin-7 stabilizes polarity protein complexes.* J Biol Chem. 8;281(49):37738-47, 2006.

Suetsugu S, Gautreau A. *Synergistic BAR-NPF interactions in actin-driven membrane remodeling.* Trends Cell Biol. 2012 Mar;22(3):141-50.

Suetsugu S, Kurisu S, Oikawa T, Yamazaki D, Oda A, Takenawa T. *Optimization of WAVE2 complex-induced actin polymerization by membrane-bound IRSp53, PIP(3), and Rac.* J Cell Biol. 2006 May 22;173(4):571-85.

Sung JY, Engmann O, Teylan MA, Nairn AC, Greengard P, Kim Y. *WAVE1 controls neuronal activity-induced mitochondrial distribution in dendritic spines*. Proc Natl Acad Sci U S A. 2008 Feb 26;105(8):3112-6.

Takahashi Y, Karbowski M, Yamaguchi H, Kazi A, Wu J, Sebti SM, Youle RJ, Wang HG. *Loss of Bif-1 suppresses Bax/Bak conformational change and mitochondrial apoptosis*. Mol Cell Biol. 2005 Nov;25(21):9369-82.

Toma C, Hervás A, Balmaña N, Vilella E, Aguilera F, Cuscó I, del Campo M, Caballero R, De Diego-Otero Y, Ribasés M, Cormand B, Bayés M. *Association study of six candidate genes asymmetrically expressed in the two cerebral hemispheres suggests the involvement of BAIAP2 in autism*. J Psychiatr Res., 45(2):280-2, 2011.

Tondera D, Czauderna F, Paulick K, Schwarzer R, Kaufmann J, Santel A. *The mitochondrial protein MTP18 contributes to mitochondrial fission in mammalian cells*. J Cell Sci. 2005 Jul 15;118(Pt 14):3049-59.

Tortarolo, M., Crossthwaite, A.J., Conforti, L., Spencer, J.P., Williams, R.J., Bendotti, C. & Rattray, M. (2004) *Expression of SOD1 G93A or wild-type SOD1 in primary cultures of astrocytes down-regulates the*

glutamate transporter GLT-1: lack of involvement of oxidative stress. J. Neurochem., 88, 481–493.

Twig G, Elorza A, Molina AJ, Mohamed H, Wikstrom JD, Walzer G, Stiles L, Haigh SE, Katz S, Las G, Alroy J, Wu M, Py BF, Yuan J, Deeney JT, Corkey BE, Shirihai OS. *Fission and selective fusion govern mitochondrial segregation and elimination by autophagy.* EMBO J. 2008 Jan 23;27(2):433-46.

van der Bliek AM, Shen Q, Kawajiri S. *Mechanisms of mitochondrial fission and fusion.* Cold Spring Harb Perspect Biol. 2013 Jun 1;5(6).

van Spronsen M, Mikhaylova M, Lipka J, Schlager MA, van den Heuvel DJ, Kuijpers M, Wulf PS, Keijzer N, Demmers J, Kapitein LC, Jaarsma D, Gerritsen HC, Akhmanova A, Hoogenraad CC. *TRAK/Milton motor-adaptor proteins steer mitochondrial trafficking to axons and dendrites*. Neuron. 2013 Feb 6;77(3):485-502.

Verstreken P, Ly CV, Venken KJ, Koh TW, Zhou Y, Bellen HJ. *Synaptic mitochondria are critical for mobilization of reserve pool vesicles at Drosophila neuromuscular junctions.* Neuron. 2005 Aug 4;47(3):365-78.

Vessey JP, Karra D. *More than just synaptic building blocks: scaffolding proteins of the post-synaptic density regulate dendritic patterning.* J Neurochem., 102(2):324-32, 2007. Review.

Wang XB, Zhou Q. *Spine remodeling and synaptic modification.* Mol Neurobiol. 41(1):29-41, 2010. Review.

Waterham HR, Koster J, van Roermund CW, Mooyer PA, Wanders RJ, Leonard JV. *A lethal defect of mitochondrial and peroxisomal fission.* N Engl J Med. 2007 Apr 26;356(17):1736-41.

Westrate LM, Sayfie AD, Burgenske DM, MacKeigan JP. *Persistent mitochondrial hyperfusion promotes G2/M accumulation and caspase-dependent cell death.* PLoS One. 2014 Mar 14;9(3):e91911.

Wong ED, Wagner JA, Gorsich SW, McCaffery JM, Shaw JM, Nunnari J. *The dynamin-related GTPase, Mgm1p, is an intermembrane space protein required for maintenance of fusion competent mitochondria.* J Cell Biol. 2000 Oct 16;151(2):341-52.

Wu C, Asokan SB, Berginski ME, Haynes EM, Sharpless NE, Griffith JD, Gomez SM, Bear JE. *Arp2/3 is critical for lamellipodia and response to extracellular matrix cues but is dispensable for chemotaxis.* Cell. 2012 Mar 2;148(5):973-87.

Wu, G., Fang, Y., Lu, Z. H. and Ledeen, R. W. (1998). *Induction of axon-like and dendrite-like processes in neuroblastoma cells.* J. Neurocytol. 27, 1–14.

Yamagishi A, Masuda M, Ohki T, Onishi H and Mochizuki N. *A novel actin bundling/filopodium-forming domain conserved in insulin receptor tyrosine kinase substrate p53 and missing in metastasis protein.* J Biol Chem. 9;279(15):14929-36, 2004.

Yang, C., Czech, L., Gerboth, S., Kojima, S., Scita, G. and Svitkina, T. (2007). *Novel roles of formin mDia2 in lamellipodia and filopodia formation in motile cells.* PLoS Biol. 5, e317.

Yang C, Hoelze M, Disanza A, Scita G, Svitkina T. *Coordination of membrane and actin cytoskeleton dynamics during filopodia protrusion.* Plos One, 4:1-9. 2009.

Yang, C. and Svitkina, T. (2011). *Filopodia initiation: focus on the Arp2/3 complex and formins.* Cell Adh. Migr. 5, 402–408.

Yeh TC, Ogawa W, Danielsen AG, Roth RA. *Characterization and cloning of a 58/53-kDa substrate of the insulin receptor tyrosine kinase.* J Biol Chem. 9;271(6):2921-8, 1996.

Yoshihara Y, De Roo M, Muller D. *Dendritic spine formation and stabilization.* Curr Opin Neurobiol.,19(2):146-53, 2009.

Yoshimura T, Arimura N, Kaibuchi K. *Signaling networks in neuronal polarization.* J Neurosci., 18;26(42):10626-30, 2006. Review.

Youle RJ, Karbowski M. *Mitochondrial fission in apoptosis.* Nat Rev Mol Cell Biol. 2005 Aug;6(8):657-63.

Zhao J, Liu T, Jin S, Wang X, Qu M, Uhlén P, Tomilin N, Shupliakov O, Lendahl U, Nistér M. *Human MIEF1 recruits Drp1 to mitochondrial outer membranes and promotes mitochondrial fusion rather than fission.* EMBO J. 2011 Jun 24;30(14):2762-78.

Zhao H, Pykäläinen A, Lappalainen P. *I-BAR domain proteins: linking actin and plasma membrane dynamics.* Curr Opin Cell Biol., 23(1):14-21, 2011.

Zhao Y, Zhang W, Kho Y, Zhao Y. *Proteomic analysis of integral plasma membrane proteins.* Anal Chem. 2004 Apr 1;76(7):1817-23.

Zhou J, Jones DR, Duong DM, Levey AI, Lah JJ, Peng J. *Proteomic analysis of postsynaptic density in Alzheimer's disease*. Clin Chim Acta. 2013 May;420:62-8.

Ziv, N. E. and Smith, S. J. (1996). *Evidence for a role of dendritic filopodia in synaptogenesis and spine formation.* Neuron 17, 91–102.

Züchner S, Mersiyanova IV, Muglia M, Bissar-Tadmouri N, Rochelle J, Dadali EL, Zappia M, Nelis E, Patitucci A, Senderek J, Parman Y, Evgrafov O, Jonghe PD, Takahashi Y, Tsuji S, Pericak-Vance MA, Quattrone A, Battaloglu E, Polyakov AV, Timmerman V, Schröder JM, Vance JM. *Mutations in the mitochondrial GTPase mitofusin 2 cause Charcot-Marie-Tooth neuropathy type 2A*. Nat Genet. 2004 May;36(5):449-51.

Zucker B, Kama JA, Kuhn A, Thu D, Orlando LR, Dunah AW, Gokce O, Taylor DM, Lambeck J, Friedrich B, Lindenberg KS, Faull RL, Weiller C, Young AB, Luthi-Carter R. *Decreased Lin7b expression in layer 5 pyramidal neurons may contribute to impaired corticostriatal connectivity in huntington disease.* J Neuropathol Exp Neurol.. 69(9):880-95, 2010.

CHAPTER 10

List of abbreviations

10. List of abbreviations

- ADHD: Attention deficit / hyperactivity disorder
- ALS: Amyotrophic lateral sclerosis
- ALS2: Alsin
- AMPA: α-amino-3-hydroxy-5-methyl-4-isoxazolepropionic acid
- ARP 2/3 complex: Actin-related protein 2/3 complex
- ASD: Autism spectrum disorder
- AJs: Adherens junctions
- BAIAP2: brain-specific angiogenesis inhibitor 1-associated protein 2
- BAR: Bin–Amphiphysin–Rvs
- Bax: Bcl-2-associated X protein
- BDNF: Brain-derived neurotrophic factor
- BGT1: Betaine-GABA transporter 1
- BSA: Albumin Bovine serum
- CAMK2: Calcium/calmodulin-dependent protein kinase type II
- CASK: Calcium/calmodulin-dependent serine protein kinase
- Cdc42: Cell division control protein 42
- CMT: Charcot-Marie-Tooth disease
- CMT1: Charcot-Marie-Tooth type 1 disease
- CMT2A: Charcot-Marie-Tooth type 2A disease
- CNS: Central nervous system
- CRIB: Cdc42/Rac interactive binding domain
- DMEM: Dulbecco's modified eagle medium

- DN: Dominant negative
- DOA: Autosomal dominant optic atrophy
- Drp1: Dynamin-Related Protein 1
- DTT: Dithiothreitol
- DYN: Dynamin
- E: Embryonic day
- ECM: Extracellular matrix
- EDTA: Ethylenediaminetetraacetic acid
- ENA: Enabled
- Eps8: Epidermal growth factor receptor pathway substrate 8
- ER: Endoplasmic Reticulum
- EtBr: Ethidium bromide
- F-actin: Filamentous actin
- FBS: Foetal bovine serum
- FH2: Formin homology 2 domain
- Fis1: Mitochondrial fission protein 1
- FMNL2: Formin-like protein 2
- FTD: Frontotemporal dementia
- G-actin: Globular actin
- GABA: gamma-Aminobutyric acid
- GAP: GTPase activating protein
- GED: GTPase Effector Domain
- GEF: Guanilate exchange factor
- GFP: Green fluorescent protein

- GSK3β: Glycogen synthase kinase 3 beta
- HR: Heptad Repeat
- Htt: Huntingtin
- I: Insoluble fraction
- I-BAR: Inverted : Bin–Amphiphysin–Rvs domain
- IGF-1: Insulin-like growth factor 1
- IMD: IRSp53 and missing in metastasis domain
- IMM: Inner Mitochondrial Membrane
- INF2: Inverted formin-2
- IP: Immunoprecipitate
- IRSp53: Insulin receptor substrate protein of 53 kDa
- JACoP: Just Another Colocalization plugin
- KIF5: Kinesin heavy chain isoform 5
- Kif17: Kinesin-like protein 17
- KO: Knock Out
- L27: Lin 2 and Lin7 domain
- LB: Luria-Bertani broth
- Let-23: Lethal protein 23
- LIN2: Lineage defective 2
- LIN7: Lineage defective 7
- LIN10: Lineage defective 10
- LTD: Long term depression
- LTP: Long term potentiation
- MAGUK: Membrane-associated guanylate kinase

- Mals: Mammalian lin-seven protein
- MCC: Mander's colocalization coefficient
- MDCK: Madin-Darby canine kidney
- mDia1: mammalian Diaphanous 1
- mDia2: mammalian Diaphanous 2
- Mena: Mammalian enabled
- MFF: Mitochondrial fission factor
- MFN1: Mitofusin 1
- MFN 2: Mitofusin 2
- MiD49: Mitochondrial dynamics proteins of 49
- MiD51: Mitochondrial dynamics proteins of 51 kDa
- Miro: Mitochondrial Rho GTPase 1
- MITO: Crude mitochondrial fraction
- mitoPLD: Mitochondrial Phospholipase D
- mtDNA: Mitochondrial DNA
- MTP18: Mitochondrial protein of 18 kDa
- N-cadherin: Neuronal cadherin
- NMDA: N-methyl-D-aspartate
- NO: Nitric Oxide
- Nox: NADPH oxidase
- NPF: Nucleation promoting factor
- N-WASP: Neuronal Wiskott- Aldrich syndrome protein
- OMM: Outer Mitochondrial Membrane
- OPA1: Optic Atrophy 1

- OXPHOS: Oxidative Phosphorilation
- P: Pellet fraction
- Pak: p21 activated kinase
- Par-3: Partitioning defective-3
- Par-6: Partitioning defective-6
- PBS: Phosphate buffered saline
- PDZ: Post synaptic density protein/Drosophila disc large tumor suppressor/zonula occludens-1 domain
- PH: Plekstrin homology domain
- PI3K: Phosphoinositide 3-kinase
- PKC: Protein kinase C
- PM: Plasma membrane
- PMS: Post-mitochondrial supernatant
- PMSF: phenylmethylsulfonyl fluoride
- PNS: Post-nuclear supernatant
- PS: Phosphatidylserine
- PSD: Postsynaptic density
- PSD-95: Postsynaptic density protein 95
- PtdIns(4,5)P_2 : Phosphatidylinositol 4,5-bisphosphate
- Rac1: Ras-related C3 botulinum toxin substrate 1
- Rho: Ras homolog gene
- RhoA: Ras homolog gene family, member A
- ROI: Region of interest
- ROS: Reactive Oxygen Species

- RT: Room temperature
- S: Soluble fraction
- Ser: Serine
- SH3: SRC homology 3 domain
- Shank 1: SH3 and multiple ankyrin repeat domains protein 1
- SDS: Sodium dodecyl sulfate
- SDS-PAGE: Sodium dodecyl sulfate Polyacrylamide gel electrophoresis
- SOD1: Copper/Zinc Superoxide dismutase 1
- STEF: SIF and Tiam 1-like exchange factor
- TAE: Tris-acetate EDTA
- TDP-43: TAR DNA-binding protein 43
- TE: TrisHCl - EDTA
- TIAM1: T-cell lymphoma invasion and metastasis-inducing protein 1
- TJ: Tight junction
- TRAK1: Trafficking kinesin-binding protein 1
- TRAK2: Trafficking kinesin-binding protein 2
- UV: Ultraviolet light
- VASP: Vasodilator-stimulated phosphoprotein
- VELI: Vertebrate lin-7 homolog
- WAVE1: Verprolin-homologous protein 1
- WAVE2: Verprolin-homologous protein 2
- WRC: WAVE regulatory complex